Sedimentological and petrographical investigations of the Early Triassic Vardebukta Formation on western Spitsbergen

Ole-Marius Solvang

Thesis for the degree of Master of Science

in Sedimentology/Petroleum Geology

Department of Earth Science
University of Bergen
November 2017

Abstract

The earliest Triassic Barents Sea Basin received sediments from three sedimentary systems. Of these, the Fennoscandian and the Uralian systems have been well studied highlighting their sedimentology, provenance, extent and reservoir parameters. Contrarily, the system originating from Greenland/Arctic Canada has received little attention and remains poorly constrained. This study has investigated the latter system by detailed sedimentological outcrop analysis of the Induan Vardebukta Formation on western Spitsbergen at Festningen, Selmaneset and Studentdalen. The composition and texture of collected sandstone samples have been investigated by thin section analysis, warranting a comparison to its synchronous deposits in the Barents Sea.

Based on the sedimentological analysis, 6 facies associations are recognized; supratidal flats, tidal sandflats, tidally influenced channels, delta front deposits, offshore transition zone and prodelta deposits. These are interpreted to have been deposited in a mixed type delta as evidenced by the great variety of sedimentary processes, and the clear progradational signature. Furthermore, the depositional environment was characterized by extensive biogenic carbonate production with a storm and wave agitated shelf.

Point counting of the sandstones reveals high mineralogical maturity whereas the textural observations do not, suggesting a short transport from a nearby sedimentary source area. Additionally, the sediments show evidence of deep burial prior to deposition expressed through the sutured grain shape and the relative abundance of quartzite grains. Also, a clear bimodal grain size distribution is found in one of the samples, implying that the Vardebukta Formation partially originates from two distinctive source areas. It is possible that the sudden influx of sediments in the Induan is linked to Late Paleozoic – Early Mesozoic tectonism, which at the time led to a general tectonic uplift of the uplands to the Barents Sea Basin. This was possibly due to the onset of rifting along the western Norway - eastern Greenland margin, creating large denudation areas of previously deeply buried sediments originally sourced from Greenland/Arctic Canada.

Acknowledgements

Ole-Marius Solvang

Bergen, 20.11.2017

Table of contents

1 Introduction

1.1 Aim of study

During the Triassic in the Barents Sea, sedimentary systems were principally prograding from Fennoscandia in present-day northern Norway and from the Uralides in the eastern Barents Sea. These have been well studied and have attracted attention from the petroleum industry for decades, but generally it is only the Fennoscandian system that displays favorable reservoir properties and has proved to contain significant amounts of hydrocarbons (e.g. the Goliat discovery (Mulrooney et al., 2017; Klausen et al., *in press*)). However, in the Lower Triassic an additional sedimentary system was prograding from the west (i.e. northeastern Greenland/Arctic Canada) supplying sediments to Svalbard and possibly the Barents Sea. This system has received little attention compared to the more well-known counterparts from the Urals and Fennoscandia. Consequently, important details relating to sedimentary environments, sediment distribution, source area and reservoir parameters remain unknown.

This study intends to create a detailed facies model of this western system through outcrop data from the Vardebukta Formation along western Spitsbergen, incorporating data gathered from proximal sandstone-rich localities by investigating petrographic properties of collected sandstones through thin-section analysis. Thus, this study has three goals:

1) To provide a reliable depositional model for the Vardebukta Formation based on sedimentary processes.
2) To investigate the source-to-sink perspectives of the Vardebukta Formation by examining sandstone composition through thin section analysis and reviewing available provenance data. Furthermore, this will be compared to the synchronous deposits in the Barents Sea.
3) To explore the reservoir properties of the Vardebukta Formation and contemporary deposits in the Arctic.

1.2 Previous work

The Triassic stratigraphy on Svalbard has been the target of numerous Swedish, Russian, English, Norwegian and Polish research groups since the 19th century, with the first work concentrating on the abundant fossil content found throughout the archipelago (Vigran et al., 2014). Presently, the research is connected to the Barents Sea as an oil and gas province.

The basal Vardebukta Formation directly overlies the Permian-Triassic boundary (P-T boundary) (Vigran et al., 2014). While the boundary has received attention from scientists researching palynoflora (Vigran et al., 2014), geochemistry (e.g. Wignall et al., 1998; Wignall et al., 2016) and investigating the transition across the boundary, the sedimentology of the Vardebukta Formation has received little scientific attention. Additionally, the Festningen area is considered one of the most popular locations for geological field trips on Svalbard (Mørk and Worsley, 2006). Yet, previous work by Mørk et al. (1982) remains the only published work with a detailed sedimentary log from the formation at Festningen. Wignall et al. (1998) and Wignall et al. (2016) also investigated the sedimentology, but as touched upon earlier this was not their main focus. Recently, Pózer Bue and Andresen (2014) investigated the provenance of the sediments through detrital zircon U-Pb age analysis.

1.3 Study area

The study area is located on Svalbard, which is an archipelago located on the northwestern corner of the Barents Shelf (Gudlaugsson et al., 1998). The Vardebukta Formation of Early Triassic age is investigated at its type location at Festningen (Fig. 1.1) on Nordenskiöld Land close to the inlet of Isfjorden. Investigations were also made at Rotundafjellet in Studentdalen (Fig. 1.1), which is located at the inlet of Billefjorden, and at Selmaneset which is situated at Oscar II Land (Fig. 1.1).
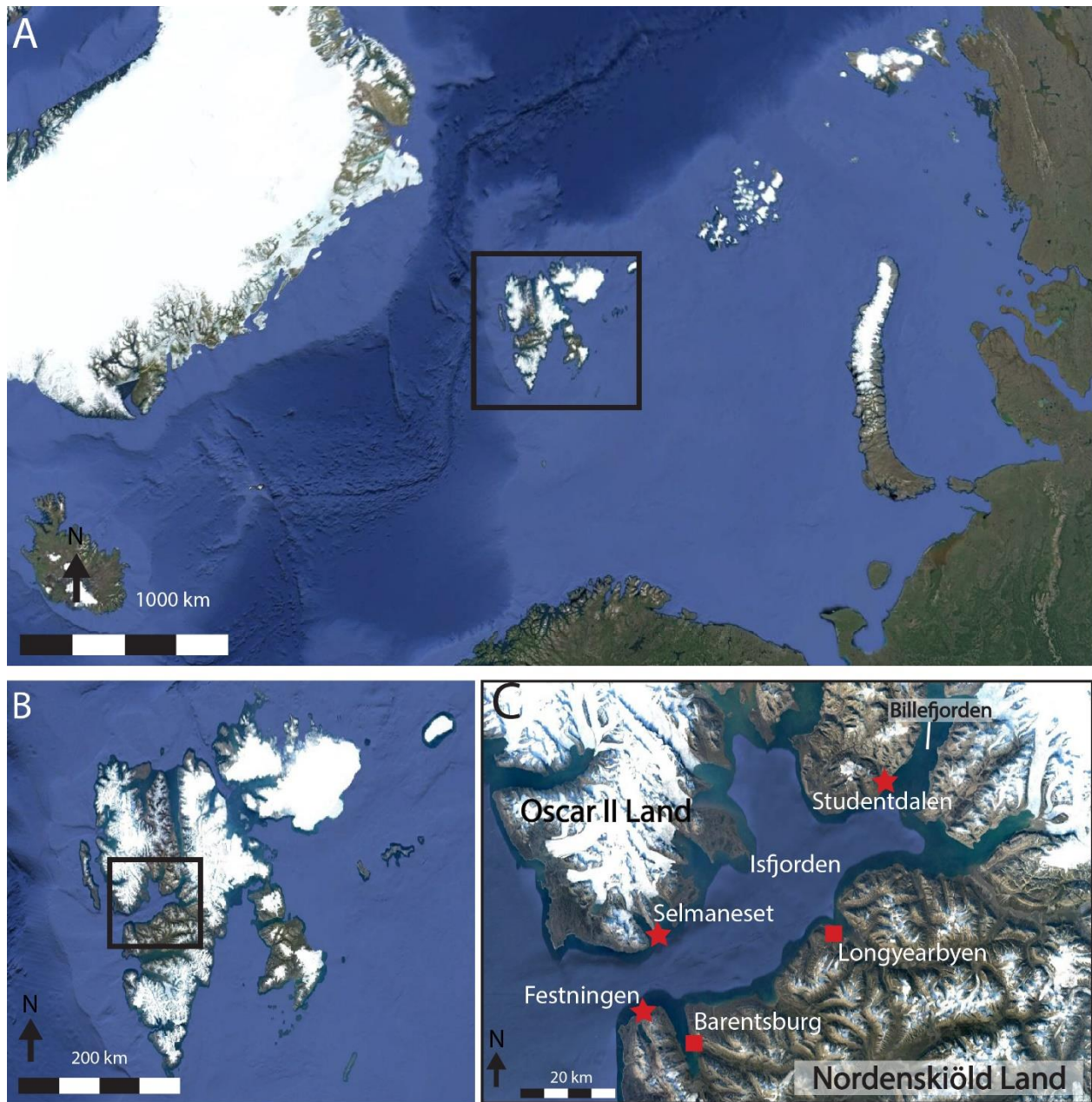
Figure 1.1: Overview of the study area on Svalbard. **A)** Highlights Svalbard while **B)** highlights Isfjorden and the surrounding areas. The three red stars in picture **C)** marks the locations were fieldwork was carried out. Satellite images © Google.

2 Geological background

2.1 Overview of Svalbard and the Barents Sea

The northwestern corner of the Eurasian continental shelf is covered by the Barents Sea. It is a wide epicontinental sea bounded by young passive margins to the west and north, the Novaya Zemlya fold and thrust-belt to the east and the Fennoscandian Shield to the south (Fig. 2.1) (Faleide et al., 1984). These passive margins, bounding the Barents Sea to the west and north, have a long history of rifting with the opening of the Atlantic Ocean in Late Cretaceous (Faleide et al., 2008). The western margin has been a passive one since Early Oligocene times, with the culmination of the opening of the Norwegian-Greenland Sea (Faleide et al., 2008). Roughly, the Barents Sea can be divided into two major geological provinces; the eastern and the western province (Smelror et al., 2009). Few major basins characterize the former while the latter has several smaller basins, widespread platform areas and generally a more complex geology (Henriksen et al., 2011b).

Svalbard is an archipelago located on the northwestern corner of the Barents Shelf (Gudlaugsson et al., 1998). It represents an uplifted and subaerially exposed part of the Barents Shelf (Worsley, 2008). Major fault zones striking N-S to NNW-SSE characterize the geology of Svalbard. These are long-lived and have frequently been active during geological time (Dallmann et al., 2015). The complex history of Svalbard with its different tectonic regimes is mirrored in the lithostratigraphy by the documentation of transport directions, provenance, facies assemblage and the thickness of sediments (Steel and Worsley, 1984). In addition, Svalbard has been drifting northwards from the Devonian to the Cenozoic (Fig. 2.2) leading to major climatic and environmental changes, which has had a pronounced influence on the lithostratigraphy (Steel and Worsley, 1984).
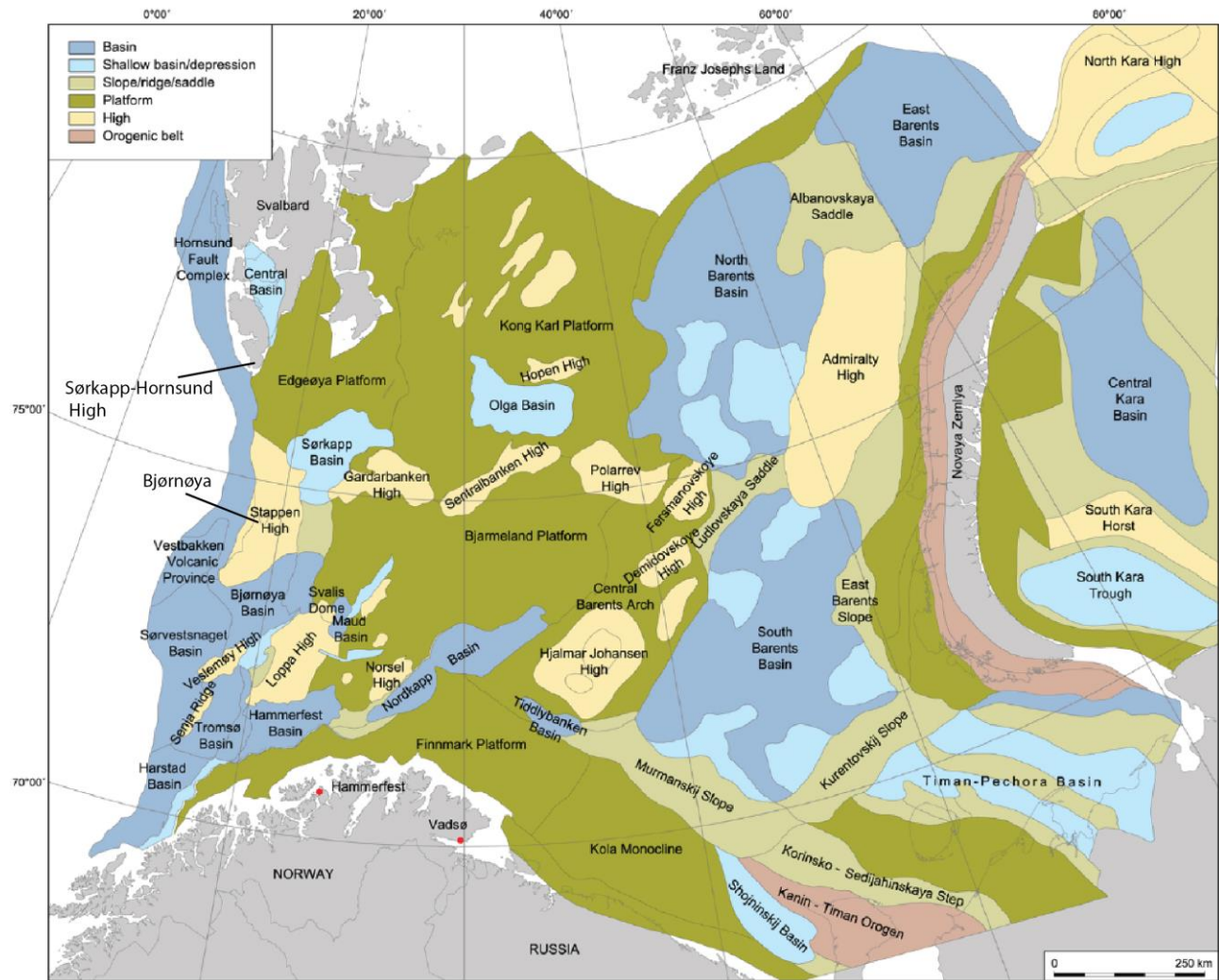
Figure 2.1: Map displaying the structural elements of the present-day Barents Sea. Modified from Henriksen et al. (2011b).
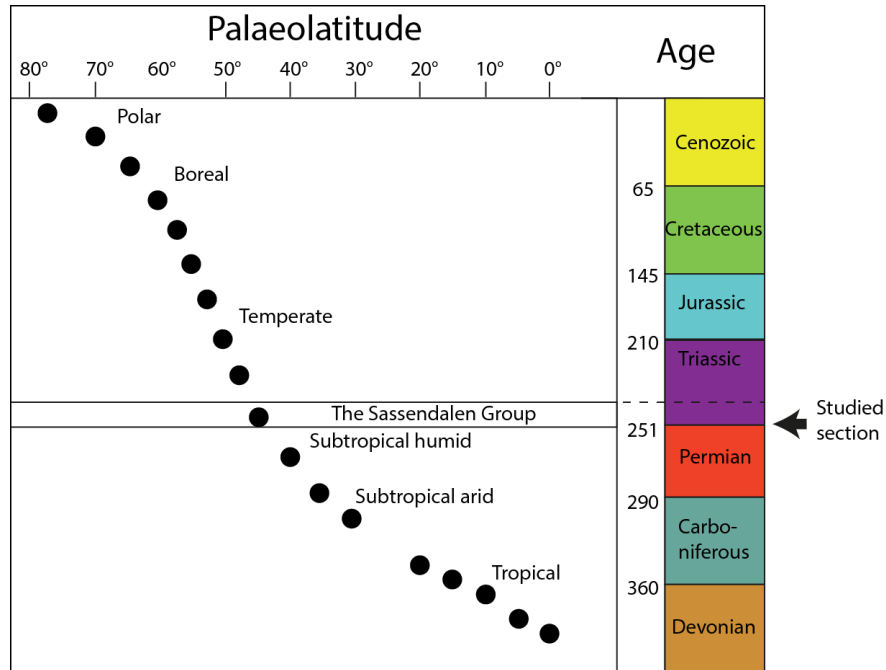
Figure 2.2: Plot displaying the palaeolatitude of Svalbard since the Devonian. Note an overall subtropical humid climate during deposition of the Sassendalen Group and the studied section (i.e. the Vardebukta Formation). Modified from Elvevold et al. (2007).

2.2 Tectonostratigraphic evolution of Svalbard and the Barents Sea.

2.2.1 The Paleozoic

The Pre-Cambrian and Lower Paleozoic basement rocks on Svalbard are referred to as "Hecla Hoek". It is a maximum 20km thick succession of metasediments, sediments and igneous rocks (Worsley, 2008). On the Barents Shelf, several of the structural trends observed today may have been established prior to the Carboniferous as shown by seismic reflection data (Gabrielsen et al., 1990). In all likelihood, remnant structural lineaments in the basement have controlled the structural development of the Late Paleozoic and Cenozoic in the Barents Sea (Gabrielsen et al., 1990). The Caledonian Orogeny caused the closure of the Iapetus Ocean in the western Barents Sea, which previously had separated Laurentia and Eurasia (Henriksen et al., 2011b). On northern Svalbard, the Late-Devonian Ellesmerian Orogeny (locally called the Svalbardian event) created a graben system where the Old Red molasse sediments were preserved in a down-faulted crustal block (Dallmann, 1999).

In the Early Carboniferous, Spitsbergen and the western margin of the Barents Shelf were located in a strike-slip transfer setting with N-S trending lineaments (Smelror et al., 2009). Active rifting and the development of subsiding rift valleys along these major, pre-existing fault zones created a distinct horst and graben structural pattern (Dallmann et al., 2015). Due to sea-floor spreading, Svalbard drifted northwards from about 20° N at the start of the Carboniferous to 35° N at the end (Fig. 2.2) (Blomeier, 2015a). As a consequence of Svalbard drifting out of the wet equatorial climate zone, the environment changed from a warm and humid climate with alluvial, fluvial and terrestrial deposits to a more semi-arid to arid climate. Rising sea-levels during the Late Carboniferous led to the flooding of Svalbard (Worsley, 2008). This resulted in a change in depositional environment, as evidenced by the evaporites and warm water carbonates of the Gipsdalen Group (Fig. 2.3) (Worsley, 2008; Blomeier, 2015b).

As the horst-graben tectonics associated with the Svalbardian orogeny terminated, the western Barents Sea experienced a shift towards moderate regional subsidence. By the end of the Paleozoic, a regional sag basin covered large portions of the Barents Sea (Smelror et al., 2009).

During the Permian, Svalbard drifted from approximately 30° N to around 45° N experiencing fundamental climatic, environmental and palaeoceanographic changes (Fig. 2.2) (Blomeier, 2015b). Permian deposits on Svalbard is divided into the cherty and siliciclastic influenced Tempelfjorden Group and the underlying carbonate-dominated Gipsdalen Group (Fig. 2.3) (Blomeier, 2015b). The transition from carbonate to siliciclastic-influenced environments was related to the developing Uralides and the opening of a seaway between Norway and Greenland. A major increase in subsidence rates occurred after the tectonic plate reconfiguration that followed the formation of the Uralides. As a result, cool water flowed across the Barents Shelf flooding the previous platform, basin and basin margin areas (Stemmerik et al., 1999; Worsley, 2008; Henriksen et al., 2011b).
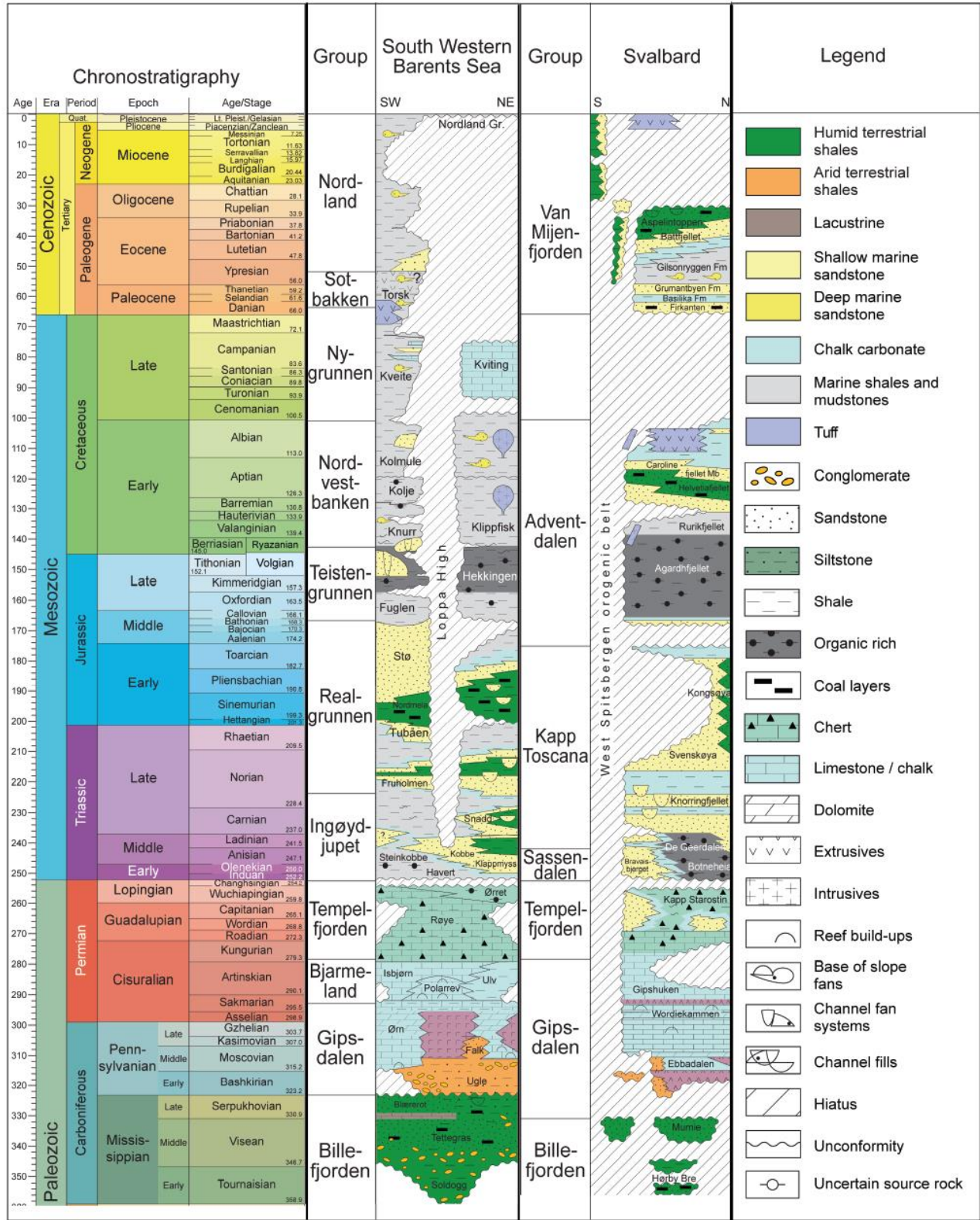
Figure 2.3: Lithostratigraphy of the southwestern Barents Sea and Svalbard. Modified from Naturhistorisk Museum (2013, http://www.nhm2.uio.no/norges/litho/Barents_Chart.html)

In the eastern Barents Sea the closing of the Uralian Seaway, due to the collision of Siberia and Euramerica in the Late Permian, led to the formation of the Uralian Mountains (Puchkov, 2009). This orogeny closed the connection to the Tethys Ocean. Plate tectonic reconstruction by Cocks and Torsvik (2007) shows that in the Late Permian, Svalbard and the Barents Sea were located on a shelf open to the north, and bounded by Pangea to the south, west and east.

2.2.2 The Mesozoic

Generally, the Triassic in the Barents Sea was characterized by regional subsidence and little tectonic activity. Svalbard and the western Barents Sea were relatively stable (Riis et al., 2008; Smelror et al., 2009; Mørk, 2015), only experiencing a passive regional subsidence with slight fault movement observed on the Finnmark and Bjarmeland platforms (Fig. 2.1) (Smelror et al., 2009; Henriksen et al., 2011b). Conditions were different in the eastern Barents Sea where the northern and southern basins (Fig 2.2) were strongly subsiding and forming important depocenters (Riis et al., 2008).

Clastic deposition prevailed during the Triassic on Svalbard as well as on the entire Barents Sea Shelf. This marked a significant change from the carbonate deposits of the Late Carboniferous to Early Permian and the spiculitic/cherty mudstone deposits of the Late Permian (Dallmann, 1999). In the Triassic, most of Svalbard was situated in a distal basinal position with the basin first being filled from the west, depositing the Sassendalen Group (Fig. 2.3) (Mørk et al., 1982). With the recently formed Uralides to the east, the sediment source shifted as a major shallow-marine to deltaic sedimentary system prograded towards the west and deposited the Kapp Toscana Group (Fig. 2.3) (Riis et al., 2008; Mørk, 2015).

Induan (i.e. the earliest Triassic, Fig. 2.3) sediments in the Barents Sea and Svalbard are sourced from the west, east and south. Sediments with an eastern source dominate and the Uralides is considered the main provenance area for Triassic sandstones in the Norwegian Barents Sea (Mørk, 1999; Riis et al., 2008; Smelror et al., 2009). Close to the Fennoscandian margin (i.e. northern Norway) there is evidence of a more limited sediment input originating from the Fennoscandian shield to the south (e.g. Mørk, 1999; Riis et al., 2008; Smelror et al., 2009; Eide et al., *in press*). Sedimentary systems were also prograding from northeast Greenland/Arctic Canada

into Svalbard during the Induan (Mørk et al., 1982; Wignall et al., 1998). These systems appear to have been of limited extent, only reaching a few tens of kilometers into Svalbard, and no evidence of these reaching the Barents Sea itself has been presented (Klausen et al., 2015; Eide et al., *in press*). In the Barents Sea, subsidence and sedimentation rates were decreasing in the Early Jurassic as the influence of the Uralides was reduced and the region shifted towards the development of coastal and shallow marine systems (Worsley, 2008). The Late Jurassic is known for its extensive clay-rich deposits in the Barents Sea region with maximum transgression occurring in the Tithonian (latest Jurassic, Fig. 2.3) (Worsley, 2008; Smelror et al., 2009). By the Early Cretaceous, the Barents Sea had established the main structural elements that are recognized today (Gabrielsen et al., 1990).

Dolerite intrusions and basaltic lavas from the latest Jurassic to Early Cretaceous are the first trace from the opening of the North Atlantic and Arctic oceans on Svalbard, due to the separation of Greenland and Europe (Dallmann, 1999). The Upper Cretaceous strata on Svalbard is lacking as a consequence of uplift and erosion related to this separation (Worsley, 2008; Grundvåg, 2015).

2.2.3 The Cenozoic

The evolution of the Barents Sea and its western margin in the Cenozoic is closely related to the opening of the Norwegian-Greenland Ocean (Henriksen et al., 2011b). This opening created a Paleocene and Eocene tectonic overprint, which led to convergent structures. The opening also involved dextral transpression between the Greenland and Svalbard plate and manifested in a wide contractional fold-thrust belt on western Spitsbergen (Fig. 2.4). To the east of the fold-thrust belt, the Central Tertiary Basin (CTB) developed as a small foreland basin (Braathen et al., 1999). Sandstones, siltstones, shales and smaller amounts of coals and conglomerates represent the sedimentary succession in the clastic CTB (Dallmann, 2015).
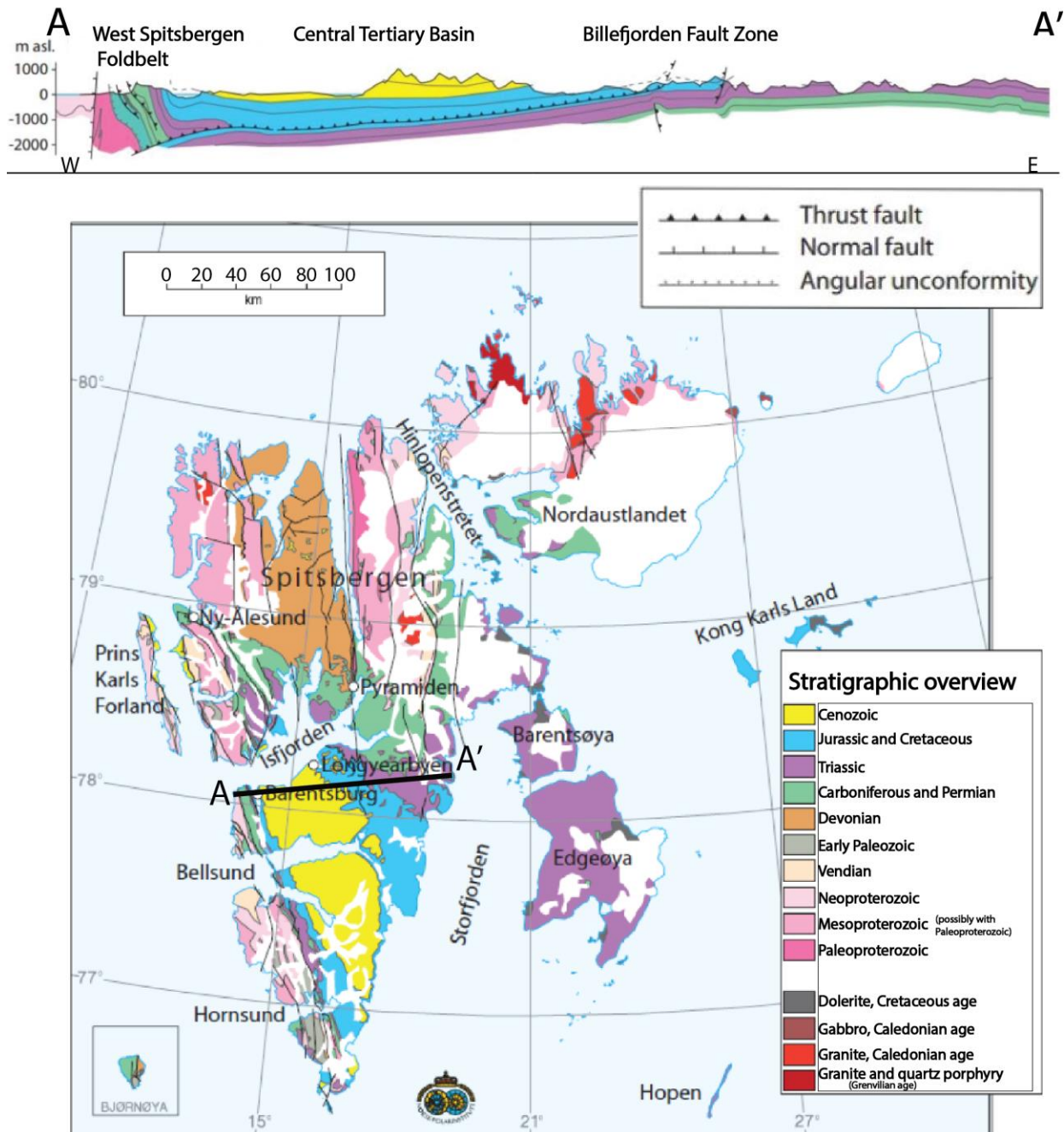
Figure 2.4: Geological map of Svalbard with cross-section A to A' showing the fold-thrust belt strata at the inlet of Isfjorden. Note how it changes eastwards of the fold belt. Modified from Elvevold et al. (2007).

Following the opening of the Norwegian-Greenland Ocean, the Barents Sea has been subjected to intense uplift, resulting in Svalbard being subaerially exposed (Dimakis et al., 1998). Although the controls on the uplift have been heavily debated, it is likely connected to the opening of the Norwegian-Greenland Ocean (Dimakis et al., 1998).

A significant feature of the Barents Sea stratigraphy is the large unconformity separating Quaternary deposits from underlying deposits (Smelror et al., 2009; Henriksen et al., 2011b). It is the result of Paleogene–Recent uplift and erosion in the Barents Sea (Riis and Fjeldskaar, 1992; Riis, 1996; Henriksen et al., 2011b). The greatest erosion and uplift occurred in the areas surrounding Svalbard and the northern platform areas (Fig. 2.3), whereas in the southwestern Barents Sea it was significantly lower (Smelror et al., 2009). Erosion products, mainly from frequent glaciations and associated isostatic uplift, are distributed in major submarine depocenters along the subsiding western margin of the Barents Sea (Smelror et al., 2009).

2.3 Early to Middle Triassic sedimentary systems on Svalbard and in the Barents Sea – The Sassendalen Group
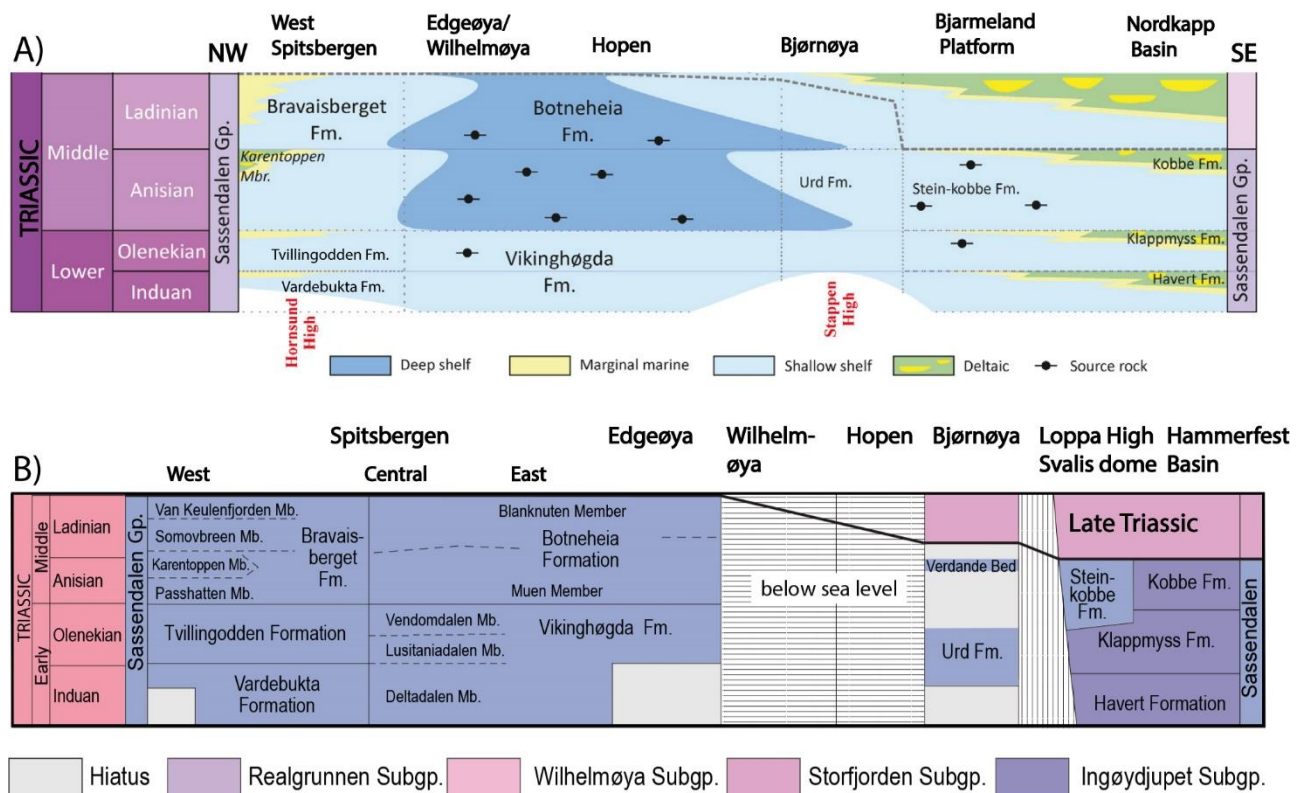
Figure 2.5: Overview of Early and Middle Triassic lithostratigraphy on Svalbard and the southern Barents Sea. **A)** Simplistic overview of the different depositional environments in the Sassendalen Group. Note that until approximately the mid-Induan, the Sørkapp-Hornsund High, located on southern Spitsbergen, acted as a basement high. However, where the Vardebukta Formation was investigated in this study it conformably overlies the underlying deposits. Modified after Fleming et al. (2016). **B)** Shows the lithostratigraphy in more detail. Modified from Vigran et al. (2014). Locations for the different areas are shown in Fig. 2.1.

At the Permian-Triassic boundary a major transgression marks the onset of the Triassic, manifesting in a switch from the Permian spiculitic shales of the Kapp Starostin Formation to the Early—Middle Triassic Sassendalen Group dominated by fine-grained clastics (Fig. 2.3 and Fig. 2.5) (Mørk et al., 1989; Mørk et al., 1999). At the start of deposition, Svalbard was situated in a shallow shelf sea, mainly receiving sediments from Greenland/Arctic Canada in the west, or from continental blocks in between Svalbard and Greenland (Mørk, 2015). The Sassendalen Group primarily consists of three coarsening-upward sequences that originate from the shallowing-upwards environments that came to exist as the basin was filled with sediment after marked transgressions (Mørk et al., 1982; Mørk, 2015). It is known to reach thicknesses of up to 700 meters on Svalbard (Dallmann, 1999) with the thickest stratal packages located by the entrance to Isfjorden, in the area known as Festningen (Fig. 1.1) (Wignall et al., 1998). In other areas of Svalbard, such as on the Sørkapp-Hornsund High, thicknesses can be less than 200 meters (Wignall et al., 1998).

Lower Triassic on southern and western Svalbard is represented by the basal Vardebukta Formation and the overlying Tvillingodden Formation (Mørk, 2015). A continuous coast profile at Festningen show the type sections for the formations and how the beds dip vertically due to Paleogene deformation (Fig. 2.4) (Mørk et al., 1982). The Vardebukta Formation is estimated to be approximately 250 – 300 meters at its type section (Harland, 1997; Dallmann, 1999). Other places, such as on the Sørkapp-Hornsund High, it can be just a few tens of meters (Dallmann, 1999). At its type locality it is primarily made up of sandstones, shales and siltstones with main facies being calcareous silty shales and shaley siltstones in the lower half, informally known as the Selmaneset Member. Higher up, in the member informally known as the Siksaken Member, calcareous siltstones and more sand rich facies showing ripple cross-lamination, cross-stratification and an abundance of ammonites and bivalves are common. Towards the boundary to the Tvillingodden Formation the facies gets increasingly more fine-grained. The Tvillingodden Formation is characterized by generally shallowing- and coarsening-upwards from a deep shelf towards a more shallow shelf. Main facies are laminated dark shale with little or no bioturbation at the base, and progressively getting into more bioturbated and ripple cross-laminated sandstone upwards (Mørk et al., 1982). Previous work by Mørk et al. (1982) has interpreted the

Vardebukta Formation and the Tvillingodden Formation as eastward prograding sand-rich barrier bars with affiliated fine-grained lagoonal systems and deeper shelf areas with extensive mud deposition.

In the Early Anisian, a large transgression led to the deposition of phosphatic black shales on Spitsbergen (Mørk, 2015). These are found in both the Botneheia Formation in the central and eastern areas of Spitsbergen, and in the lower parts of the more proximal Bravaisberget Formation along western Spitsbergen (Fig. 2.6). Together, these constitute the Middle Triassic on Spitsbergen (Mørk, 2015) with the high organic content of the Botneheia Formation making it a prolific source rock (e.g. Krajewski, 2008).

In the Barents Sea, the Sassendalen Group is defined by the Ingøydjupet Subgroup (Fig. 2.3), known from the Hammerfest Basin (Fig. 2.1, Dallmann, 1999), and the Steinkobbe Formation (Fig. 2.6) on the Svalis Dome (Fig. 2.1) (Mørk and Elvebakk, 1999). The latter is known to exhibit high organic contents forming a fruitful source rock in the Barents Sea (Vigran et al., 1998; Mørk and Elvebakk, 1999), comparable to the Botneheia Formation on Svalbard. The Ingøydjupet Subgroup, including the southerly derived sediments briefly mentioned in subchapter 2.2.2, is thought to be partially sourced from both the south (i.e., the Fennoscandian Shield) and the east (i.e., the Uralides), thus having a different provenance area than their corresponding units on Svalbard (Pózer Bue and Andresen, 2014; Fleming et al., 2016). Work by Glørstad-Clark et al. (2010), Henriksen et al. (2011b) and Lundschien et al. (2014) show Induan clinoforms near the coast along the Finnmark Platform (Fig. 2.1) prograding into the Barents Sea, thus indicating a source in Scandinavia and nearby land areas to the south-east.

The Havert Formation represents the start of the Lower Triassic in the southern Barents Sea (Fig. 2.3 and Fig. 2.5), and resembles the synchronous Vardebukta Fm. on western Spitsbergen in regards to palynoflora and sequence evolution (Worsley et al., 1988). It was first described by Worsley et al. (1988) as shallow marine to open marine deposits with a coastline to the south and southeast of the Hammerfest Basin (Fig. 2.1). Recent work has interpreted it to represent a deltaic system, which in the Early Induan was being fed with sediments from the Fennoscandian Shield

(Eide et al., *in press*). Gradually, the sediment source shifted to the Uralian system which was prograding from the east in Middle and Late Induan (Eide et al., *in press*).

3 Methodology

Fieldwork and laboratory work have been carried out to obtain the results of this thesis.

3.1 Fieldwork and sampling

The first season of fieldwork was conducted on Svalbard in the late summer of 2016. Outcrops at Festningen were investigated from 31st August to 4th September and reached by Zodiac from the camp in Barentsburg (Fig. 1.1). Fieldwork in Studentdalen was carried out from 6th – 9th September, outcrops were reached by hiking approximately 30 minutes from camp (Fig. 1.1).

In August of 2017 a second field season was carried out at Selmaneset at Oscar II Land (Fig. 1.1) together with master students from NTNU and geoscientists from the Norwegian Petroleum Directorate. Here, the outcrops were reached by Zodiac from camp onboard the vessel *Youexplore*. Rock samples were collected at all locations from fresh and unweathered surfaces with the use of a geological hammer.

3.1.1 Sedimentological outcrop study

Lithostratigraphic logging was performed in the field by measuring vertical sections. Grain size, sedimentary structures, layer boundaries, layer thickness, mineralogy, texture and geometry were carefully examined. The studied features were recorded using millimeter paper, meter stick, hand lens, geological hammer, and grain size card. Furthermore, a camera was used to document observations, a compass to measure paleocurrents obtained from sedimentary structures and a GPS was used to acquire precise coordinates for the location of the sedimentary logs. The results were plotted on millimeter paper in different scales such as 1:25 and 1:50, making the basis for further work. Bioturbation was also registered following Fig. 3.1.

Grade	Classification	Visual Representation
0	Bioturbation absent	
1	Sparse bioturbation, bedding distinct, few discrete traces	
2	Uncommon bioturbation, bedding distinct, low trace density	
3	Moderate bioturbation, bedding boundaries sharp, traces discrete, overlap rare	
4	Common bioturbation, bedding boundaries indistinct, high trace density with overlap common	
5	Abundant bioturbation, bedding completely disturbed (just visible)	
6	Complete bioturbation, total biogenic homogenization of sediment	
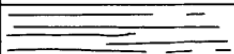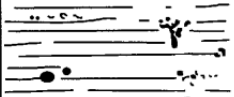
Figure 3.1: The bioturbation index (BI) used in this study with six different grades of bioturbation. Figure from Bann et al. (2004) based on the concepts of Reineck (1963) and Taylor and Goldring (1993).

3.2 Laboratory work

The rock samples from the field were delivered to the Preparation Lab for thin sections at the Department of Earth Science at the University of Bergen where they were prepared. From the two best sandstone samples, thin sections were stained with blue epoxy to highlight the porosity, while eight thin sections were point counted to determine the composition.

3.2.1 Thin section descriptions

The studied thin sections were described in terms of grain contacts, roundness, grain size and sorting, as well as being photographed using the equipment shown in Fig. 3.2.
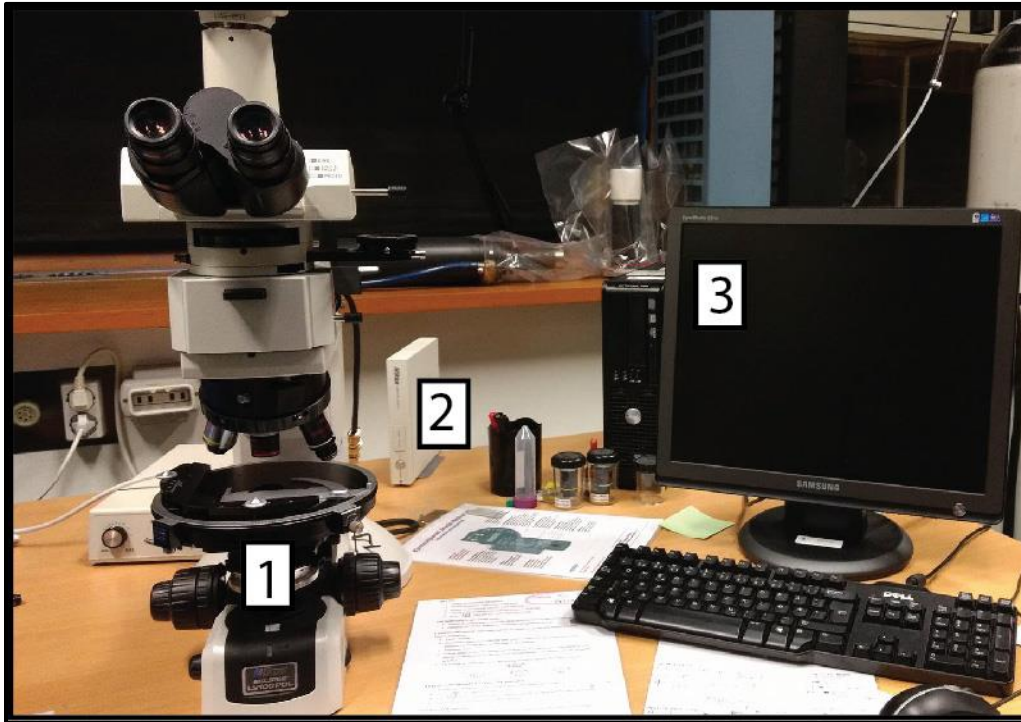
Figure 3.2: Equipment used for describing and taking pictures of the studied thin sections. **1)** Nikon Eclipse LV100POL, polarizing microscope with a camera attached **2)** Camera control unit **3)** Computer with NIS Elements software.

Grain size

To decide the grain size in the microscope, the average of the longest and the shortest axis for 100 random detrital grains were measured. Furthermore, these averages were converted to millimeters, summarized and divided by the sample size (i.e. 100).

When logging in the field, grain size was decided visually. The Wentworth scale after Wentworth (1922) was used to classify the grain size (Table 3.1), both in the field and for describing the studied thin sections.

Table 3.1: Grain size classes as defined by Wentworth (1922).

Millimeters (mm)		Micrometers (μm)	Phi (φ)	Wentworth size class	
	4096		-12.0	Boulder	
	256		-8.0	Cobble	Gravel
	64		-6.0	Pebble	
	4		-2.0	Granule	
	2.00		-1.0	Very coarse sand	
	1.00		0.0	Coarse sand	
1/2	0.50	500	1.0	Medium sand	Sand
1/4	0.25	250	2.0	Fine sand	
1/8	0.125	125	3.0	Very fine sand	
1/16	0.0625	63	4.0	Coarse silt	
1/32	0.031	31	5.0	Medium silt	
1/64	0.0156	15.6	6.0	Fine silt	Silt
1/128	0.0078	7.8	7.0	Very fine silt	
1/256	0.0039	3.9	8.0	Clay	Mud
	0.00006	0.06	14.0		

Sorting

The sorting of a sediment indicates the grain sizes present as well as the spread among grain sizes (Boggs, 2014). In this study, sorting was determined by using the terminology and examples from Longiaru (1987) (Fig. 3.3) and further implementing these in the descriptions of the studied thin sections.
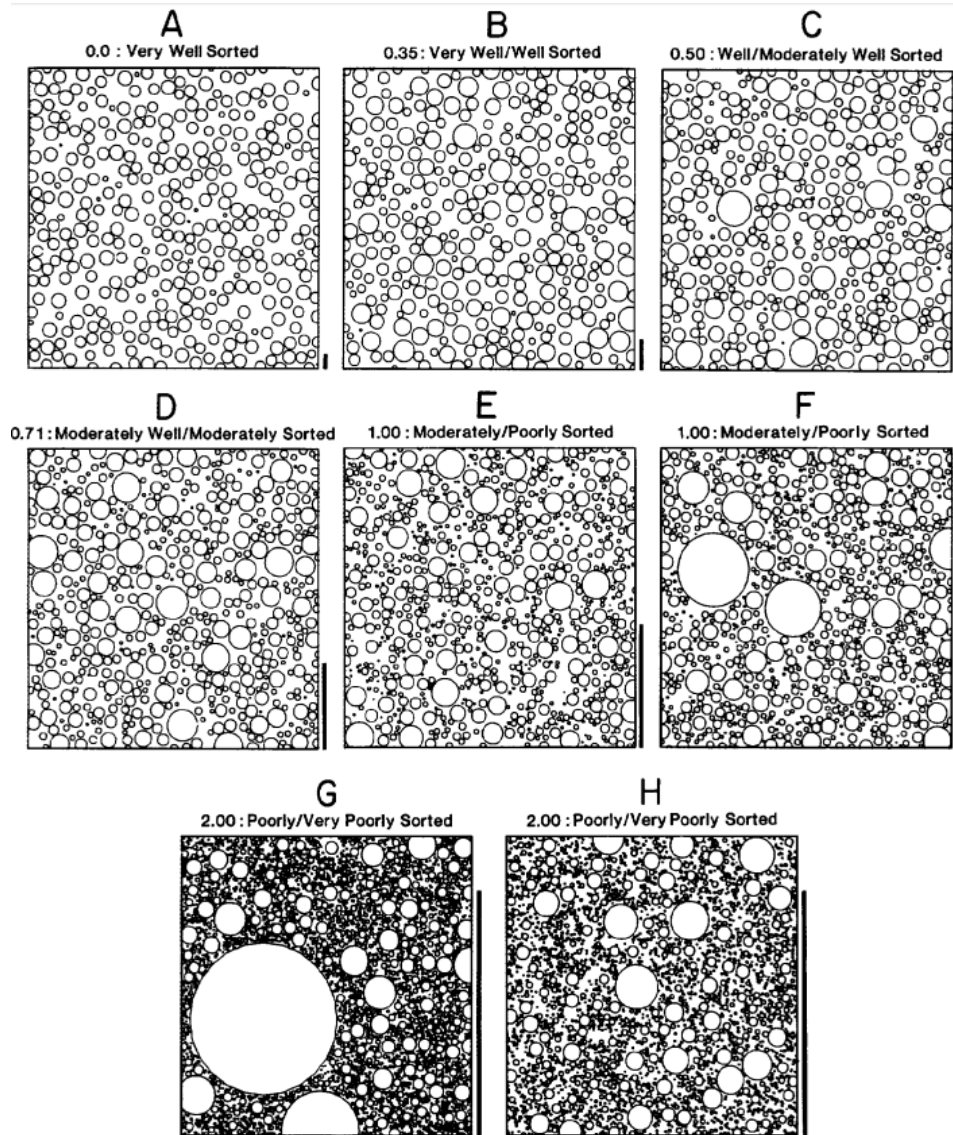
Figure 3.3: Grain sorting terminology and examples from Longiaru (1987). The numbers specify the standard deviation. Based on the descriptive terminology from Folk (1966).

Roundness

The roundness and sphericity of the grains were decided by using the definitions and examples from Powers (1953) visible in Fig. 3.4, and further applying these to the examined thin sections.
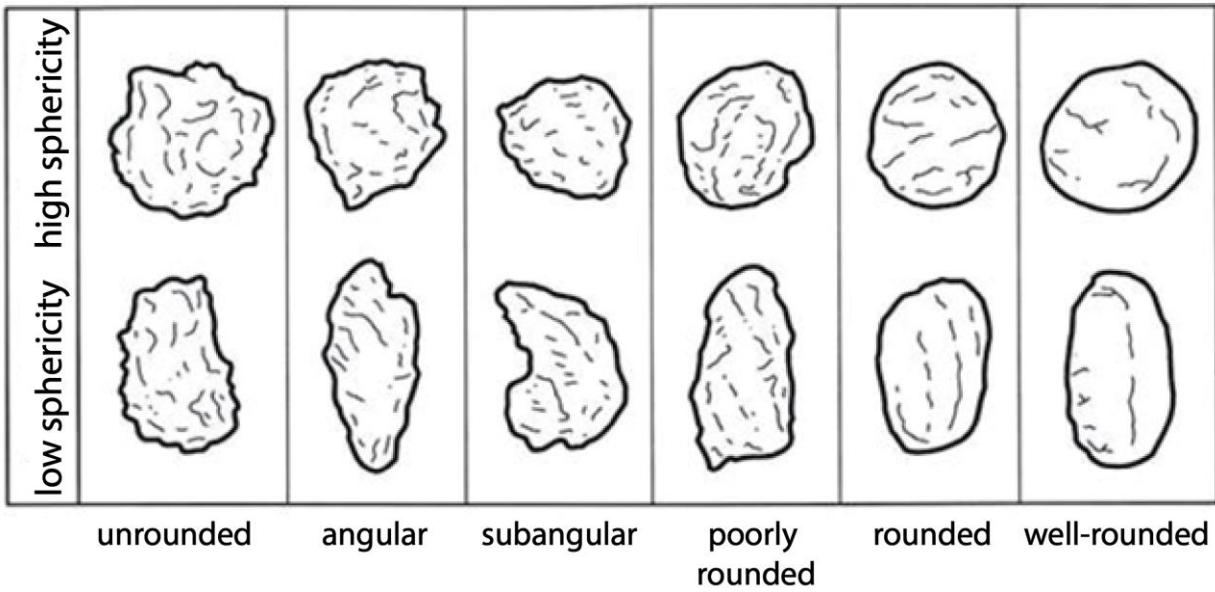
Figure 3.4: Grain roundness and sphericity terminology used for describing the thin sections in chapter 5. The figure is from Lundberg (2015) and is modified from Powers (1953).

Grain contacts

Grain contacts were described as in Taylor (1950) with the recognition and identification of point contacts, concavo-convex contacts and sutured contacts (Fig. 3.5). Additionally, the term floating grains was introduced and used for describing grains floating encased in cement with no apparent grain to grain contact (Fig. 3.5).
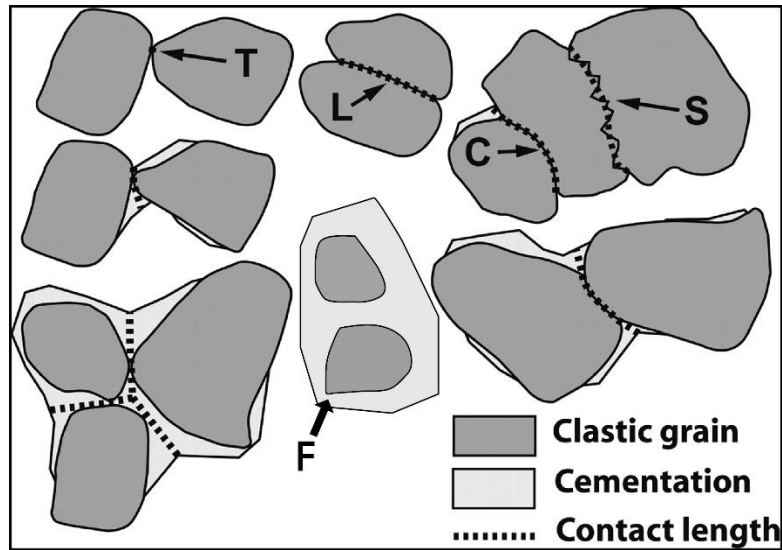
Figure 3.5: Illustration showing the concepts of Taylor (1950) with T and L being point contacts, C = Concavo-convex contacts and S being sutured contacts. F represents floating grains that are encased in cement with no apparent grain to grain contact and has been added for the purpose of this study. The figure is modified from Storvoll and Bjørlykke (2004).

3.2.2 Point counting

Thin sections were point counted to help determine sandstone composition. In each thin section, 300 points were counted to calculate the composition. It was carried out by moving the stepping stage 300 times by using the PETROG Lite software and recording the grain composition in the same software. The equipment that was used is shown in Fig. 3.6.
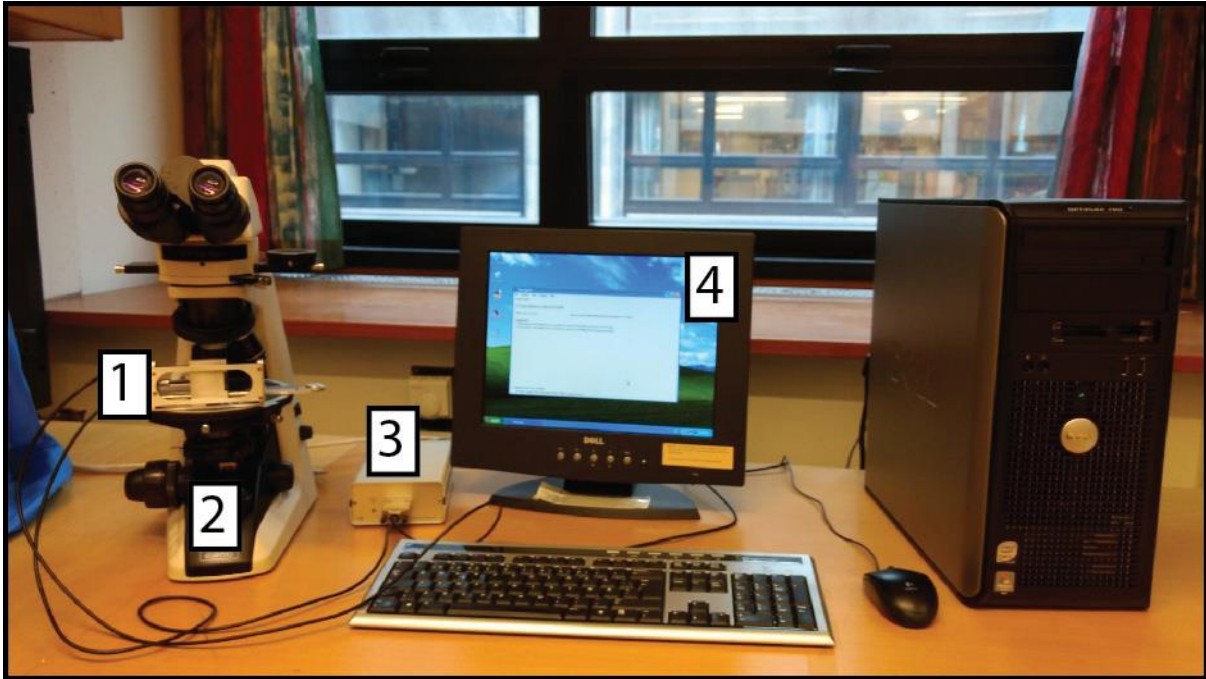
Figure 3.6: Equipment used for point counting chosen thin sections. **1)** "Wire-connected" MicroStepper Stage, Mk1.5 **2)** Nikon ECLIPSE E200, polarizing microscope **3)** MicroStepper Stage control box **4)** Computer with PETROG Lite Software.

Sources of error connected to point counting

There are errors concerned with point counting and Solomon (1963) described three principal sources of error;

1. *The operator error,* operators with different knowledge and background will provide contrasting results. Solomon (1963), as well as Van der Plas and Tobi (1965), considered this negligible compared to other sources of error.

2. *The counting error,* errors that are controlled by the size of the area counted, grain size and the stepping length. Of these, the stepping length was considered the most significant source of error for the variance and Solomon (1963) advised that it should be half the grain radius or more.

3. *The sampling error,* errors concerned with the problem of estimating the composition of a volume by just looking at a small fraction (e.g. a thin section). The volume should have a random distribution of grains with a regular shape and a low variance in grain composition to ensure the error being kept to a minimum (Solomon, 1963).

3.2.3 Cathodoluminescence

The cathodoluminescence of chosen thin sections was investigated by a petrographic microscope with an attached optical cathodoluminescence (Optical CL) stage. By using this technique, it is possible to separate between different generations of calcite cement as well as providing information about the provenance of siliciclastic grains (Richter et al., 2003). As the thin section is bombarded with electrons, electromagnetic radiation is released. CL is the image of this radiation expressed as colors in the visible electromagnetic spectrum (Grant, 1985).

3.3 Software

3.3.1 Adobe Illustrator 2014

Adobe Illustrator is a vector-based graphics software that was used to make and edit figures as well as digitize the sedimentary logs.

4 Sedimentological results

4.1 Overview

As previously noted, the Vardebukta Formation was investigated by Mørk et al. (1982) at Festningen, and was described as "a major barrier bar progradation with the development of barrier sands with tidal inlets and lagoonal back-barrier systems" (Mørk et al., 1982, p. 375). It is interpreted to represent the first of three major coarsening upwards cycles (Fig. 2.5A), which together constitute the Sassendalen Group on western Spitsbergen (Mørk et al., 1982). The basal 140 meters of the formation (Fig. 4.1) is dominated by fine-grained deposits (e.g. shales and siltstones) with an upwards increase in siltstones (i.e. gradual regression) showing ripple cross-lamination, gutter casts and currents moving eastwards (Mørk et al., 1982). Further regression is evidenced by the deposition of a 90 meters sandstone-rich section (Fig. 4.1) displaying cross-stratification, shell debris and several erosional surfaces (Mørk et al., 1982). Above these 90 meters the formation becomes more fine-grained again (Fig. 4.1), showing siltstones and shales interbedded similar to those below the sandstone-rich interval (Mørk et al., 1982). These finer grained sections were interpreted by Mørk et al. (1982) to be storm-generated and the result of a gradual transgression following the deposition of the sandstone-rich portion.

The focus of this study has mostly been on the sand-rich parts of the Vardebukta Formation, which relates back to the aims of this study, as proclaimed in subchapter 1.1. As a consequence, as well as time constraints, only the most relevant parts of the Vardebukta Formation at Festningen were logged (Fig. 4.1).

Through lithostratigraphic logging of outcrops at Festningen, Studentdalen and Selmaneset (Fig. 1.1 and Fig. 4.2) the present study has defined 16 sedimentary facies and 6 facies associations (FA) (Table 4.1 and subchapter 4.3, respectively). It should be noted that the outcrops, especially at Selmaneset and Festningen, are extremely cemented, which in many cases gives them an apparent structureless appearance.
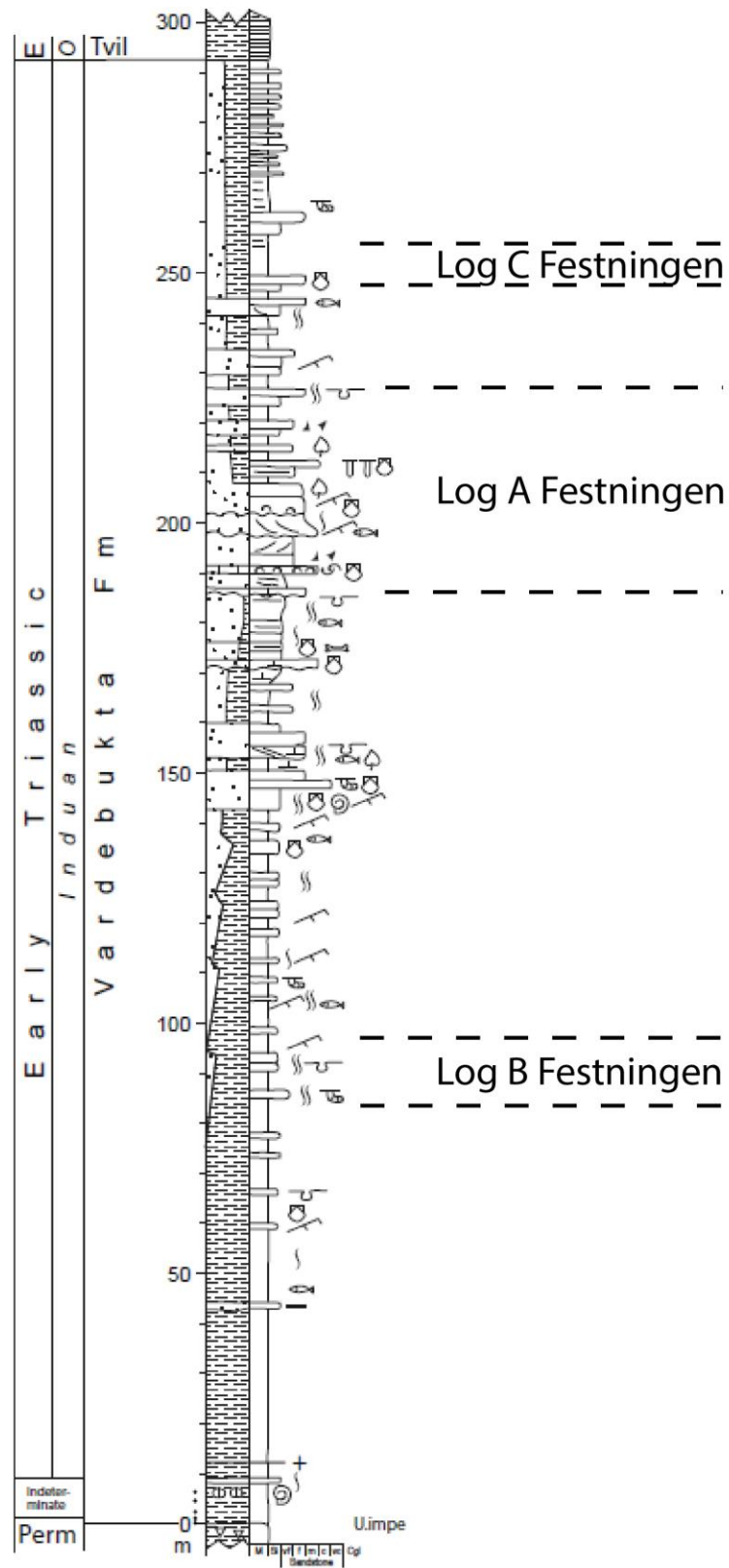
Figure 4.1: Log from the Vardebukta Formation at Festningen by Mørk et al. (1982). The stapled lines show the logged intervals at Festningen from this study. Logs A, B and C are shown in Appendix A.
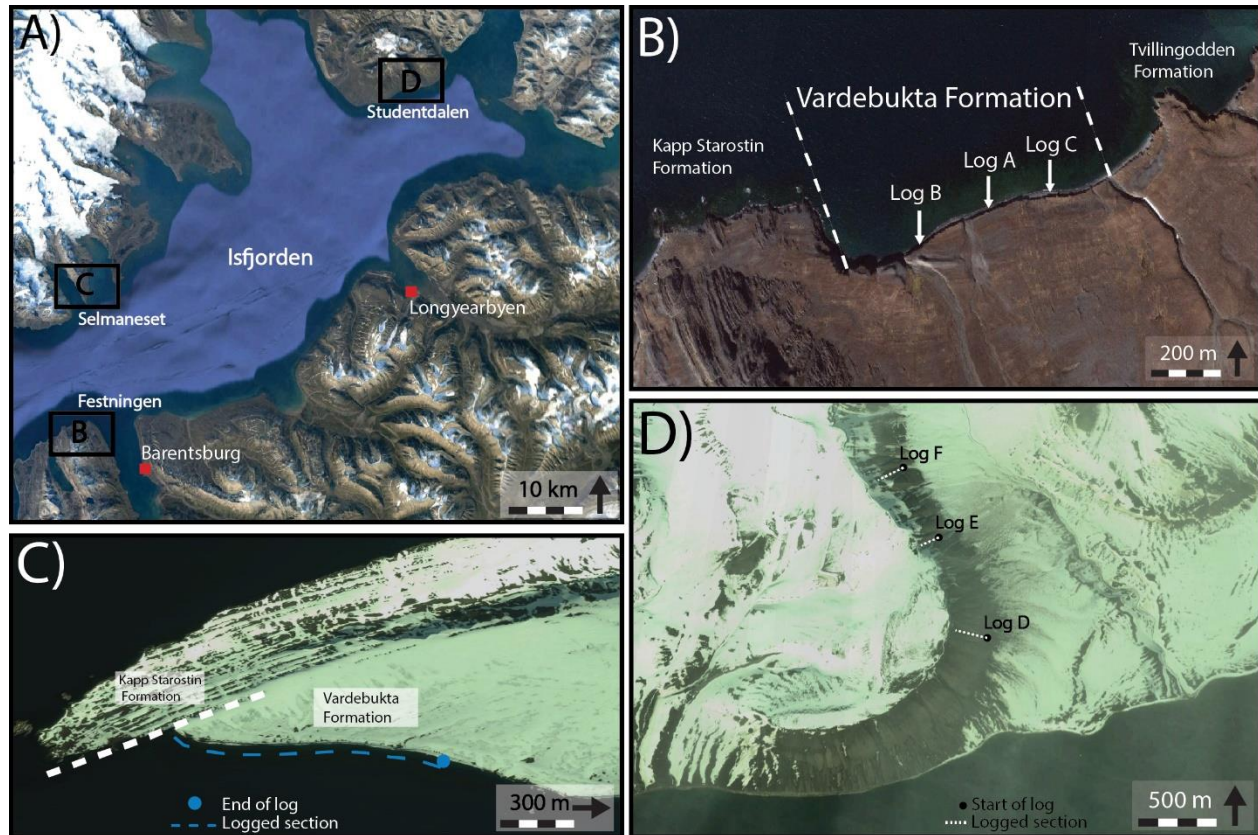
Figure 4.2: The geographical location of the different logs. **A)** Is an overview showing the location of the field areas B, C and D (Festningen, Selmaneset and Studentdalen, respectively). **B)** shows Vardebukta at Festningen and where logging was performed. **C)** Shows the study area at Selmaneset and the logged section. Finally, **D)** Shows the logged intervals at Rotundafjellet in Studentdalen. Satellite images © Google. Coordinates for the start of the logged sections are given in Appendix A.

Festningen

The outcrop at Festningen (Fig. 4.2A-B), represents the best exposure of the Vardebukta Formation. It displays a wide array of sedimentary structures and geometries in addition to being a largely conformable succession.

Hence, the logged section at Festningen (See Log A, B and C in Appendix A) constitutes the most valuable data for this study. Figure 4.2B shows the location of the logs.

Selmaneset

Selmaneset is located on Oscar II Land (Fig. 1.1, Fig 4.2A and C), and is a highly tectonized region due to the intense deformation by the Cenozoic fold-and-thrust belt mentioned in subchapter 2.2.3. This deformation has been documented in detail by e.g. Bergh et al. (1997), while the sedimentology remains poorly understood.

The tectonized nature of the region is reflected in the outcrop at Selmaneset where the stratigraphy is interrupted by folds and faults resulting in abundant repeated sections (Fig. 4.3). Therefore, establishing a continuous stratigraphic log showing the original stratigraphy has proved problematic. This will be addressed in more detail by students from NTNU as a part of their master theses. Thus, this study will not present a continuous log as from the outcrops at Festningen and Studentdalen (Fig. 1.1). Instead, smaller sections will be presented and compared with the more detailed logs from the other outcrops.

Figure 4.3: Example of the intense deformation in the deposits at Selmaneset on Oscar II Land. Sections like this were frequently encountered along the outcrop making the logging more challenging. Geologist for scale.

Studentdalen

The outcrops in Studentdalen (Fig. 4.2D) were scree-covered to a much greater degree than the outcrops at Festningen and Selmaneset. This is likely due to the abundance of fine-grained deposits (i.e. mudstone and shales) (See Log D, E F in the Appendix). In some instances, the deposits in Studentdalen had a peculiar dark color, likely due to contact metamorphism from adjacent Cretaceous dolerites (cf. Senger et al., 2013; Senger et al., 2014). Thin sandstone layers observed amidst these finer-grained deposits are dominated by sedimentary structures characterized by planar parallel stratification, current and wave ripples (Facies A, B and G; Fig. 4.4A, B and G, respectively). Three logs were obtained from this location and their location is shown in Fig. 4.2D. For the position of the logs, see Log D, E and F in Appendix A.

4.2 Sedimentary facies

Table 4.1: Description and interpretation of sedimentary facies in the Vardebukta Formation.

Facies	Bedding and lithology	Sedimentary structures, fossils and remarks	Bioturbation index (BI) and trace fossils	Process interpretation
A) **Planar parallel stratified sandstone** Fig. 4.4A	Very fine sand to fine sand, medium sand may occur. Layers range in thickness from 5-100 cm. However, most are 5-30 cm.	Planar parallel stratification. Often found below wave ripple cross-laminated- and planar-cross stratified sandstones. Ammonites. Glauconites observed in thin section (Fig. 5.7).	None observed / no data.	Most likely formed by tractional unidirectional currents in the lower parts of the upper flow regime when co-occurring with cross-stratified deposits (Collinson et al., 2006). Contrarily, together with Facies G (Fig. 4.4G) or Facies O (Fig. 4.4O), strong waves are inferred (Komar and Miller, 1975).
B) **Current ripple cross-laminated silt- and sandstone** Fig. 4.4B	Very fine sand to silt. Layers range in thickness from 2.5-25 cm. Mean thickness of 7 cm.	Asymmetric current ripples.	Generally, no BI data. Short intervals with BI 0, 1 and 2. *Planolites.*	Generally, forms by a relatively weak unidirectional current in the lower reaches of the lower flow regime (Allen, 1982; Collinson et al., 2006; Boggs, 2014).
C) **Deformed sandy siltstone** Fig. 4.4C1-C2	Very fine sand to silt. Layers vary in thickness from 15-55 cm with a mean thickness of 33 cm. Lateral thickness variations from 10s of cm to meter scale.	Convex shape (elongated U). Coarser units seem to "sink" into underlying fine-grained material, squeezing the latter up between the former ones. Erosive bases are observed. Glauconites observed in thin section.	None observed / No data.	Deposition by mechanical forces (e.g. gravity) acting upon weak sediment soon after burial or at the sediment surface (Collinson et al., 2006), causes the soft-sediment deformation features. Rapid deposition in proximity to nearby sediment source. Loading is normally restricted to just a few layers, while slumping involves many layers that deform together (Collinson et al., 2006).
D) **Structureless silt- and sandstones** Fig. 4.4D	Very fine sand to silt.	Massive, structureless with a few Fe concretions. A few glauconites observed in thin section.	Generally, BI = 0. Rare BI of 4 and 5. *Arenicolites*, *Teichichnus*, *Planolites*.	Reflects depositional conditions or post-depositional destruction of structures. The former can be attributed to rapid deposition, the latter to heavy bioturbation by organisms or liquefaction (Collinson et al., 2006).
E) **3D-current ripple cross-laminated sandy siltstone** Fig. 4.4E	Very fine sand to silt. Occurs in two layers that both are 35 cm.	3D current-ripple cross-lamination occasionally draped by mud. Ripple- and grain size generally decrease upwards.	None observed / No data.	Deposited in the lower flow regime by migrating 3D ripples, indicating a relatively weak unidirectional current (Allen, 1982).

F) **Crude plane parallel laminated silt- and sandstone** Fig. 4.4F	Very fine sand to silt. Layers vary in thickness from 5-85 cm, Mean thickness: 27.5 cm.	Plane parallel lamination. Shell imprints.	Moderate to high BI of 3-4 in most layers. BI up to 6 observed. *Planolites*.	Original planar lamination modified by bioturbation after deposition. Bioturbation may destroy original laminae completely (Boggs, 2014), but in this case this process is not completed. Periods of bioturbation may be attributed to short periods of sparse sediment input.
G) **Wave ripple-cross-laminated sand- and siltstone** Fig. 4.4G	Silt to fine sand. The layer thickness range from 1-35 cm Mean thickness is approximately 5 cm.	Wave ripples. Often found above muddy deposits. May display erosive bases. At times, it is found overlying Facies A.	Generally, no BI data. Spikes up to BI=5 observed. *Planolites*, *Rosselia*, *Arenicolites*.	Formed by oscillatory currents with low orbital velocity (Komar and Miller, 1975). May indicate a position above fair weather wave base or formation below during powerful storms (Howell and Flint, 2003). Erosive bases can be attributed to particularly strong waves or storms.
H) **Wavy bedded sandstone** Fig. 4.4H	Interlaminations of 1-2 cm mud laminae and 1-5 cm sand laminae. Approximate 50-50 relationship between the two. Layers vary in thickness from 15-130 cm, mean thickness at around 55 cm.	Ripple cross-laminated sand. Paleocurrents in ripples generally towards the east. Interbedding of ripples and paper shales observed. Shell imprints.	BI= 2-5. Unknown vertical and horizontal burrows. *Arenicolites*, *Cylindrichnus*, *Planolites*, *Paleophycus*.	Wavy bedding is used when there are approximately equal amounts of mud vs. sand and where ripple forms are visible (Collinson et al., 2006). It represents a net increase in current speed compared to Facies I, and a net decrease in current speed compared to Facies J (Dalrymple, 2010).
I) **Lenticular bedded mudstone** Fig. 4.4I	Interlaminations of mud and sand with a dominance of the former. Layers vary in thickness from 30-35 cm.	Ripple cross-laminated sand encased in mud.	No trace fossils observed and BI is 0 or unknown.	Compared to flaser bedding and wavy bedding, lenticular bedding represents a net reduction in current speed and the increased deposition and preservation of mud drapes (Collinson et al., 2006).
J) **Flaser bedded sandstone** Fig. 4.4J	Interlaminations of mud and sand with a dominance of the latter. Usually, 1-5 cm sand laminae separated by mm scale mud drapes. Layers range in thickness from 20-95 cm.	Ripple cross-laminated sand with mud draping the ripple form with thin and often discontinuous mud laminae.	The BI is commonly 2-3. *Arenicolites*, undifferentiated vertical burrows.	Formed by alternating periods of currents depositing sand and slack-water periods allowing suspension settling of mud (Boggs, 2014). Notably forms on tidal flats and in subtidal environments where both oscillatory and unidirectional currents are present (Reineck and Singh, 1980). Still, formation also occurs in marine delta-front environments where the energy and sediment flux is varying (Boggs, 2014).
K) **Planar cross-stratified sandstone** Fig. 4.4K	Very fine to fine sand with one short interval of coarse sand. Layers range in thickness from 10-95 cm. Most layers are 15-20 cm.	Planar cross-stratification with tabular sets. Both angular and tangential foresets, occasionally mud draped. Faint shell imprints. 0.3-1 cm muddy rip up clasts found at the toe of angular sets.	None observed / No data.	Deposited by a unidirectional current in the upper part of the lower flow regime. Angular foresets form during bedload transport as migrating 2D dunes (Allen, 1982), while tangential foresets form at a higher velocity with an additional high suspension load (Jopling, 1963). Sparse mud drapes imply times of still stand (Reineck and Singh, 1980).

L) **Laminated mudstone** Fig. 4.4L1-L2	Mudstone interbedded with silt. Light to dark grey color. Very fine sandstone streaks may also be observed. Thicknesses vary from sections with a few to tens of cm thick, to sections dominated by laminated mudstone (10s of meters).	Planar parallel laminations.	Generally, none observed / no data. However, a few intervals of 4 exist.	Deposition from suspension fall-out during quiescent times in a low-energy environment, possibly between storms. May originate from hyperpycnal suspension plumes (i.e. density underflow; turbidity currents with low density) and buoyant suspension plumes (e.g. Nemec, 1995). Laminae indicate variations in energy and therefore variations in the sediment input (Pickering et al., 1986), which may be ascribed to periodic river flooding (Bhattacharya and MacEachern, 2009). The general lack of bioturbation is possibly related to the Induan shallow water anoxia on Spitsbergen (cf. Wignall et al., 2016).
M) **Mottled sandstone** Fig. 4.4M	Yellow-brown mud sections interrupted by grey irregular very fine sand sections. Present in two layers that are approximately 15 cm and 50 cm.	No apparent structures, possible desiccation cracks observed in thin section (Fig. 4.10A-B).	None observed / No data.	Desiccation cracks are found in several environments, e.g. supratidal and intertidal flats. Commonly form at the surface and is strongly linked with subaerial exposure. Usually originate from drying of mud-rich sediments, causing contraction and fracturing (Collinson et al., 2006).
N) **Shell-rich limestone.** Fig. 4.4N	Packstone following the classification of Dunham (1962). Only found in one layer that is approximately 20 cm.	Tightly packed shell imprints with mud drapes. Siliciclastic grains evident from viewing in thin section.	None observed / No data.	Bioclastic sandstones are described by Mørk et al. (1982) from the Tvillingodden Formation (Fig. 2.5) and thought to form from stillstand around wave base. A similar explanation is imagined here with abundant mud drapes implying times of stillstand (Reineck and Singh, 1980).
O) **Hummocky and swaley cross -stratification** Fig. 4.4O	Fine to medium sand, unclear boundaries to deposits above and below. Found confidently at one location in a nearly 40 cm thick layer.	Hummocky and swaley cross-stratification.	Sparse to none bioturbation, *Cylindrichnus.*	Deposition by combined-flow during powerful storms (Arnott and Southard, 1990; Duke et al., 1991; Cheel and Leckie, 1993) and form due to a combination of storm waves and storm-generated bottom currents (Walker, 1984; Dumas and Arnott, 2006).
P) **Ripple cross-laminated silt- and sandstone** Fig. 4.4P	Very fine sand to silt with occasional fine-grained sand.	Unspecified/unclear ripple form.	Generally, BI is 2-4. *Planolites.*	Indicates a combination of weak unidirectional currents and weak oscillatory currents (Collinson et al., 2006; Baas et al., 2016).

A — Planar parallel stratified sandstone — 5 cm

B — Current ripple cross-laminated silt- and sandstone — 10 cm

C₁ — Deformed silty sandstone — 40 cm

C₂ — Deformed silty sandstone — dl — 75 cm

D — Structureless silt- and sandstones — 10 cm

E — 3D-current ripple cross-laminated sandy siltstone — la — la — th — 15 cm

F — Crude planar parallel laminated silt- and sandstone — 4 cm

G — Wave ripple cross-laminated silt- and sandstone — 8 cm

Wavy bedded sandstone

Lenticular bedded mudstone

Flaser bedded sandstone

Planar cross-stratified sandstone

Laminated mudstone

Laminated mudstone

Mottled sandstone

Shell-rich limestone

Hummocky and swaley cross-stratified deposits

Ripple cross-laminated silt- and sandstone

Figure 4.4: Photographs of lithofacies. **A)** Planar parallel stratified sandstone. Note the white lines highlighting the stratification. **B)** Current-ripple cross-laminated sandstone in plan view. White arrow indicates ripple migration direction. **C)** Deformed sandy siltstone. Distorted layering (dl) visible in C2). **D)** Structureless sandstone. **E)** 3D current-ripple cross-laminated sandy siltstone with well-exposed laminae (dl) and easily recognizable troughs (th). **F)** Crude plane parallel laminated siltstone and sandstone. **G)** Wave ripple cross-laminated sandstone. **H)** Sandstone with wavy bedding. Note the interlaminations of sand (s) and abundant mud drapes (md) as well as the wavy shape/geometry (wa). **I)** Mudstone with lenticular bedding displaying well-defined mud drapes (md). **J)** Sandstone with flaser bedding. Note the isolated mud drapes (md) encased in sand and the well preserved vertical burrow (vb). **K)** Planar cross-stratified sandstones. Note the stapled lines which highlight the tangential foresets (ts). **L)** Laminated mudstone. Note the laminae (la). **M)** Mottled sandstone with sand (s) and rustier (ru) colored intervals. **N)** Shell-rich limestone. Note the abundant shell fragments/imprints (Sf) encased in mud drapes (md). **O)** Hummocky and swaley cross-stratified deposits. Black stapled line separates the hummock from the overlying swale. **P)** Ripple cross-laminated silt- and sandstone.

4.3 Facies associations

LEGEND

- Sandstone
- Mudstone
- Angular cross-stratification
- Flaser bedding
- Wavy bedded sandstone
- Wavy bedded mudstone
- Lenticular bedding
- Plane parallel laminations
- Planar parallel stratification
- Tangential cross-stratification
- Low-angle cross-stratification
- Crude laminations
- Mud drapes
- Shell fragments, shell hash
- Soft-sediment deformation
- Very cemented
- Organic fragments
- Wave ripples
- Indistinct ripples
- Fe Iron concretion
- Current ripples
- Planolites
- Arenicolites
- Ammonite
- Unidirectional current orientation
- Oscillatory current orientation

Figure 4.5: Legend for the log portions shown in Fig. 4.7, Fig. 4.9, Fig. 4.10, Fig. 4.11, Fig. 4.12 and Fig. 4.13. Complete legend as well as full logs are available in Appendix A.

4.3.1 Facies association A – Tidally influenced channel

Observations:

Facies association A is dominated by planar cross-stratified sandstones (Facies K; Fig. 4.4K) showing a dominant paleocurrent direction towards the NE. Additionally, it fines upward from coarse to fine sand and occasionally displays mud draped foresets. However, one set of cross-strata with an SW paleocurrent direction and mud draped foresets is also observed. Additionally, mud-pebbles/rip-up clasts, shell hash and shell material are recognized in the basal 1.5-2 meters of the succession while for the remaining 5 meters such features are mostly absent.

Amidst these cross-stratified sandstones there are several layers with planar parallel stratification (Facies A; Fig. 4.4A) and an almost rhythmic pattern with alternations between these facies can be distinguished. BI is generally zero except for a few *Planolites*. A sharp undulating boundary to the deposits below marks the start of this FA. Sample FES19 (Fig. 5.5) is taken at the base of FA A in Fig. 4.5A while samples FES20 (Fig. 5.6), FES6 (Fig. 5.4) and FES3 (Fig. 5.3) are from successively higher up in the FA.
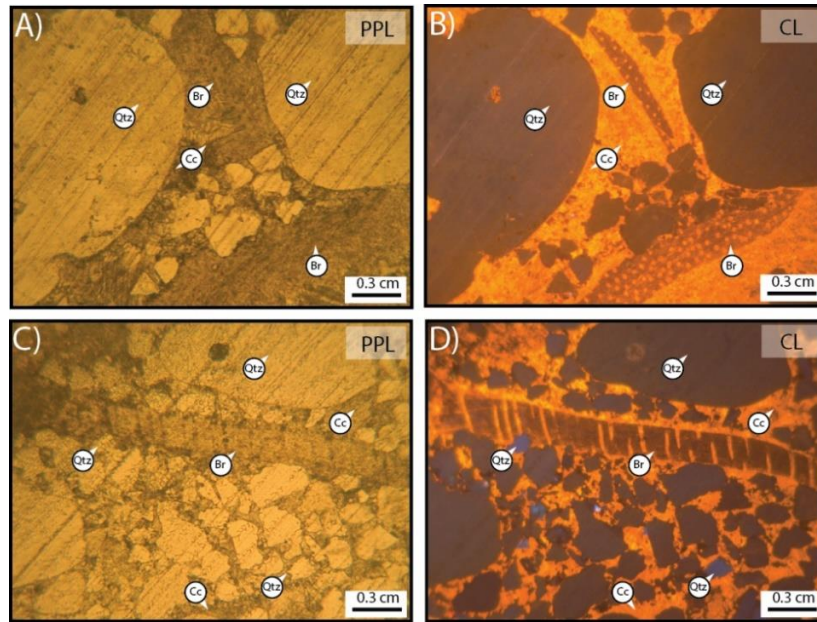
Figure 4.6: Thin section pictures of sample SES7 from Selmaneset in both plane polarized light (PPL) and cathodoluminescence (CL). The sampled layer is visible in Fig. 4.7C and has been interpreted to belong to FA A (Tidally influenced channel. Please note the *Brachiopod punctae* (Br) shell fragments visible in pictures **A-D)** as well as the quartz grains (Qtz) mainly displaying a non-luminescent color. However, clear examples of luminescent (blue colored) quartz grains are observed, particularly in picture D. Additionally, note that the calcite cement (Cc) have the same luminescent appearance both in the pore space between the siliciclastic grains as well as within the shell fragments.

Interpretation:

The sedimentary structures observed testifies to a strong unidirectional flow with sand primarily being transported as 2D dunes, and secondarily by upper stage plane bed transport (cf. Allen, 1982). Mud draped foresets accounts for periods of stillstand (Reineck and Singh, 1980) and together with bidirectional cross-strata sets implies a tidal component to the current. Furthermore, a fining upwards motif (Fig. 4.7A-B) coupled with an erosive base exhibiting abundant debris (i.e. mud clasts and shell fragments), and a decreasing amount of such debris upwards, is recognized. Together with the gentle u-shaped erosional surface (Fig. 4.7A), this leads to the interpretation of it being a channelized deposit.

However, mud drapes are only observed on the foresets in a few cross-strata sets and only one cross-strata set demonstrating a reversed paleocurrent direction is found. Furthermore, the identified sedimentary structures represent high-energy conditions (i.e. Facies A and K). The absence of bioturbation, except for a few *Planolites* which are tolerant of stressed conditions, supports the idea of conditions with persistent high sedimentation rates unfavorable for trace fossils (Maceachern et al., 2005). Moreover, many of the shell fragments have been identified as

brachiopods (Fig. 4.6), suggesting a marine influence. The samples from this FA at Festningen shows a trend of upwards decreasing content of calcite cement and a weak trend of increasing quartz cement upwards (see change from sample FES19; Table 5.2 to sample FES3; Table 5.2), perhaps related to reduced availability of biogenic carbonate as the flow persisted.

Finally, this leads to an interpretation of a tidally influenced channel with minor tidal modulation where waves reduce the suspension settling of mud during times of stillstand. The subordinate current (i.e. flood tide) is rarely able to deposit sand in the form of 2D dunes or even 2D ripples.
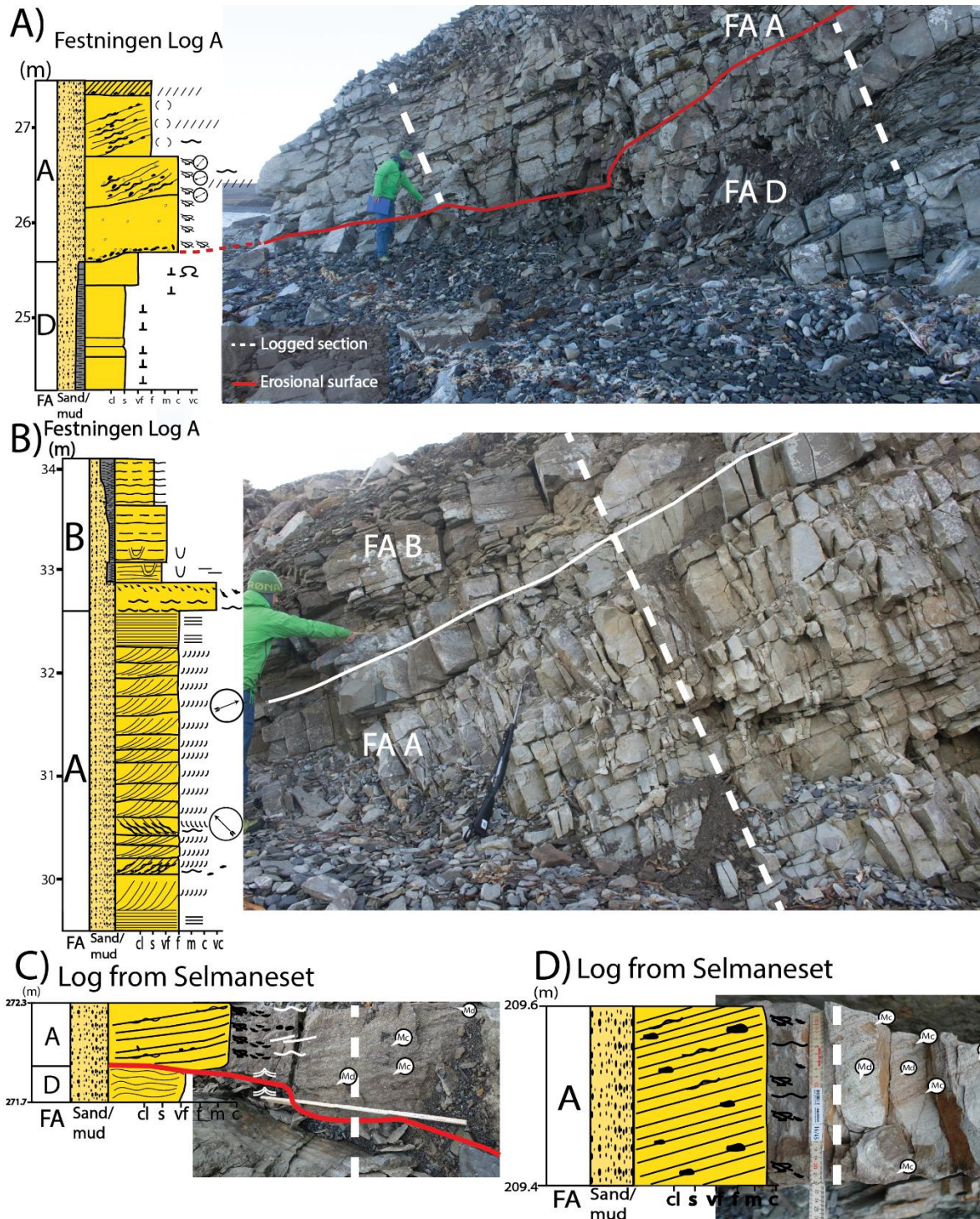
Figure 4.7: Overview photos of facies association (FA) A illustrating the main features. **A)** Interpreted as a channel cutting into underlying FA D (Delta front deposits) and overlain by FA B (Tidal sandflat, red line marks proposed erosive boundary and separates FA A and D, **B)** Continuation of FA A and eventually overlain by FA B, **C-D)** Showing that this FA possibly exists on Selmaneset exhibiting abundant mud clasts (Mc) and sparse mud drapes (Md). For legend please see Fig. 4.5 or Appendix A.

4.3.2 Facies association B – Tidal sandflat

Observations:

Facies association B contains flaser bedded sandstone (Facies J; Fig. 4.4J), wavy and lenticular bedded mudstone (Facies H and I; Fig. 4.4H and Fig. 4.4I) as well as crudely laminated siltstone (Facies F; Fig. 4.4F) with some streaks of very fine sandstone. Furthermore, a coarser layer with abundant mud drapes, shell hash and shell material are recognized. Bioturbation is generally low to moderate (BI=3) and is primarily observed in the more sand-rich deposits. Only u-shaped burrows are found. Another key observation is that this FA is almost exclusively found in association with FA A (tidally influenced channel) and FA C (supratidal deposits). Thin section FES2 is sampled within the more sand-rich parts of this FA and when viewed in cathodoluminescence (Fig. 4.8), reveals possible *Brachiopod punctae* shell fragments.
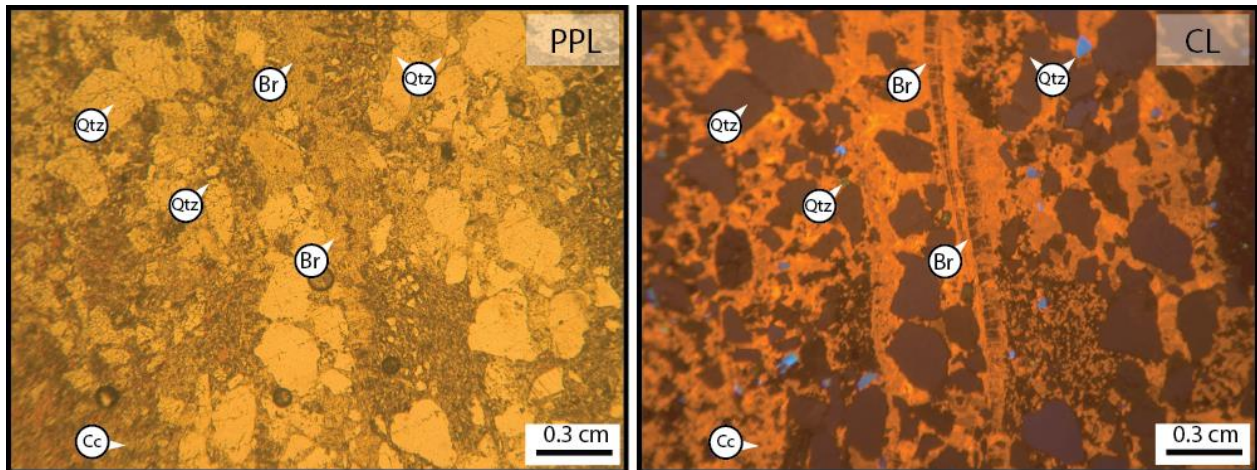

Figure 4.8: Thin section photos of sample FES2 from Festningen in both plane polarized light (PPL) and cathodoluminescence (CL). The sample is taken from the base of FA B in Fig. 4.9 Please note the possible *Brachiopod punctae* (Br) shell fragments as well as the quartz (Qtz) with one dominant color in cathodoluminescence. The calcite cement (Cc) shows a similar luminescent color throughout.

Interpretation:

Flaser, wavy and lenticular bedding found adjacent to each other may signify a tidal depositional control and may represent parts of a tidal flat similar to the classical illustration by Dalrymple (1992). Crude laminations can form due to moderate bioturbation at times when the sediment input is limited. The presence of brachiopod shell fragments (Fig. 4.8) infers some marine influence. Additionally, the nearby FAs (FA A and C, tidally influenced channels and supratidal deposits, respectively) are both interpreted to exhibit a tidal component, which strengthens the notion of this being a tidal flat.

The u-shaped burrows have been interpreted as *Arenicolites* and these are typical for high-energy deposits (e.g. deposition by storms or migrating dunes) (Knaust, 2017). However, *Arenicolites* in a low diversity with other trace fossils may indicate a stressed environment with alternating salinity (Knaust, 2017), such as a tidal flat environment.
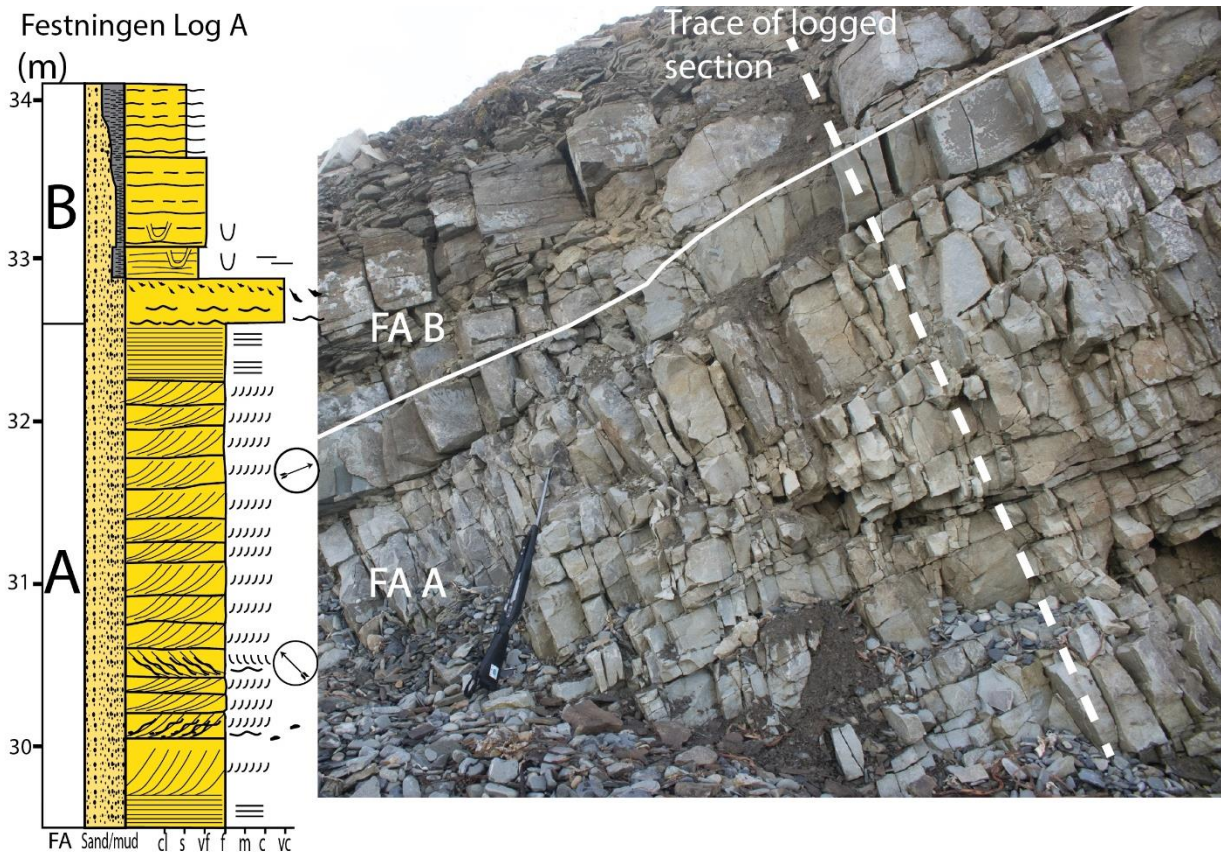
Figure 4.9: Picture of FA B with an associated log showing the main features. Note the flaser- and wavy bedded sandstone found together, the abundant Arenicolites burrows as well as the nature of the underlying FA. Rifle for scale. For legend, see Fig. 4.5 or Appendix A.

4.3.3 Facies association C – Supratidal deposits

Observations:

Facies association C consists of the mottled sandstone facies (Facies M; Fig. 4.4M), and is only confidently observed at Festningen (Fig. 1.1). Similar facies are possibly present at Selmaneset (Fig. 1.1), but no compelling evidence has been found due to the challenging outcrop conditions. Thin section FES1 from this FA display abundant fractures which have a curved appearance and generally appears to be subparallel to one another (Fig. 4.10A-B). That coupled with the nature of the under- and overlying deposits (FA A and B, tidally influenced channel and tidal sandflat, respectively) are key observations in this FA. Furthermore, sections of well sorted very fine-grained sand, as well as mud-sized and coarser grained calcite cements (possibly ?micrite and sparite), are observed in thin section FES1 (Fig. 4.10A-B).

Interpretation:

In FA C, the most important facies is the mottled sandstone, which has been interpreted to be possible desiccation cracks (cf. Goldstein et al., 1991), reflecting deposition close to or at the surface and may thus give valuable information about subaerial exposure.

The very fine sand intervals present in Facies M (Fig. 4.10A) are interpreted to represent overbank flood deposits from nearby channels, possibly related to times of flooding (Boggs, 2014). Additionally, the presence of carbonate mud (possibly micrite, Fig. 4.10A and Fig. 5.9) implies suspension settling of sediments, perhaps connected to periods after spring tides. Between times of sediment supply the deposits are subjected to subaerial conditions so that desiccation can occur (Davis Jr, 2012). Finally, this leads to an interpretation of a supratidal flat incised by channels.

Previous studies by Mørk et al. (1982) and Mørk et al. (1989) found evidence of desiccation cracks on Selmaneset and possibly in the shallowest part of the formation at Festningen (Fig. 1.1). These evidences and the findings of the present study, suggests that subaerial conditions were briefly attained along western Spitsbergen in the Induan (Fig. 2.5).
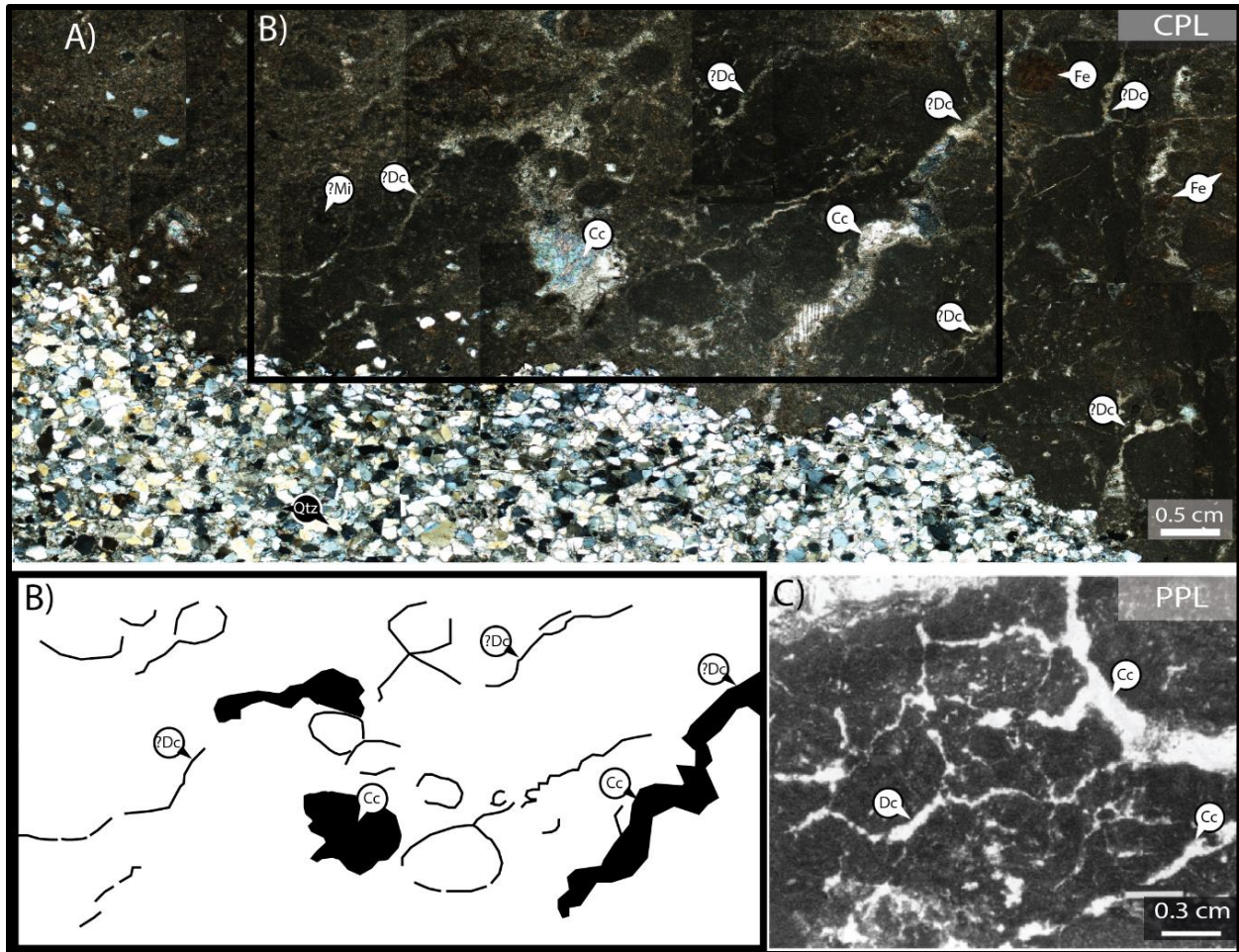
Figure 4.10: Thin section photo of sample FES1. **A)** Combination of several thin section photos. Represents desiccation cracks on a supratidal flat with the influx of sand from a nearby channel and is an argument for subaerial exposure in FA C. Note the possible desiccation cracks (?Dc) which in many cases have a curved appearance and generally appears to be subparallel to one another. These cracks are in most cases filled in with calcite cement (Cc). Also note the iron oxides (Fe), quartz (Qtz) and (?Mi) = possible microcrystalline calcite. **B)** Attempt to highlight some of these fractures. **C)** Example of desiccation cracks (Dc) viewed in plane polarized light from Goldstein et al. (1991) with calcite (Cc) infilled cracks.

4.3.4 Facies association D – Delta front deposits

Observations:

Facies association D contains a mixture of several facies and a large variance in sedimentary processes is observed. However, the dominating facies are rippled intervals (Facies B, G, and P; Fig. 4.4B, G and P). Another characteristic feature is the abundant soft-sediment deformation (Facies C; Fig. 4.4C1-C2), which is clearly visible in Fig. 4.11. It shows evidence of loading, possible erosive bases and slightly contorted internal layering (Fig. 4.11B-C). Mud clasts are also observed and are only found in association with soft-sediment deformed and current ripple cross-laminated deposits. Additionally, shell remains are frequently observed throughout and a shell-rich limestone with abundant mud drapes is identified in one layer (Facies N; Fig. 4.4N). Sections enriched in mud compared with their over- and underlying deposits are also recognized, i.e. wavy bedded and flaser bedded sandstone (Facies H and J). One instance of planar cross-stratified sandstone (Facies K) and 3D-current ripple cross-laminated siltstone (Facies E; Fig. 4.4E) is found. Furthermore, at least two faintly coarsening upwards packages can be distinguished in Log A (See Appendix A), from roughly 0-5 meters and 7 to 10.5 meters, respectively. Minor coarsening upwards cycles are also noticed (Fig. 4.11). Where present, the BI is generally between 2-4. However, intervals with a BI of 1 and 6 as well as sections with no recorded data or a BI of 0, are also recorded. Paleocurrent measurements indicate a transport direction towards S-SE and N-NE (See Appendix A for paleocurrent measurements).

Interpretation:

Soft-sediment deformation (Facies C), especially when found with erosive bases and potential slump features (contorted layering), implies the presence of a slope. Additionally, the soft-sediment deformation suggests (periodic) high sedimentation rates. The latter can be expected from FA A (tidally influenced channel), which is found directly overlying this FA at Festningen. Coarsening upwards packages in relatively quick succession are interpreted as signs of a progradational system slightly landwards of this FA. It signifies gradual infilling of available accommodation space, separated by times of sudden increase in accommodation space (i.e. transgressions). The dominance of rippled intervals suggests that both fluvial, wave and tidal processes were influencing the deposits. Current rippled and 3D-current rippled intervals may

correspond to hyperpycnal flows originating from a nearby channel mouth. Additionally, the mud clasts observed, especially accompanying the soft-sediment deformation, may indicate proximity to a nearby terrigenous source. The intervals with increased mud content (i.e. the flaser and wavy bedded sections) signify that, at times, both the wave action and the unidirectional currents must have been sufficiently suppressed to allow the suspension settling of mud. Adding to that, waves are occasionally strong enough to form ripples. The isolated instance of planar cross-stratified sandstone may signify that at times the conditions were able to form dune-scale bedforms, possibly as subaqueous bars. Furthermore, the irregular bioturbation pattern and BI observed in this FA is interpreted to reflect the sedimentation conditions, i.e. sporadic high rates of deposition separated by quiescent times where organisms could thrive. Finally, the mixture of deposits seen in this FA with indications of both wave, fluvial and tidal components is interpreted as delta front deposits.
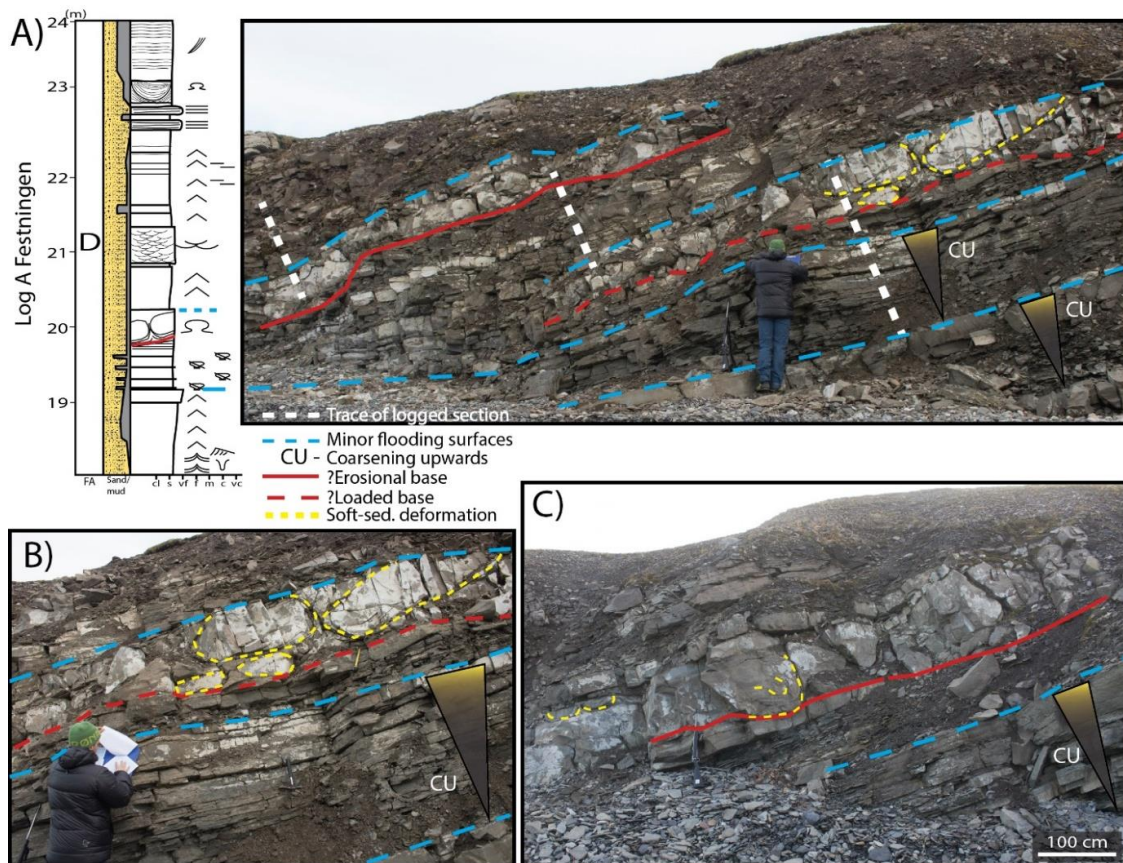
Figure 4.11: Typical expression for FA D. **A)** Shows a logged section with minor coarsening upwards cycles separated by minor flooding surfaces. Soft-sediment deformation features are also recognized along with potential erosional bases underlying the deformed strata. **B)** Is a closer look at these deformed layers. **C)** Illustrates soft-sediment deformed layers on different scales as well as showing potential erosion and flooding surfaces. See Fig. 4.5 or Appendix A for legend.

4.3.5 Facies association E – Offshore transition zone

Observations:

Facies association E predominantly consists of laminated mudstones (Facies L; Fig. 4.4L1-L2), which in some cases exhibit a more structureless appearance, separated by thin wave ripple cross-laminated- (Facies G; Fig. 4.4G) and planar parallel stratified (Facies A; Fig. 4.4A) very fine sandstone layers. In some of the sandstone layers it is possible to distinguish a transition from planar parallel stratification at the base, to wave ripple cross-lamination towards the top. Structureless sandstones (Facies D; Fig. 4.4D) may display short intervals of wave ripple cross-lamination. Furthermore, at Selmaneset (Fig. 4.2A), hummocky and swaley cross-stratification (Facies O; Fig. 4.4O) in very fine to fine sandstone was observed. Additionally, even though not included in the logged sections, observations were made of probable hummocky cross-stratification at Festningen in proximity with deposits belonging to this FA. It is also possible to recognize minor coarsening upwards packages capped by flooding surfaces (Fig. 4.12).

Where present, the BI is generally moderate (BI=3) while some intervals of higher BI (4-5) occur. Most frequently observed ichnofossils include *Planolites*, *Teichichnus* and *Arenicolites*, other recognized ichnofossils were *Paleophycus*, *Cylindrichnus*, *Rosselia* as well as undifferentiated vertical burrows.

Interpretation:

Laminated mudstone is attributed to suspension settling of mud with minor incursions of silt and very fine sand. The occurrence of structureless layers with both sand- and mudstone is interpreted to be the result of intense bioturbation. Abundant thin wave ripple cross-laminated sandstone layers between the more fine-grained deposits, likely represent deposition below fairweather wave base and may give an indication of the paleo-water depth. The observation of planar parallel stratification grading into wave ripple cross-lamination is thought to be the result of higher energy waves (i.e. minor storms), with the wave ripple cross-laminations representing the waning flow.

Furthermore, the rare occurrences of hummocky and swaley cross-stratification could indicate unfavorable current speeds, sediment fall out rates and/or orbital wave velocities as suggested by Dumas and Arnott (2006). However, their absence may also suggest that powerful storms were

rare in the study area during the Early Triassic (Wignall et al., 2016), or that the steepness of the depositional slope was not favorable. Adding to that, the coarsening upwards packages indicates proximity to a prograding system. This supports the interpretation of a wave-dominated offshore transition (e.g. sensu Howell and Flint, 2003) or a distal lower shoreface (e.g. sensu Hampson and Storms, 2003) environment. Deposition mostly takes place below fairweather wave base as evidenced by the abundance of laminated mudstone. Contrarily, deposits above fairweather wave-base would show progressively less-fine-grained sediments (e.g. clay and silt) as the seabed would be under continuous agitation (Howell and Flint, 2003). During storms, sand is being supplied from erosion of more proximal deposits nearby, allowing the formation of wave ripple cross-lamination, planar parallel stratification and occasionally hummocky cross-stratification. The trace fossil assemblage seen in this FA includes *Teichichnus*, *Arenicolites*, *Planolites*, *Rosselia*, *Cylindrichnus* and *Paleophycus* and is suggestive of the *Cruziana* ichnofacies, which is common, although not exclusive, in offshore transition deposits (Pemberton et al., 2012; Knaust, 2017).
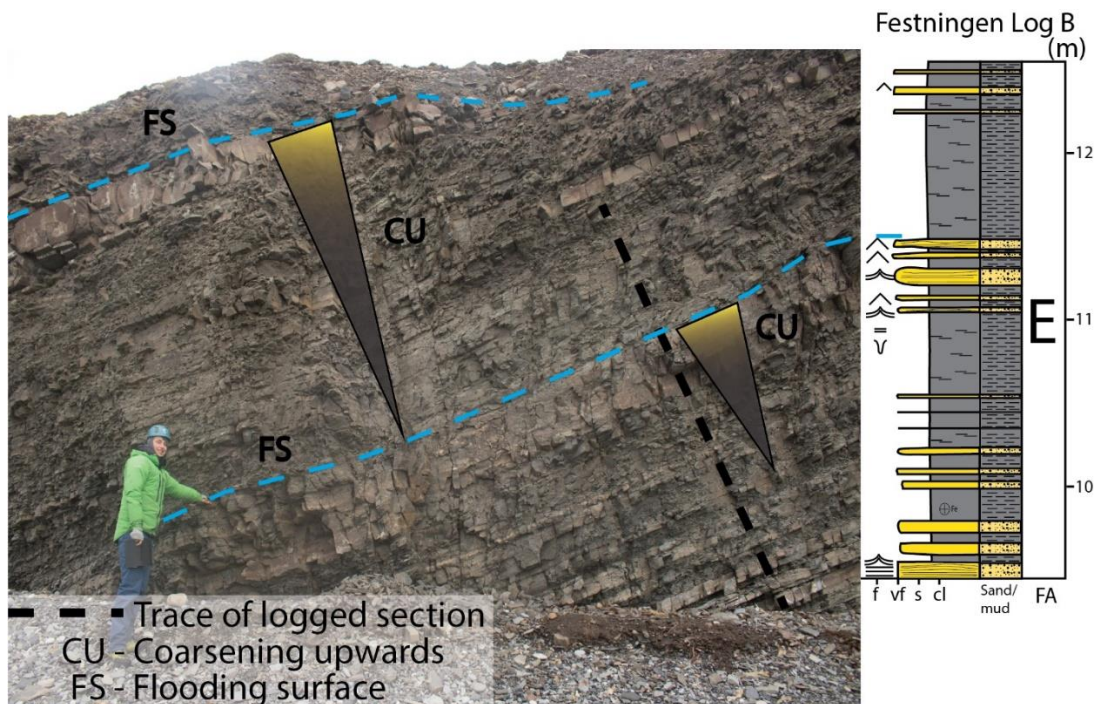
Figure 4.12: Photo and idealized log for FA E. The log is an interval from Log B from Festningen. Note the upwards coarsening cycles separated by minor flooding surfaces and the overall dominance of oscillatory currents. For legend see Fig. 4.5 or Appendix A. Complete log available in Appendix A.

4.3.6 Facies association F – Prodelta deposits

Observations:

Facies association F is dominated by mudstone with thin layers of siltstone and occasional very fine sandstone layers. The sandstone layers are, with a few exceptions, laterally continuous and often show erosive bases, wave ripple cross-lamination and in some instances planar parallel stratification (Facies A and G). Additionally, a few instances of current ripple cross-laminated sandstone are documented (Facies B) as well as one interval of 3D-current ripple cross laminated deposits. Contrarily, the mudstone and siltstone layers are dominated by planar parallel laminations (Facies L). These layers are often partially to completely scree covered and are interpreted as mudstone and siltstone, since these weathers easier than sandstone layers which tend to stand out more in cliff sides. No progradational or retrogradational trend can be distinguished within this FA as the lithological patterns in the logged section is too monotonous (Fig. 4.13A). Typically, the mudstone layers have a thickness of a few meters, up to several tens of meters and are separated by thin silt- and sandstone layers that are commonly a few tens of centimeters. Sparse to no bioturbation is observed.

Interpretation:

The dominance of laminated mudstone with variations in silt content suggests a basinal low energy environment. However, the very fine sandstone layers with wave ripple cross-lamination and planar parallel stratification signify times of higher energy. Wave action during storms is a probable explanation when these deposits are found co-occurring as well as for isolated instances of wave rippled sandstones. Having said that, isolated planar parallel stratified sandstones may originate from multiple processes.

The dominance of laminae in the deposits suggests small variations in the sediment input (Pickering et al., 1986), possibly by deltaic hyperpycnal plumes (i.e. low-density turbidity currents). Although laminae are not exclusive for such plumes, it makes sense with some contribution from these in association to the other FAs, as hyperpycnal plumes are likely to occur in front of prograding deltas (e.g. Bhattacharya and MacEachern, 2009). Therefore, hyperpycnal plumes, along with buoyant hypopycnal plumes, are believed to be the main suppliers of mud to this FA. At times of river flooding, hyperpycnal plumes may also transport silt and possibly sand to this distal part of the system (Bhattacharya, 2010). The absence of any progradational

signatures is an important distinction between this FA and FA E (Offshore transition zone; Fig. 4.12), and further suggests that this FA is situated in more a distal position. Additionally, the preservation of laminae suggests little bioturbation (Bhattacharya, 2010). Adding to that, the Induan, as well as the rest of the Lower Triassic on Spitsbergen, was characterized by shallow marine anoxia (Wignall et al., 2016), which may help explain the absence of bioturbation in this FA.
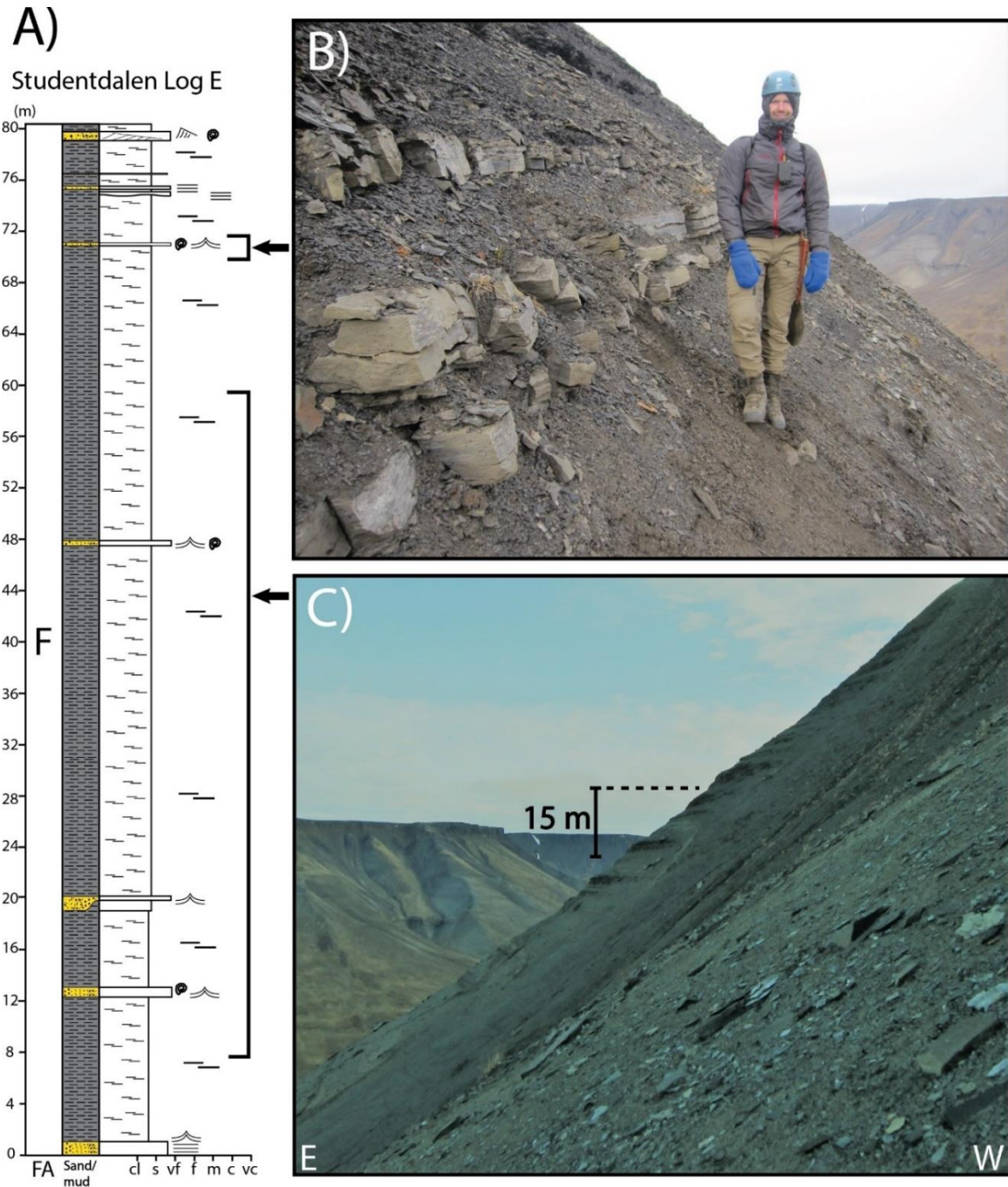
Figure 4.13: Photos from Rotundafjellet in Studentdalen (Fig. 1.1). **A)** Typical log expression of FA F. **B)** Yellow colored very fine sand deposits dominated by wave ripples separated by thicker packages of partially scree covered laminated mudstone. **C)** Overview photo of the mountainside. Note the sand prone layers sticking out with scree cover in between. For legend please see Fig. 4.5 or Appendix A.

5 Petrographic results

Here, the results of the petrographic work carried out in the lab will be presented. The work was performed following the procedures given in chapter three. This includes results from point counting, photographing and description of chosen thin sections. In total, the texture in ten sections was described focusing on grain roundness, sphericity, sorting, size as well as grain contacts (Table 5.1). Additionally, eight thin sections were point counted (Table 5.2) and classified in QFL and QmFLt diagrams based on their composition (Table 5.3). Table displaying which facies and FA the samples are from is shown in Appendix B.

5.1 Textural characteristics

Table 5.1: Description of chosen thin sections from both Festningen and Selmaneset with focus on grain size, sorting, roundness, sphericity and grain contacts. *Possible bimodal grain size distribution like in sample SES3, but few siliciclastic grains in the sample makes it problematic to calculate.

Location	Sample	Grain size	Grain sorting	Grain roundness	Grain sphericity	Grain contact
Festningen	FES2 (Fig. 5.2)	Silt – F.	Poorly sorted.	Poorly rounded to subangular.	Dominance of high sphericity.	Dominance of concavo-convex, subordinate floating grains.
	FES3 (Fig. 5.3)	F – VF.	Well to very well sorted.	Rounded to poorly rounded.	High to moderate sphericity.	Dominance of concavo-convex, but also a lot of sutured contacts.
	FES6 (Fig. 5.4)	F.	Moderately sorted.	Poorly rounded.	Dominance of high sphericity.	Dominance of concavo-convex, subordinate floating grains.
	FES9	F – VF.	Well sorted.	Poorly rounded.	Low sphericity.	Concavo-convex dominate.
	FES19 (Fig. 5.5)	F – M.	Poorly to very poorly sorted.	Angular to poorly rounded.	Low sphericity.	Dominance of floating grains, subordinate concavo-convex.
	FES20 (Fig. 5.6)	F – M.	Moderately sorted.	Poorly rounded to rounded.	Dominance of high sphericity, although several with low.	Dominance of concavo-convex, subordinate floating grains.
Selmaneset	SES2	Silt – VF.	Very poorly sorted.	Angular to subangular.	Low sphericity.	Floating grains dominate, subordinate concavo-convex.
	SES3	Large grains M-C, smaller grains silt to F*.	Very poorly sorted.	Rounded to well-rounded large grains. Smaller grains are angular to subangular.	Larger grains show high sphericity while smaller grains display low.	Floating grains.
	SES5 (Fig. 5.7)	VF – F.	Well sorted.	Subangular to poorly rounded.	Low sphericity.	Dominated by concavo-convex contacts.
	SES7 (Fig. 5.8)	Bimodal, peak at F sand as well as C and VC sand.	Very poorly sorted	Rounded to well-rounded large grains. Smaller are angular to poorly rounded	Large grains with high sphericity. Smaller grains have low.	Large grains and small grains dominated by floating.

5.2 Point counting

During point counting, detrital quartz (monocrystalline quartz), feldspar, chert (microcrystalline quartz), quartzite (polycrystalline quartz), mica and opaque minerals were registered. Authigenic minerals including quartz cement and calcite cement were also noted. The relative abundance of feldspars and opaque minerals is generally very low (<2%) in the studied samples, therefore no major attempts were made to investigate these in more detail. However, Raman spectroscopy was used to accurately identify grains with an uncertain composition. These investigations showed a dominance of rutile among the opaque minerals and that grains suspected of being feldspars, generally were monocrystalline quartz.

Table 5.2: Name and composition of point counted thin sections. VF = Very fine sand, F = Fine sand, M = Medium sand. *Note that the bimodal grain size is further described in Table 5.1 and shown in Fig. 5.8 and Fig. 6.8.

Sample information			Detrital minerals							Diagenetic minerals (%)		
			Monogranular grains (%)				Polygranular grains (%)					
Locality	Sample	Grain size	Quartz	Feldspar	Mica	Opaque	Polycrystalline quartz	Chert	Other	Quartz cement	Calcite cement	SUM (%)
Festningen												
	FES3	F - VF	78.0	0.3	2.3	0.0	3.7	3.3	0.0	10.3	2.0	99.9
	FES6	F	52.5	0.9	0.9	1.5	2.5	3.7	0.0	0.0	38.0	100.0
	FES9	VF	60.0	0.0	0.3	0.0	2.0	3.0	0.0	0.0	34.7	100.0
	FES19	F-VF	31.4	0.3	1.0	0.0	2.7	2.3	0.0	0.0	62.3	100.0
	FES20	F-M	53.3	0.3	0.3	0.0	3.3	4.0	0.0	6.7	32.0	99.9
Selmaneset												
	SES2	Silt - VF	56.7	0.0	0.3	0.0	1.3	3.0	0.0	3.7	35.0	100.0
	SES5	VF- F	75.3	0.0	2.0	0.0	2.7	3.3	0.0	10.7	6.0	100.0
	SES7	Bimodal*	34.0	0.0	0.3	0.0	11.3	5.0	1.3	0.7	47.3	99.9

5.3 Sandstone classification

To classify the sandstones, the results from the point counting (Table 5.2) was used to determine the relative proportions of quartz, feldspar and lithic fragments (Table 5.3). These were plotted accurately on QFL and QmFLt diagrams to investigate provenance as well as highlighting possible differences in sandstone composition (Fig. 5.1).

Table 5.3: Relative proportions of quartz, feldspar and lithic fragments in chosen thin sections. Values are calculated for both QmFLt and QFL diagrams following the reasoning that is given in subchapter 5.3.1. *Note that the bimodal grain size is described further in Table 5.1 and illustrated in Fig. 5.8 and Fig. 6.8.

Sample information			QmFLt Diagram						QFL Diagram						
Locality	Sample	Grain size	Quartz		Feldspar		Lithic fragments		Quartz		Feldspar		Lithic fragments		
Festningen			n	%	n	%	n	%	n	%	n	%	n	%	Nsum
	FES3	F - VF	234.0	89.0	1.0	0.4	28.0	10.6	255.0	97.0	1.0	0.4	7.0	2.7	263.0
	FES6	F	171.0	84.7	3.0	1.5	28.0	13.9	196.0	97.0	3.0	1.5	3.0	1.5	202.0
	FES9	VF	180.0	91.8	0.0	0.0	16.0	8.2	195.0	99.5	0.0	0.0	1.0	0.5	196.0
	FES19	F-VF	94.0	89.5	1.0	1.0	10.0	9.5	101.0	96.2	1.0	1.0	3.0	2.9	105.0
	FES20	F-M	160.0	87.0	1.0	0.5	23.0	12.5	182.0	98.9	1.0	0.5	1.0	0.5	184.0
Selmaneset															
	SES2	Silt - VF	170.0	92.4	0.0	0.0	14.0	7.6	183.0	99.5	0.0	0.0	1.0	0.5	184.0
	SES5	VF- F	226.0	90.4	0.0	0.0	24.0	9.6	244.0	97.6	0.0	0.0	6.0	2.4	250.0
	SES7	Bimodal*	102.0	67.1	0.0	0.0	50.0	32.9	151.0	99.3	0.0	0.0	1.0	0.7	152.0

5.3.1 QmFLt and QFL diagrams

The composition of the sandstones (Table 5.3) was classified in ternary QFL and QmFLt diagrams following the descriptive terms of Pettijohn et al. (1987) (Fig. 5.1A-B). Additionally, the same values (Table 5.3) were plotted on ternary QFL and QmFLt diagrams similar to Dickinson and Suczek (1979) in an attempt to highlight the provenance of the samples (Fig. 5.1C-D).

For the QFL diagram all quartzose grains are plotted together, both mono-, micro- and polycrystalline quartz. Contrarily, the QmFLt diagram only regards monocrystalline quartz as quartzose grains. Thus, in the QFL diagram used in this study only mica and opaque minerals are considered lithic fragments following Dickinson and Suczek (1979) and Dickinson et al. (1983), barring the inclusion of mica. For the QmFLt diagram lithic fragments include polycrystalline quartz, chert, mica and opaque minerals, which is in agreement with the QmFLt diagram used by Dickinson and Suczek (1979) and similar to the classification used by Mørk (1999). Another key thing to be aware of is the importance of separating mono- and polycrystalline quartz from microcrystalline quartz. The two former is most likely originating from Greenland (discussed in subchapter 6.3), while the chert (microcrystalline quartz) is probably derived from uplifted parts of the Kapp Starostin Formation in nearby areas, which contains abundant chert (e.g. Ehrenberg et al., 2001).

In the QmFLt diagrams seven of the eight samples are classified as sublitharenites due to their high quartz content and low to moderate content of lithic fragments (Fig. 5.1A). Additionally, one of the samples is classified as a litharenite due to the lower ratio between the relative abundance of quartz and lithic fragments. Following Dickinson and Suczek (1979) this is indicative of a craton interior or recycled orogen source area (Fig. 5.1C). Contrarily, the QFL diagrams classify all 8 samples as quartz arenites (>95% quartz content, Fig. 5.1B) and exclusively suggests a craton interior source area (Fig. 5.1D).

For the purpose of this study, the QmFLt diagrams are the most interesting, since these are similar to the method used by Mørk (1999), which these deposits will be directly compared to in subchapter 6.2. Thus, when specifying sandstone composition in this chapter and discussing QFL-diagrams for the Vardebukta Formation/Study area in chapter 6 it is the QmFLt diagrams (Fig. 5.1A and C) that are referred to, unless otherwise stated.
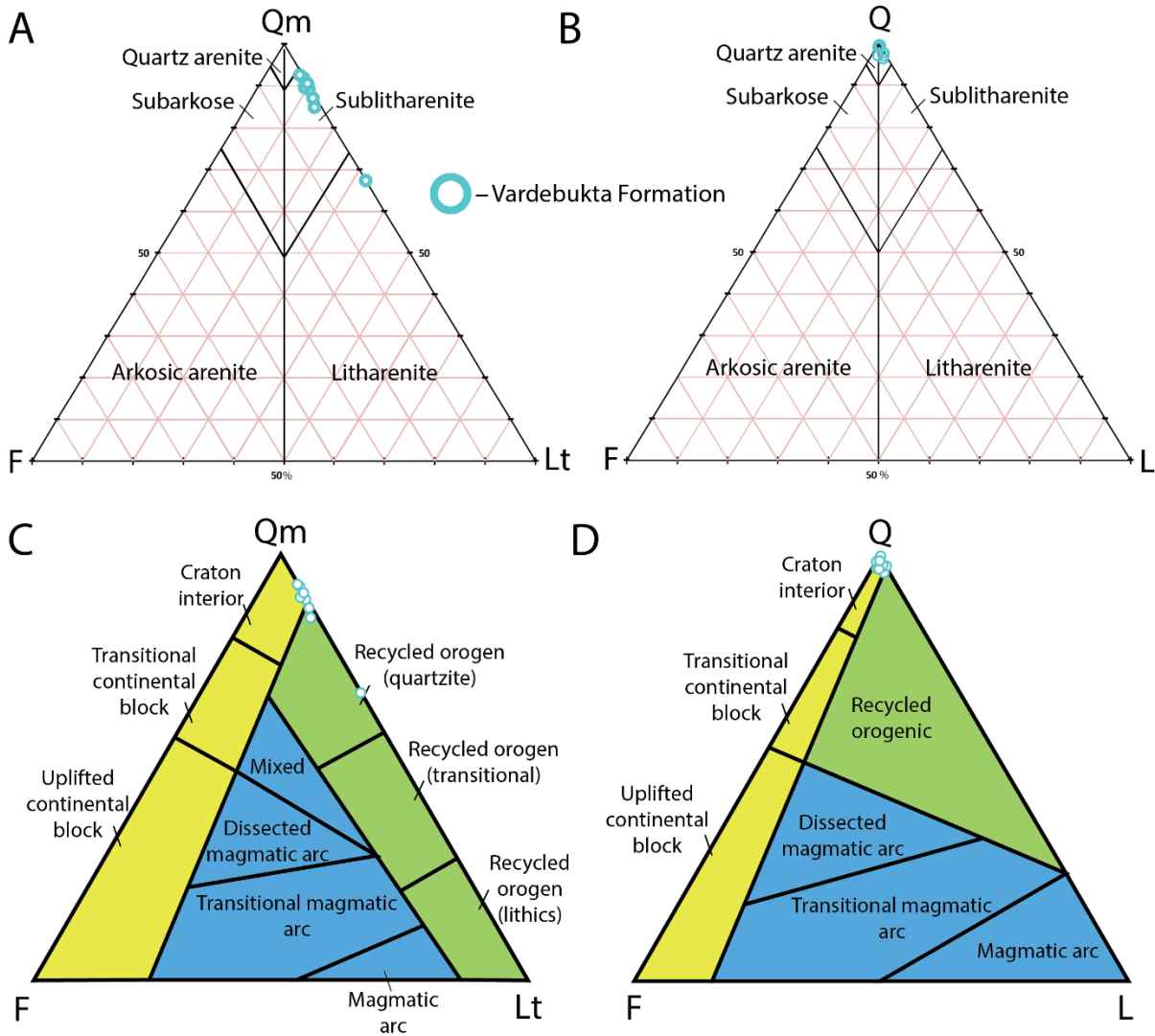
Figure 5.1: QmFLt and QFL diagrams showing the composition, classification as well as the suggested provenance areas for the 8 studied thin sections presented in Table 5.3. **A-B)** are modified from Pettijohn et al. (1987) while **C-D)** are modified from Dickinson and Suczek (1979).

5.4 Evidence from thin sections

Photographs of the thin sections document the results from the point counting (Table 5.2 and Table 5.3) and the textural descriptions (Table 5.1). Many of the samples are relatively similar with high contents of calcite cement, a dominance of spherical, poorly to moderately sorted and poorly rounded grains showing similar sizes (e.g. sample FES2; Fig. 5.2, FES6; Fig. 5.4, FES20; Fig. 5.6). Other samples are better sorted, display relatively high contents of quartz cement and are dominated by concavo-convex grain contacts (e.g. sample FES3; Fig. 5.3, sample SES5; Fig. 5.7). One of the samples (Sample FES19; Fig. 5.5) show an extreme content of calcite cement. Samples FES3 (Fig. 5.3) and FES6 (Fig. 5.4) were stained with blue epoxy to highlight potential porosity.

The observations in sample SES7 (Fig. 5.8) from Selmaneset with a massive spread in grain sizes as well as large differences in roundness and sphericity were rather unexpected, and has implications for the source area for the Vardebukta Formation. Furthermore, the textural descriptions of the thin sections (Table 5.1), as well as the textures observed in several of the thin section photos (e.g. sample FES2; Fig. 5.2) are interesting, as they do not exhibit the same degree of maturity compared to the mineralogical maturity of the deposits (Fig. 5.1; Table 5.2; Table 5.3).

Thin sections were investigated in a cathodoluminescence microscope to provide additional information for the sedimentological part of this thesis as well as help determine if most of the calcite cement was formed during early burial stages, or if the cement originated from multiple stages of formation. Of the investigated samples, sample FES19 (Fig. 5.10) provided evidence of multiple generations of calcite cement. In Fig. 4.6 and Fig. 4.8 the bulk of the calcite cement has a similar color in cathodoluminescence, both within the pore filling calcite and within the intact *Brachiopod punctae* shell fragments, indicating that it is of early diagenetic origin.

The significance of the remarks in the two preceding paragraphs will be addressed in detail in chapter 6.
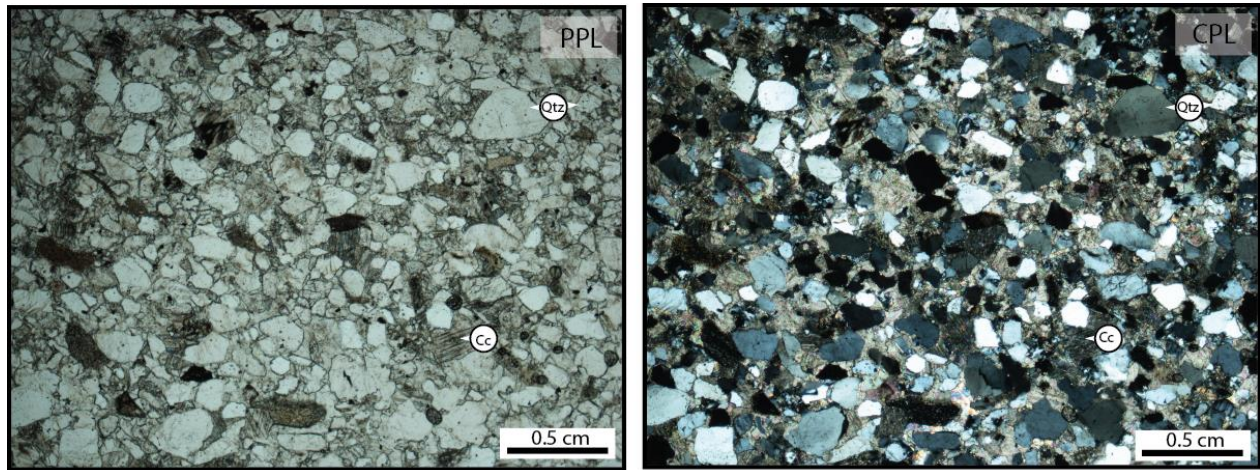
Figure 5.2: Thin section photos of sample FES2 from Festningen in plane polarized light (PPL) and cross-polarized light (CPL) showing a poorly sorted calcite-cemented sublitharenite. Note the poorly rounded to subangular grains with a dominance of high sphericity. Abbreviations: Qtz = Quartz, Cc = Calcite cement.
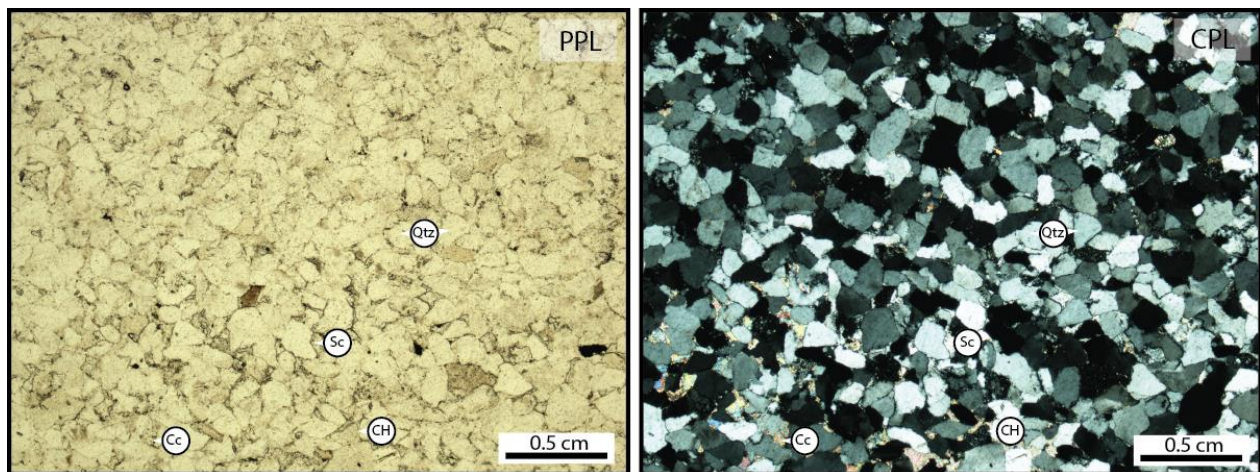
Figure 5.3: Thin section photos of sample FES3 from Festningen in plane polarized light (PPL) and cross-polarized light (CPL) showing a well sorted to very well sorted and tightly cemented sublitharenite. Grains are usually rounded to poorly rounded with a high to moderate sphericity. Abbreviations: Qtz = Quartz, Cc = Calcite cement, Sc = Sutured contacts, CH = Chert.
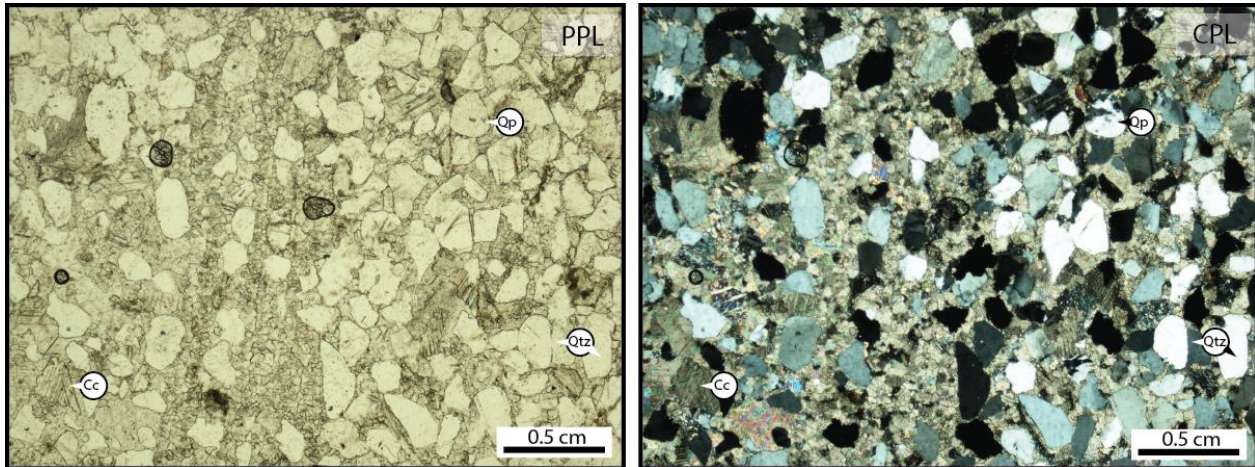
Figure 5.4: Thin section photos of sample FES6 from Festningen in plane polarized light (PPL) and cross-polarized light (CPL) showing a moderately sorted cemented sublitharenite. The grains are usually poorly rounded with a dominance of high sphericity. Abbreviations: Qtz = Quartz, Cc = Calcite cement, Sc = Sutured contacts, CH = Chert.
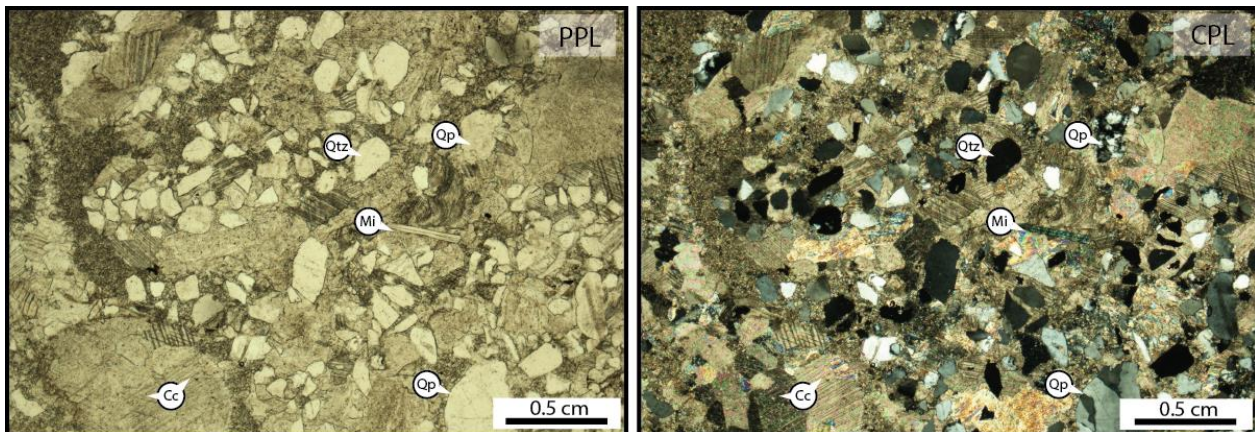
Figure 5.5: Thin section photos of sample FES19 from Festningen in plane polarized light (PPL) and cross-polarized light (CPL) showing a poorly to very poorly sorted calcite-cemented sublitharenite. The grains are usually angular to poorly rounded with a low sphericity. Abbreviations: Qtz = Quartz, Qp = Polygranular quartz, Cc = Calcite cement, Mi = Mica.
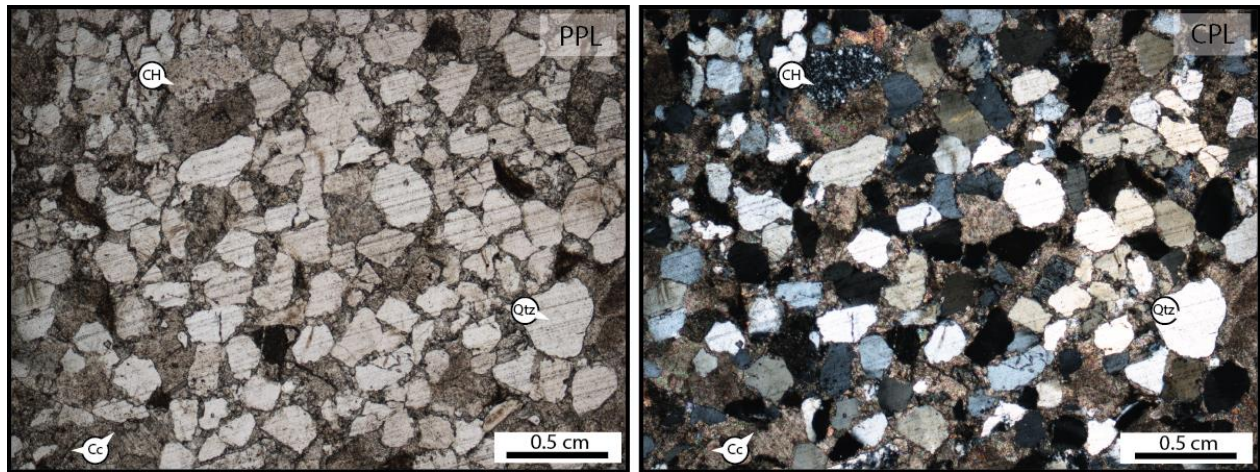
Figure 5.6: Thin section photos of sample FES20 from Festningen in plane polarized light (PPL) and cross-polarized light (CPL) showing a moderately sorted calcite-cemented sublitharenite. The grains vary from poorly rounded to rounded with a dominance of high sphericity, although several with low sphericity are distinguished. Abbreviations: Qtz = Quartz, Cc = Calcite cement, CH = Chert.
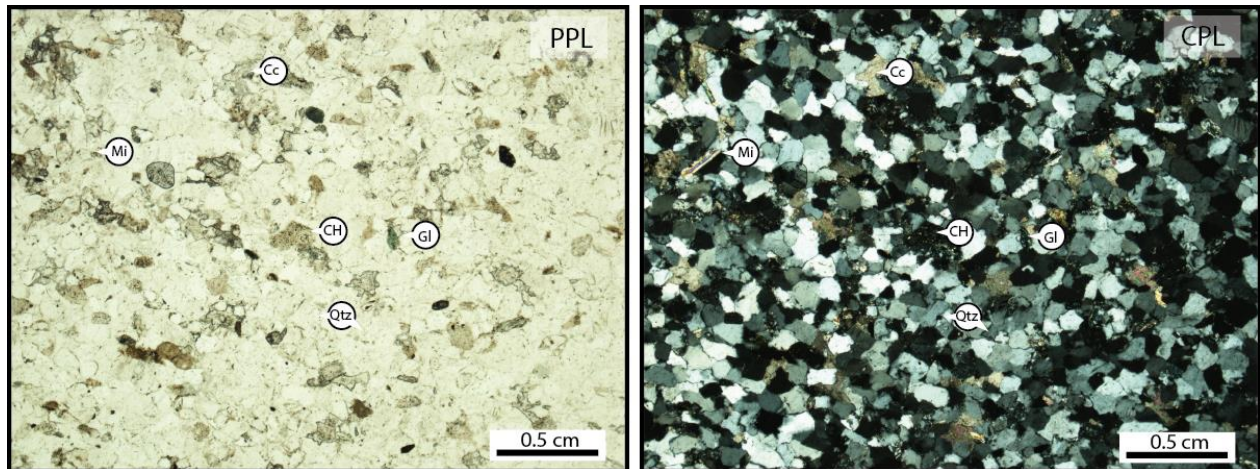

Figure 5.7: Thin section photos of sample SES5 from Selmaneset in plane polarized light (PPL) and cross-polarized light (CPL) showing a well sorted and tightly cemented sublitharenite. The grains are usually subangular to poorly rounded with a low sphericity. Abbreviations: Qtz = Quartz, Cc = Calcite cement, Gl = Glauconite, CH = Chert, Mi = Mica.
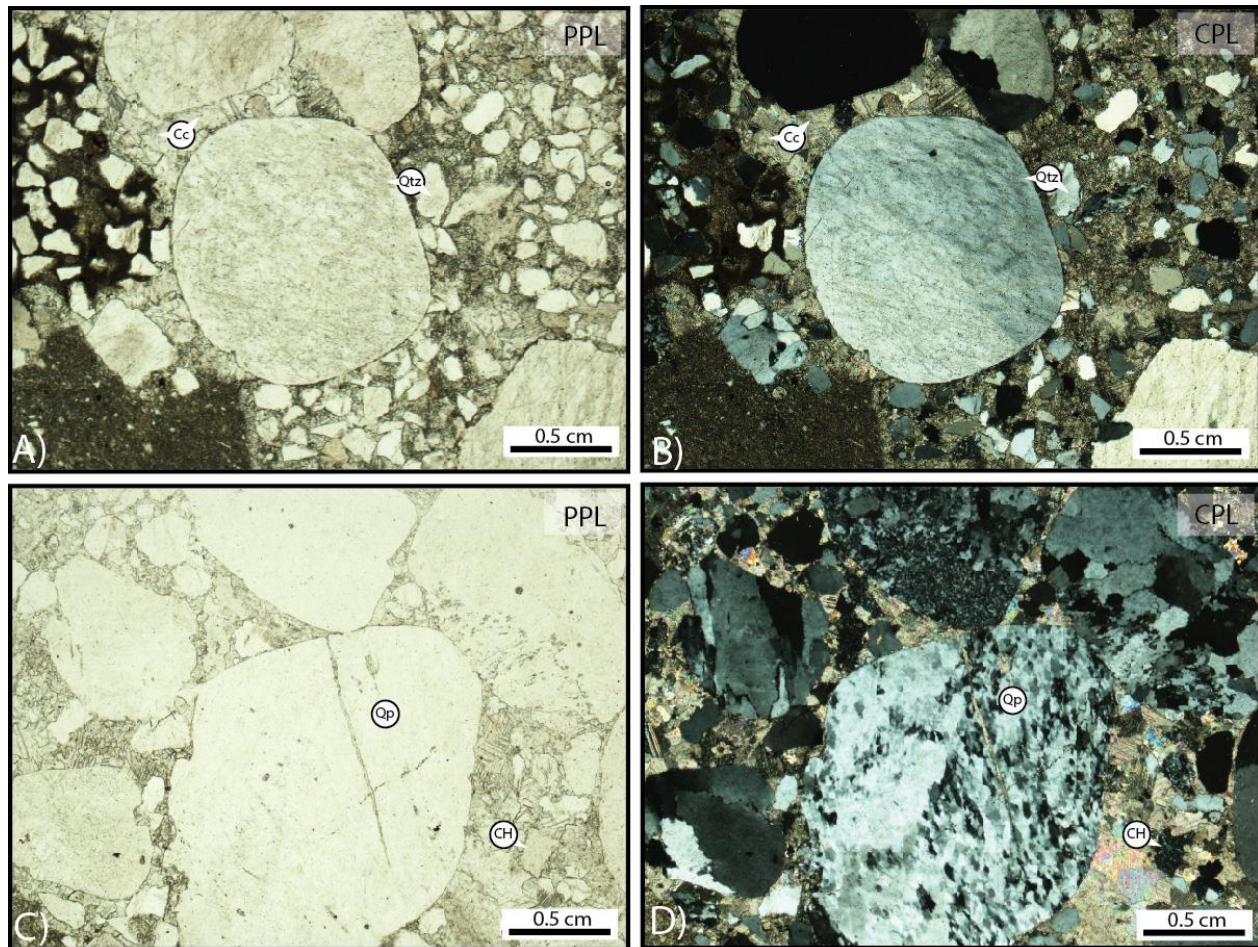
Figure 5.8: A compilation of thin section photos of sample SES7 from Selmaneset in plane polarized light (PPL) and cross-polarized light (CPL). It has been classified as a litharenite. **A-D)** Showing the variation in grain size. **A-B)** Displays large rounded to well-rounded grains and the contrasting angular to poorly rounded smaller grains with significantly lower sphericity. **C-D)** Again, note the large well-rounded quartz and polygranular grains (quartzite) with high sphericity. Abbreviations: Qtz = Quartz, Cc = Calcite cement, Qp = Polygranular quartz, CH = Chert.
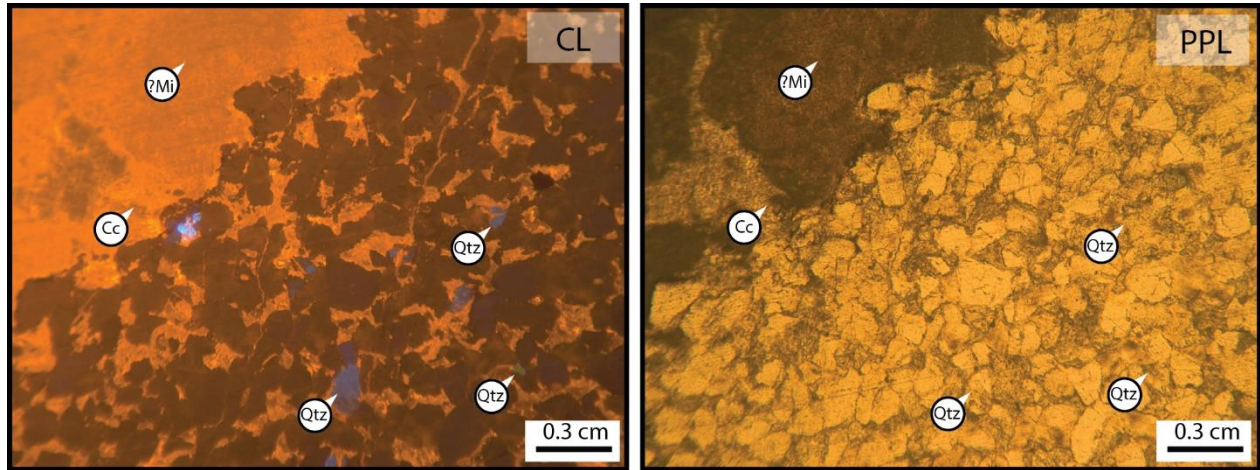
Figure 5.9: Thin section photos of sample FES1 from Festningen in both plane polarized light (PPL) and cathodoluminescence (CL). The sample is taken from FA C (Fig. 4.10) in what has been interpreted as possible desiccation cracks on a supratidal flat. Note the non-luminescent as well as the luminescent (blue colored) quartz (Qtz) grains. Furthermore, both coarse and fine-grained calcite cements are observed. The coarse cement (Cc) with visible crystals is interpreted as sparite, while the fine grained cement might represent micrite (?Mi).
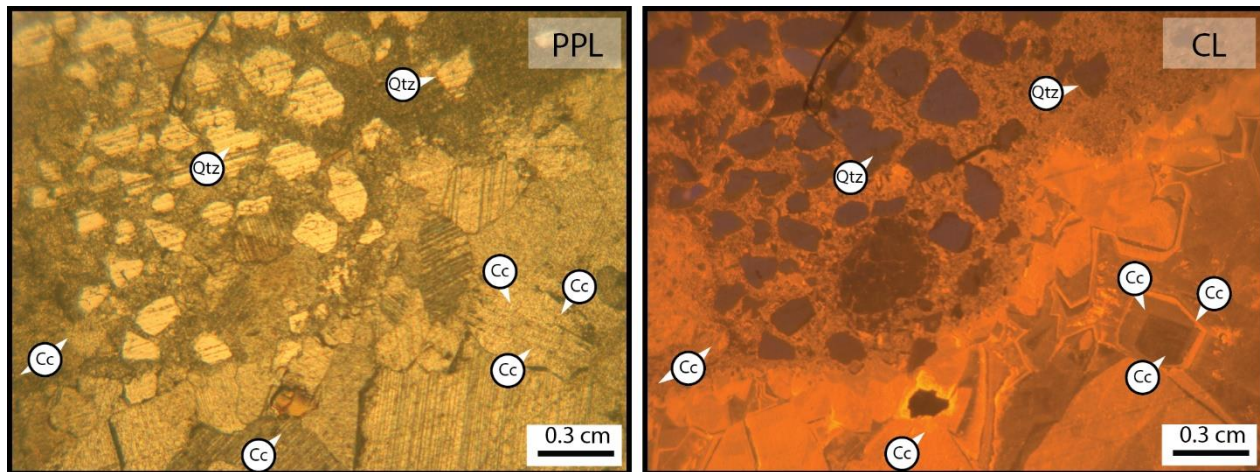
Figure 5.10: Thin section photos of sample FES19 from Festningen in both plane polarized light and cathodoluminescence. The sample is taken from the base of FA A (Fig. 4.7A). Note the non-luminescent quartz (Qtz) grains as well as the several generations of calcite cement (Cc) identified by zonation in the calcite crystals in the right-hand corner of the CL photo. At least three generations of cement are recognized.

6 Discussion

In the following chapter, the results of this study are discussed in the context of what is already published about the Vardebukta Formation and the regional situation in the Early Triassic Barents Sea. Firstly, in subchapter 6.1 the sedimentology of the formation will be discussed for the sake of establishing a depositional model. Secondly, in subchapter 6.2 the mineralogical characteristics of the three principal sedimentary systems characterizing the Triassic Barents Sea will be presented, to provide some regional background. Thirdly, in subchapter 6.3 the mineralogical characteristics of the Vardebukta Formation will be further examined and possible source areas discussed. Finally, in subchapter 6.4 the reservoir properties of the Vardebukta Formation will be debated and potential implications for regional reservoir exploration will be provided.

6.1 Depositional model for the Vardebukta Formation

As mentioned previously in Section 4.1, the Vardebukta Formation was studied by Mørk et al. (1982) and classified as a barrier bar system with tidal inlets and the development of lagoonal facies. Other studies (Wignall et al., 1998; Wignall et al., 2016) have suggested a shoreface depositional model, grading from offshore deposits in the basal part of the formation to foreshore deposits in the most proximal deposits.

Isopach maps from Wignall et al. (1998) (Fig. 6.1) and Lord et al. (2017, (Fig. 3 p. 207)) show the thickness distribution of the Sassendalen Group (Lower and Middle Triassic) and the Lower Triassic on Svalbard, respectively. Both studies reveal the highest sediment thicknesses at the inlet of Isfjorden and successively lower thicknesses towards the N/NE and SE. Although this study only focuses on the Vardebukta Formation, it is reasonable to assume that the same thickness distribution applies as for the Lower Triassic and the Sassendalen Group.
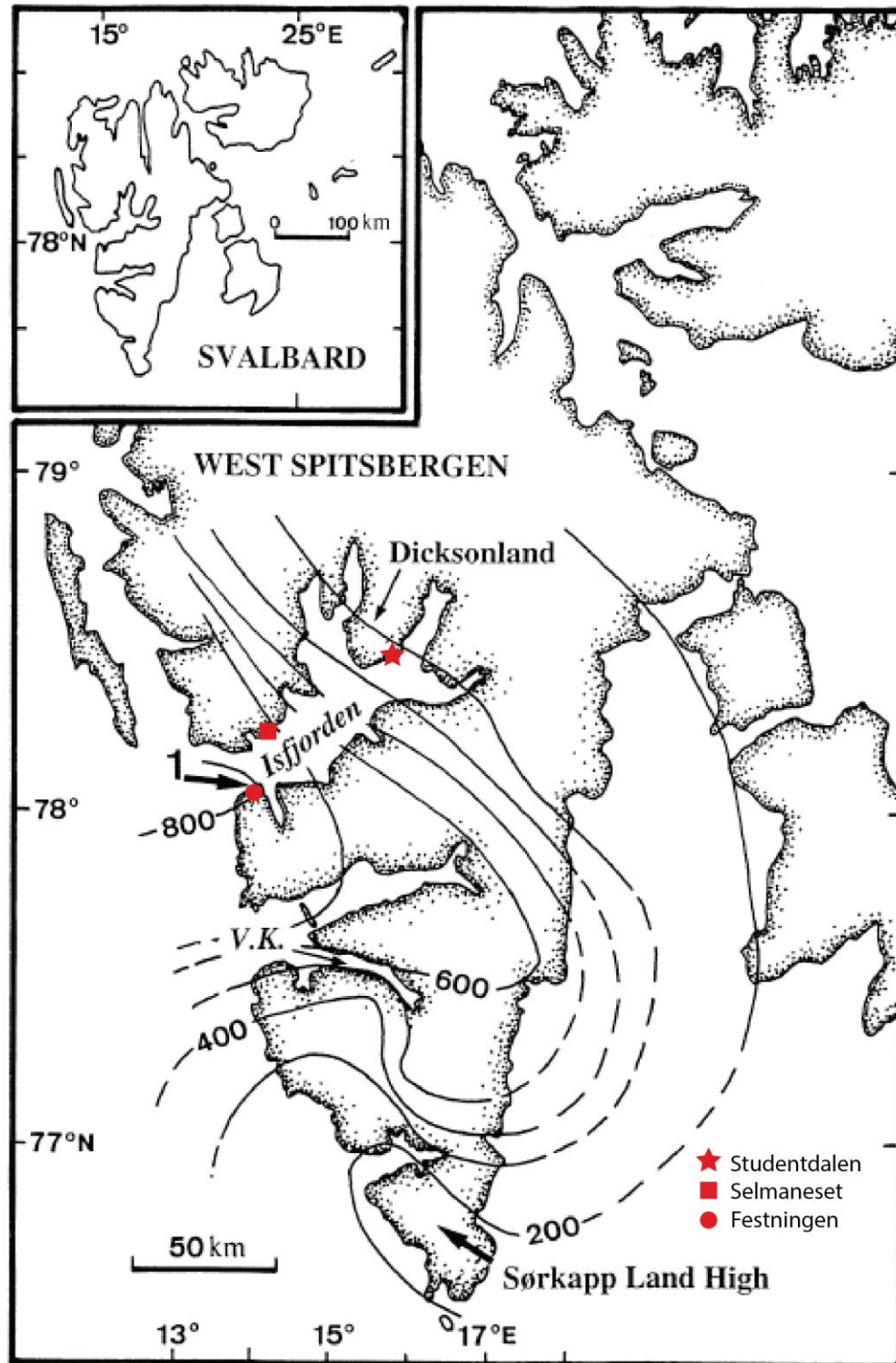
Figure 6.1: Thickness map for the Sassendalen Group (Lower and Middle Triassic) on western and central Spitsbergen. The red symbols mark the different locations were the Vardebukta Formation was investigated in this study. Modified after Wignall et al. (1998).

As the Vardebukta Formation was deposited in a shallow marine clastic ramp (Wignall et al., 2016), which is typically characterized by shallow dip angles (Coe and Church, 2003), storm and wave processes would have had a large area to influence deposition (Emery and Myers, 1996). This is in accordance with the more distal deposits found in this study, e.g. FA E (Offshore transition zone; Fig. 4.12) and FA F (Prodelta deposits; Fig. 4.13), which show a dominance of storm and wave impact between periods of quiescence and mud deposition. However, the sparse occurrences of hummocky and swaley cross-stratification in the Vardebukta Formation have been noted in the present study as well as in previous studies (Wignall et al., 1998; Wignall et al., 2016). Such stratification is usually attributed to storm deposition (Dumas and Arnott, 2006), and its rare occurrence may thus give the impression that storms were rare in the earliest Triassic (Wignall et al., 2016). Another possible, and perhaps more likely, explanation is that the Sørkapp-Hornsund High (Fig. 2.1 and Fig. 6.5), which was acting as a basement high where sedimentation did not start until the mid-Induan (Nakrem and Mørk, 1991; Worsley, 2008; Vigran et al., 2014), provided shelter for storm waves and thus restricted the formation of hummocky- and swaley cross-stratification. Nonetheless, this study documents an unambiguous example of hummocky and swaley cross-stratified sandstone (Facies O; Fig. 4.4O), likely hummocky cross-stratification in the area above Log C Festningen (Fig. 4.2B), as well as multiple gutter casts, evidencing that the shelfal conditions most likely were dominated by waves. Therefore, this study agrees with the findings of Mørk et al. (1982) who interpreted the shelf to mainly being influenced by wave and storm action. Other studies have suggested a river-fed hyperpycnal turbidite origin of these shelfal sandstones (Wignall et al., 2016). Although this cannot be excluded, neither this study or Wignall et al. (2016) observed any coarsening- or fining-upwards trends, which are diagnostic of turbidite deposits (Mulder et al., 2003).

Like previous studies (Mørk et al., 1982; Mørk et al., 1989; Wignall et al., 1998; Wignall et al., 2016), this study has documented abundant shell material in the Vardebukta Formation in the form of shell hash, shell imprints and shell-rich limestone layers, especially at Festningen and Selmaneset (Fig. 1.1). Adding to that, thin section analyses reveal high contents of calcite cement (e.g. sample FES19; Fig. 5.5). Strictly speaking, based on the point counting (Table 5.2) some of these samples could be classified as limestones given their carbonate-rich nature. However, since

most of the carbonate is in the form of cement and not carbonate grains, it is sufficient to refer to them as cemented sandstones (G. Sælen, pers. comm., 2017). It is also the clastic system that is of interest for this study.

Calcite cementation is known to occur during shallow burial at temperatures between 50-70 °C or at even lower temperatures between 15-40 °C (Saigal and Bjørlykke, 1987), and is commonly complete before quartz cementation (Walderhaug, 1990). Previous studies have documented a connection between heavily calcite-cemented intervals and the presence of dissolved or intact carbonate fossils (e.g. Fürsich, 1982; Olaussen et al., 1984). Bjørkum and Walderhaug (1990) suggested that the principal control on calcite cementation in shallow marine sandstones was through the dissolution of internal carbonate fossils deposited together with the siliciclastic material.

Consequently, most of the calcite cement seen in the deposits in the Vardebukta Formation, especially at Festningen and Selmaneset, is thought to originate from dissolved biogenic carbonate. This assumption is strengthened by the findings from cathodoluminescence investigations of thin section SES7 (Fig. 4.6) and FES2 (Fig. 4.8), which show dissolved brachiopods with the same luminescent color as the surrounding calcite cement. Adding to that, the calcite cement may act as an inhibitor to subsequent quartz cementation as the pore space is already occupied (McBride, 1989; Walderhaug, 1990). Had this not been the case, one would expect the deposits in the Vardebukta Formation to be influenced by sutured contacts and quartz cementation to a higher degree.

However, cathodoluminescence investigations of thin section FES20 (Fig. 5.6) show the presence of multiple generations of calcite cement as evidenced by the zonation in the calcite crystals. It has most likely formed at a later stage than the dominant early burial cement. The extent of this cementation is poorly understood. In all likelihood, it has a connection to pore water (e.g. meteoric) circulation in the abundant fractures seen in the outcrops at Festningen and Selmaneset, which again is related to the uplift these deposits have undergone after being buried to 4-5 kilometers (Michelsen and Khorasani, 1991).

This study concurs with several of the findings of Mørk et al. (1982), especially that the shelf was subject to a predominance of storm and wave action and the abundance of shell material as pointed out in the preceding paragraphs. Furthermore, their observations of dominant paleocurrents to the east and southeast (see Log A in Appendix A for paleocurrents), as well as the recognition of tidal influence, i.e. tidally influenced channel (FA A; Fig. 4.7) in this study and tidal inlet in Mørk et al. (1982), are not contested by the author. Having said that, barrier island systems are largely transgressive in nature (Kraft et al., 1973; Boyd et al., 1992), while on Festningen a clear progradational and shallowing-upward signature is observed both by this study (Fig. 6.3) and previous studies (e.g. Mørk et al., 1982; Wignall et al., 1998). Such a signature transitioning from the mud-rich prodelta (FA F; Fig. 4.13) to the delta front (FA D; Fig. 4.11) and further to the lower delta plain (FA A, B and C; Fig. 4.7, Fig. 4.9 and Fig. 4.10)) are symptomatic of prograding deltas (Bhattacharya, 2010). Also, tidal inlets are usually affiliated with flood tidal deltas building into the back-barrier environments and ebb tidal deltas establishing themselves on the seaward side of the inlet (Howell and Flint, 2003; Boyd, 2010). Furthermore, the ebb tidal deltas have the lowest preservation potential as they are exposed to wave and storm action (Howell and Flint, 2003; Boyd, 2010). Contrarily, the flood tidal deltas, which build into more protected environments (e.g. a lagoon), have a higher chance to be preserved (Howell and Flint, 2003). Such an ebb-flood relationship is not observed by this study, and neither is the development of diagnostic lagoonal facies.

Following this, the present study does not see the necessity of classifying the deposits as barrier and back barrier deposits when other depositional models may be equally, or more, credible. Instead, a simpler depositional model is proposed comprising a mixed type delta. This is supported by the wide array of sedimentary processes expressing similar influence of tidal, wave and fluvial influence, which is documented in this study, especially in FA D. An approximate quantification of the distribution of sedimentary structures, following the work of Ainsworth et al. (2011) and Rossi et al. (*in press*), was done for FA E (offshore transition zone), FA D (delta front deposits) and FA A (tidally influenced channel). It reveals a change from a wave and tide-dominated offshore transition zone to an almost equally wave, tide, and fluvial influenced delta front and further to a tide-dominated channel influenced by more fluvial than wave processes

(Fig. 6.2). Although not conclusive, it strengthens the general assumption that the deposition of the Vardebukta Formation was affected by a diversity of processes. Mixed-energy deltas have traditionally received little attention, but are documented in the literature (e.g. Plink-Björklund, 2012; Hassan et al., 2013).
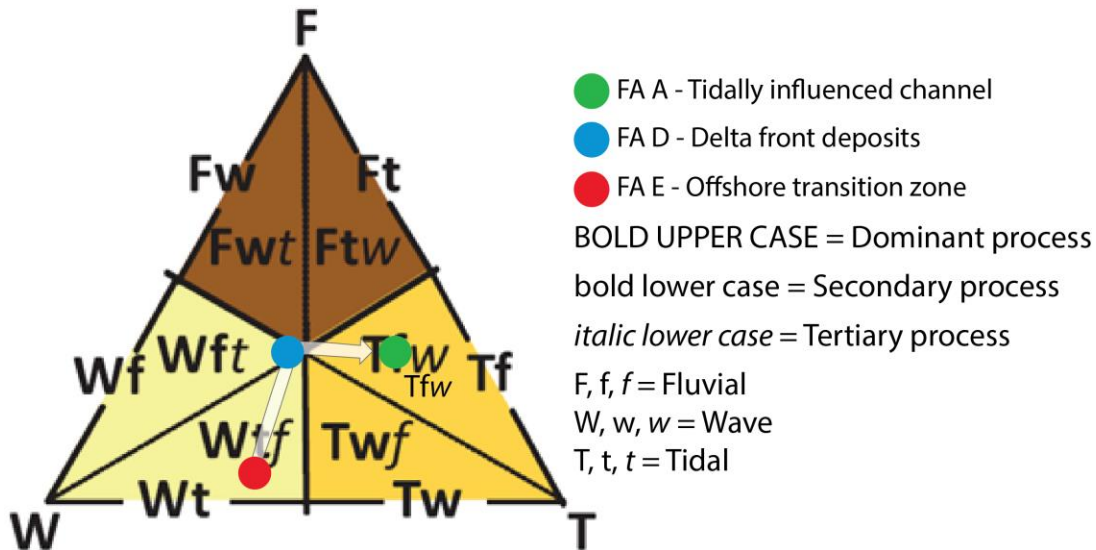
Figure 6.2: Illustration showing the distribution of fluvial, wave and tidal processes within FA A, D and E. The sedimentary structures relative abundance from these FA were quantified following the work of Rossi et al. (*in press*), while the ternary diagram was modified from Ainsworth et al. (2011).

Figure 6.3 is a conceptual drawing showing the distribution of facies associations in the Vardebukta Formation on Spitsbergen during the Induan stage. T1 (Fig. 6.3A-B) delineates the system as it approached Isfjorden in the early Induan expressed by a prograding offshore transition zone (FA E; Fig. 4.12) directly overlying the basal prodelta deposits. T2 (Fig. 6.3C) illustrates the maximum extent of the system with the most proximal facies documented in this study, found on both Festningen and Selmaneset (Fig. 6.3A). This includes the development of tidally influenced channels, tidal sandflats and supratidal deposits. The presence of desiccation cracks at Festningen and possibly on Selmaneset as contemplated in this study, is in line with previous research which documented such features at Selmaneset (Mørk et al., 1982). This means that subaerial conditions were attained along western Spitsbergen in the Induan. T3 (Fig. 6.3A and D) illustrates the subsequent transgression that followed, expressed on Festningen by the stacking of consecutively more distal deposits towards the overlying Tvillingodden Formation.
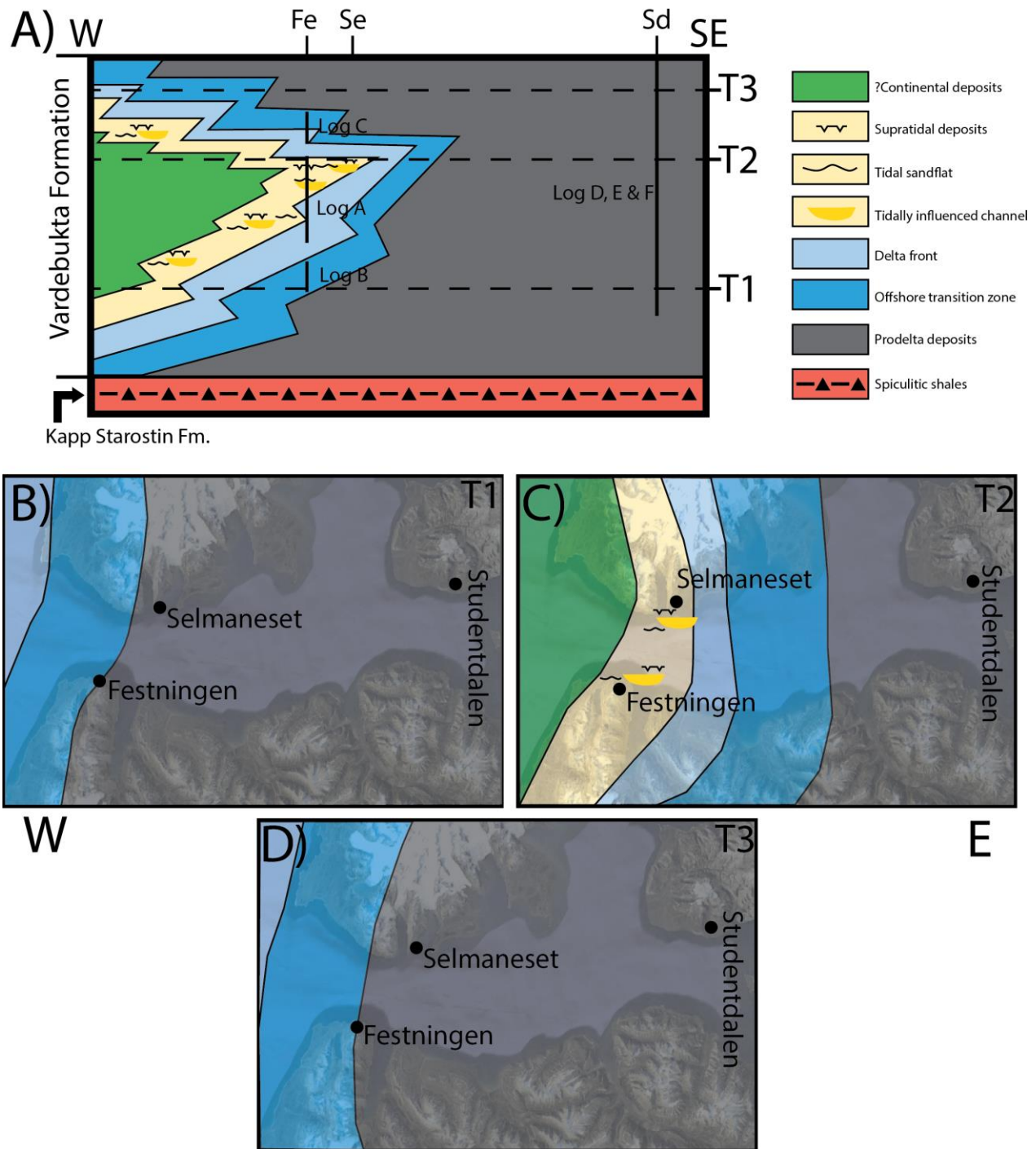
Figure 6.3: A schematic figure showing the extent of the Vardebukta Formation during the Induan. **A)** Is a cross-section showing the sedimentary development at the field localities. These are denoted by: Fe = Festningen, Se = Selmaneset and Sd = Studentdalen. Note that there is no stratigraphic control at Selmaneset due to intense tectonic deformation. T1, T2 and T3 in **B)**, **C)** and **D)** illustrate how the system may have approached Svalbard with T1 showing the initial progradation, T2 showing the max extent of the system with the brief development of subaerial conditions and finally T3 illustrating the retreat of the system. Drawn on top over satellite images © Google from Isfjorden.

Figure 6.4 illustrates how the present study visualizes the depositional environment of the Vardebukta Formation. The facies associations shallow upwards from the prodelta (FA F) to the supratidal flat (FA C). The prodelta is dominated by fine-grained suspension settling of sediments from both hyperpycnal plumes and/or buoyant hypopycnal plumes, whereas the offshore transition zone (FA E) contains abundant thin sand layers assigned to storm and wave deposition. A mixed signature of processes is seen on the delta front with isolated carbonate shell banks accumulating at times of stillstand separated by times of wave agitation and periods of high fluvial influx of sediment, as evidenced from the soft-sediment deformed layers. Shell banks may also form due to little sediment input to specific areas on the delta front, perhaps connected to avulsing channels landwards of this FA. At times, subaqueous bars may also form. Channels incise the tidal flat and frequently provide sand through flooding. Following the floods, mud suspension settles furthest away from the channels and the shoreline. The tide level is only occasionally high enough to flood the supratidal flat, possibly associated with spring or equinoctial tides, providing mostly mud (e.g. the ?micrite in Fig. 4.10A) while overbank flood deposits from nearby channels contribute mostly sand. In between these influxes of sediments, the supratidal flat is subjected to drying and fracturing forming desiccation cracks (Fig. 4.10 and Fig. 6.4).

Finally, as discussed in this subchapter, a depositional model consisting of a barrier island complex with associated lagoonal back-barrier deposits, as imagined by Mørk et al. (1982), cannot be omitted. It is perhaps more valid for the transgressive upper part of the Vardebukta Formation at Festningen (Fig. 4.1, Log C; Appendix A) as delta abandonment is one way of forming barrier-lagoon systems (Boyd et al., 1989; Bhattacharya, 2010). Having said that, this study does not see the necessity of such a model when simpler depositional models may be equally valid. Thus, it is the belief of this study that the Vardebukta Formation was deposited as a mixed type delta with a storm and wave-dominated shelf in an environment with extensive biogenic carbonate production (Fig. 6.4).
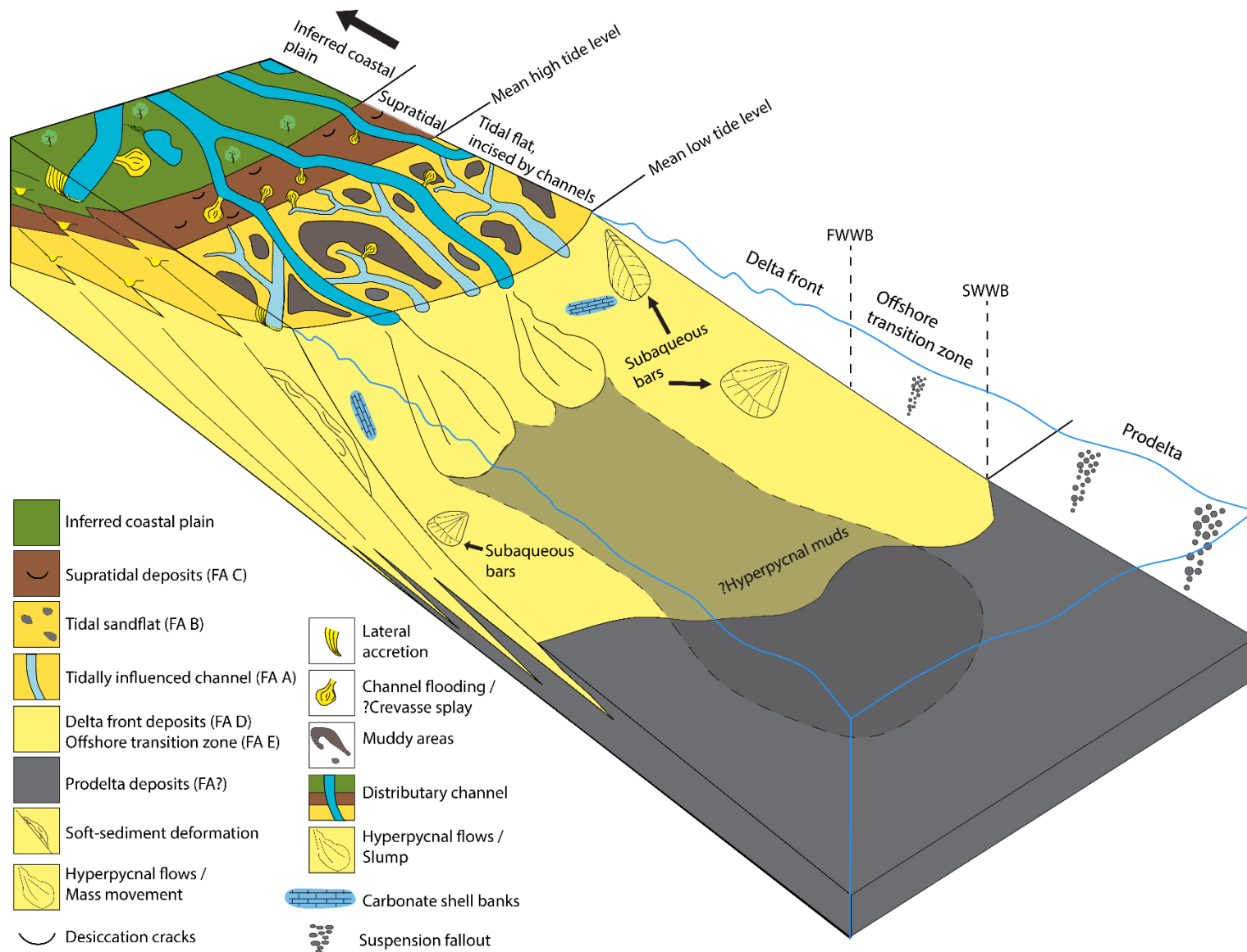
Figure 6.4: Depositional model of the Vardebukta Formation. It is envisaged as a mixed type delta based on the sedimentary processes interpreted from the different facies, documented in subchapter 4.1, and their association with other facies (documented in subchapter 4.3 Facies associations).

6.2 Sediment routing in the earliest Triassic Barents Sea

In the earliest Triassic (i.e. the Induan), sediments were predominantly supplied to the Barents Sea from three sources (Fig. 6.5). The Uralian system, associated with erosion of the Uralian mountains, was feeding sediments into the Barents Sea from the east and southeast (Puchkov, 2009; Glørstad-Clark et al., 2010; Norina et al., 2014). From the south, the Fennoscandian system was shedding sediments into the basin sourced from the shield terrane in northern Norway (Glørstad-Clark et al., 2010; Henriksen et al., 2011a; Hall et al., 2015; Eide et al., *in press*). Lastly, from the west-northwest, a third system was delivering sediments originating from Greenland/Arctic Canada (Mørk et al., 1982; Wignall et al., 1998; Riis et al., 2008; Lundschien et al., 2014; Pózer Bue and Andresen, 2014).

Interesting observations have been made about the deposits of the Vardebukta Formation warranting comparison to existing literature highlighting the sediment dispersal in the Barents Sea during the Induan. This subchapter will firstly present the large-scale setting that characterized the time interval to provide context about the sedimentary systems and their deposits. Secondly, the Vardebukta Formation and its mineralogical resemblance to the other systems will be discussed.

A) Greenland/Arctic Canada

Thin section photographs   QFL diagrams   Detrital zircon ages   Samarium-neodymium (sm-nd) ages
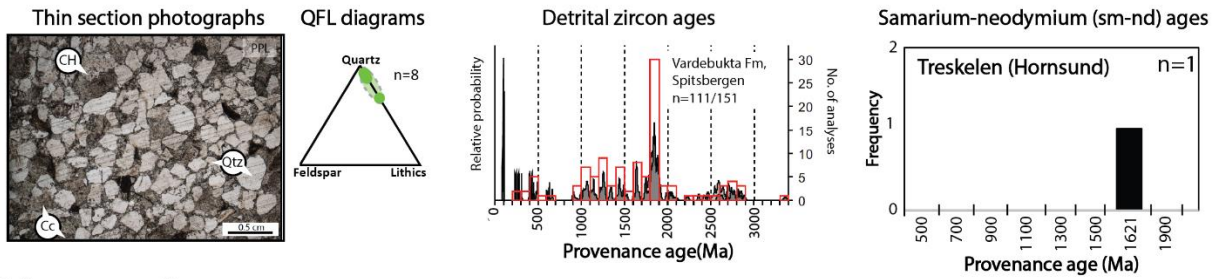
B) Fennoscandian
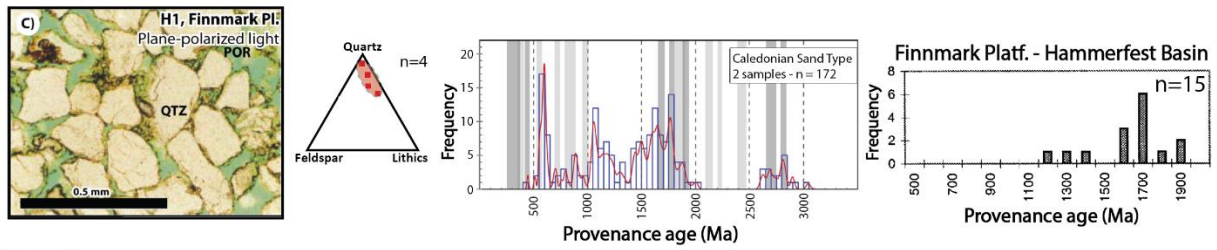
C) Uralian
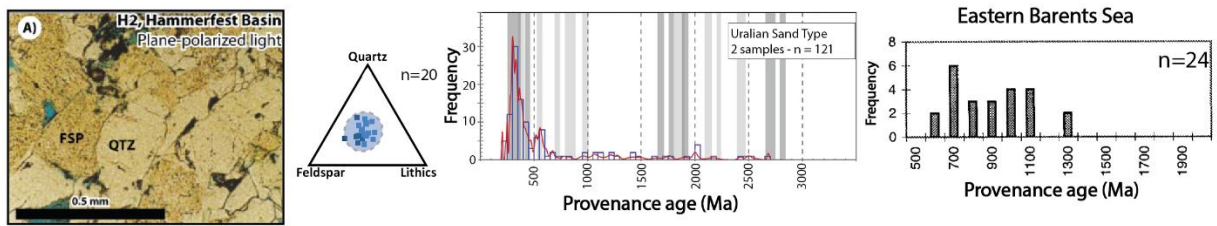
D) Sediment routing in the Barents Sea during the Induan
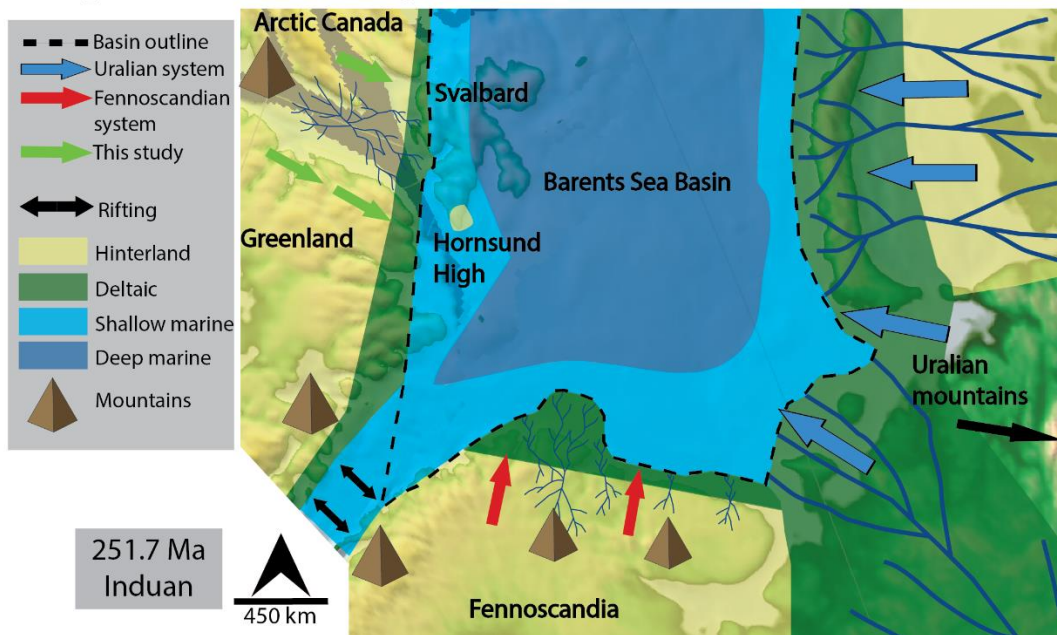
Figure 6.5: Sediment routing in the Induan in the Barents Sea showing the three main systems and their mineralogical characteristics. **A)** Characteristics of the sediments in the study area. From the left showing typical sandstone expression in thin section followed by a QFL-diagram of the point counted sandstones based on data from this study. Detrital zircon provenance ages diagram modified from Pózer Bue and Andresen (2014). Sm-Nd age diagram was created based on one Lower Triassic sample from Treskelen (Hornsund area) in Mørk (1999). **B)** Fennoscandian sediment characteristics expressed in the same manner as A) with the exception of detrital zircon ages being from Fleming et al. (2016) (Figure slightly modified). **C)** Uralian sediment characteristics as in B). **D)** Sediment routing in the Barents Sea during the Induan. The basin outline and the extent of the different sedimentary systems are based on multiple sources such as Glørstad-Clark et al. (2010), Henriksen et al. (2011a), Norina et al. (2014) and Eide et al. (*in press*) and the present study. QFL-diagrams in B-C) are modified from Eide et al. (*in press*) based on data from Mørk (1999), while thin sections and Sm-Nd provenance data in B-C) are from Mørk (1999). Background map is a plate tectonic model for the Triassic Barents Sea generously provided by Statoil.

The Uralian system has been well studied in the Barents Sea, highlighting both the sedimentological (e.g. Glørstad-Clark et al., 2010; Klausen et al., 2015) and mineralogical (e.g. Mørk, 1999; Fleming et al., 2016) characteristics. Lower Triassic sandstones sourced from this system provide mineralogically immature compositions that contain similar amounts of quartz, feldspar and lithic fragments. Sm-Nd isotopic signatures from Mørk (1999) reveal an average age of 776 million years (Ma) for the Lower Triassic sandstones in the eastern Barents Sea (Fig. 6.5C). Closer to the Fennoscandian margin, in the Nordkapp Basin and on the Bjarmeland Platform (Fig. 2.1), synchronous deposits display higher provenance ages (960-1630 Ma) representing a mixture of Uralian and Fennoscandian sediments (Mørk, 1999). Furthermore, Fleming et al. (2016) conducted detrital zircon U-Pb analysis of Triassic deposits in the Barents Sea. In the study, mineralogically immature deposits with a dominance of Late Paleozoic and Late Neoproterozoic zircon ages, similar to those of (Mørk, 1999), were classified as Uralian sand (Fig. 6.5C) (Fleming et al., 2016).

Contrarily, deposits from the Fennoscandian system show different mineralogical characteristics (Fig. 6.5B and Fig. 6.5D). This system has been briefly described by several authors (Hadler-Jacobsen et al., 2005; Glørstad-Clark et al., 2010; Henriksen et al., 2011a). More recently, Eide et al. (*in press*) investigated the system in more detail. Lower Triassic sandstones derived from this system show a mature composition, and preserve porosity to a much larger degree than the Uralian deposits (Mørk, 1999; Fleming et al., 2016), and have been interpreted to originate from late Neoproterozoic rocks in northern Norway (Fleming et al., 2016; Eide et al., *in press*). By Sm-Nd analysis, Mørk (1999) showed that Lower Triassic sandstones from the Finnmark Platform and

the Hammerfest Basin (Fig. 2.1) typically yield provenances ages between 1500 Ma and 1880 Ma, thus highlighting the contrast to the distinctly younger Uralian deposits. Similar results were found by Fleming et al. (2016) who labeled it Caledonian sand (Fig. 6.5B).

As this study has demonstrated, the deposits belonging to the Vardebukta Formation show an extreme enrichment in quartz and generally classify as quartz arenites or sublitharenites, depending on which classification scheme that is used (Fig. 5.1A-B). Similar findings were reported by Mørk (1999) from two Lower Triassic samples from Spitsbergen, hence supporting the petrographic findings of this study. Pózer Bue and Andresen (2014) investigated the provenance of Mesozoic sediments on Svalbard by detrital zircon U-Pb analysis. One of their samples was from the Vardebukta Formation and their results show a dominance of middle to late Paleoproterozoic and Mesoproterozoic grains (1900-1000 Ma), with some Archean grains and a negligible amount of Neoproterozoic, Paleozoic and Mesozoic grains (Fig. 6.5A). Additionally, one Lower Triassic Sm-Nd age of 1621 Ma from Treskelen (Sørkapp-Hornsund High area; Fig. 2.1) highlights the difference to the Uralian system (Fig. 6.5A).

When looking solely on the mineralogical characteristics of the sandstones (Mørk, 1999; This study) and the nature of the detrital zircon ages (cf. Pózer Bue and Andresen, 2014), the system originating from Greenland/Arctic Canada with extremely mature sands and high detrital zircon ages bears a closer resemblance to the Fennoscandian system, than it does the Uralian system (Fig. 6.5A-B and Fig. 6.6). Previous work has documented Caledonian basement on northeastern Greenland (e.g. Gee and Teben'kov, 2004), thus comparable provenance ages to the sediments of the Fennoscandian system, which was affected by the Caledonides, seems a natural consequence. As mentioned previously, sandstones from the Fennoscandian system are known to exhibit satisfactory reservoir properties (Mørk, 1999; Fleming et al., 2016; Mulrooney et al., 2017). Unfortunately, that is not the case for the deposits investigated in this study, as will be explained further below. However, possible reservoir intervals may exist closer to its source area (i.e. W/NW of the field localities) in similar, as well as synchronous deposits on Greenland/Arctic Canada. These issues will be addressed in subchapters 6.3 and 6.4.
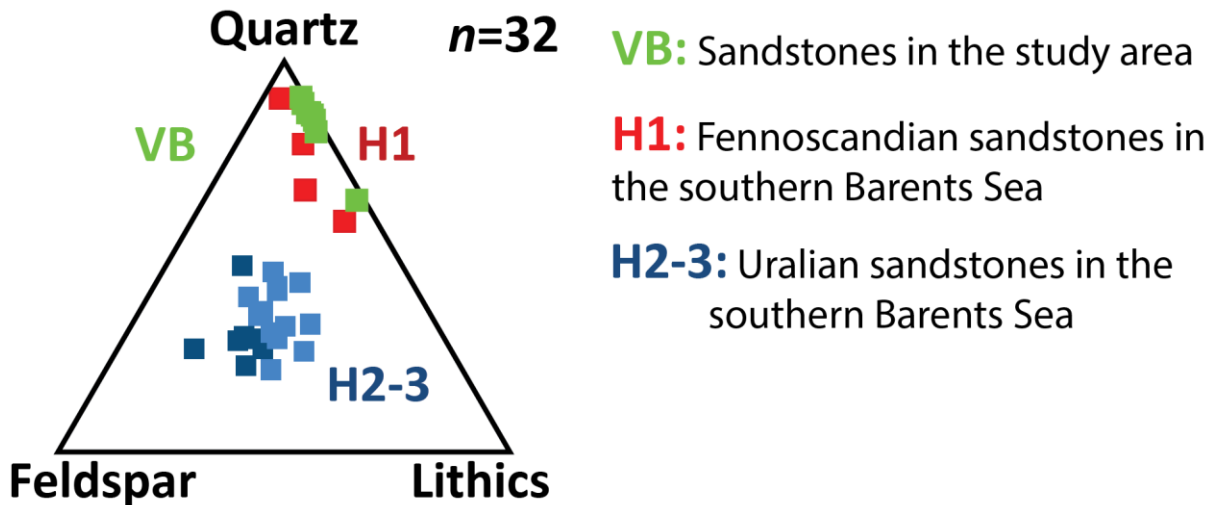
Figure 6.6: QmFLt-diagram showing sandstone composition of Induan deposits in the Barents Sea and Svalbard. Modified from (Eide et al., *in press*). Data for samples H1, H2 and H3 are based on petrographic data from Mørk (1999), while the VB samples are the results of this study.

6.3 The source area for the Vardebukta Formation

As evidenced by the petrographic investigations, the Vardebukta Formation has a highly mature mineralogy. The QmFLt and QFL diagrams generally classify the sandstones as sublitharenites and quartz arenites (Figure 5.1A-B), respectively. Furthermore, by using the QmFLt and QFL diagrams following Dickinson and Suczek (1979), it is possible to infer likely provenance terranes. The former diagram advocates that the sandstones were derived from a craton interior or a recycled orogen source area (Fig. 5.1C), while the latter only suggests a craton interior source area (Fig. 5.1D).

Detrital zircon U-Pb provenance data from the Vardebukta Formation by Pózer Bue and Andresen (2014) demonstrated a dominance of Mesoproterozoic and Paleoproterozoic zircons with a distinct population peak at 1800-1900 Ma. This supports the petrographic findings of the present study (e.g. Fig. 5.1), in the sense that the detrital zircon data also testify of a mature source area. Such an area is present to the W/NW of the study area (i.e. Greenland/Arctic Canada), where several studies have documented detrital zircon populations like those found in the Vardebukta Formation (Røhr et al., 2008; Kirkland et al., 2009; Røhr and Andersen, 2009; Anfinson et al., 2012).

However, the quartz-rich nature of the deposits, as well as the high detrital zircon U-Pb ages displaying few zircons younger than 1000 Ma (cf. Pózer Bue and Andresen, 2014) makes it problematic to establish one definite provenance terrane. Most likely, the deposits have been recycled several times and the original grains did, in all likelihood, form in contrasting tectonic environments. Andersen et al. (2016) addressed such limitations affiliated with detrital zircon provenance analysis.

Midwinter (2012) documented equally mature Early Triassic deposits from the Sverdrup Basin (Fig. 6.7) by point counting 24 thin sections. The quartz-rich nature of the deposits was attributed to recycling of Devonian foreland basin siliciclastics, derived from the Ellesmerian and the Greenland Caledonian mountains (Patchett et al., 2004; Anfinson et al., 2016). Detrital zircon analysis of Lower Triassic deposits in the Sverdrup Basin has yielded results that suggest a partially similar origin to the recycled deposits in the Vardebukta Formation (cf. Miller et al., 2006; Pózer Bue and Andresen, 2014).

Figure 6.7: Present day map showing some of the discussed areas in this chapter. The approximate position of Svalbard in the Induan is based on Cocks and Torsvik (2006). Kap Stosch denotes the area studied by Oftedal et al. (2005). Satellite images © Google.

As previously noted, all the studied thin sections display a high content of quartz and classify as mineralogical mature deposits (Table 5.2). At the same time, the grains do not demonstrate an equal textural maturity. Generally, the deposits are characterized by being moderately sorted with poorly rounded to rounded grains with low to medium sphericity (e.g. FES20, Fig. 5.6). Furthermore, in the samples not dominated by sutured and concavo-convex contacts, the grains generally display at least one smooth curved edge (e.g. sample FES6; Fig. 5.4 and FES20; Fig. 5.6), like the grains in the samples with abundant sutured contacts (e.g. sample FES3; Fig. 5.3). This may suggest that prior to erosion and subsequent deposition in the Vardebukta Formation, these grains were deeply buried and dominated by sutured as well as concavo-convex contacts. The presence of many quartzite grains (i.e. polycrystalline quartz, cf. Fig. 5.8) within the samples strengthens the notion of the source having been deeply buried at some point. A similar scenario is inferred for the porous sandstones from the Finnmark Platform (Fig. 2.1) derived from the mainland of northern Norway (cf. Fig. 5E; Mørk, 1999).

From the petrographic investigations of this study, one of the samples (Sample SES7; Fig. 5.8) shows a bimodal grain size distribution (Fig. 6.8). The coarse fraction of coarse to very coarse sand generally appears as well rounded spherical grains (Fig. 5.8), while the finer grained fraction dominated by fine sand is angular to poorly rounded with lower sphericity (Fig. 5.8). Such a grain size distribution is often attributed to two different sediment source areas as in Oftedal et al. (2005), where Induan deposits were investigated in a rift basin on northeastern Greenland (see Fig. 6.7 for location). In their study, well-rounded pebble- and cobble-sized quartzite, granite and gneissic granite clasts were credited to long transport or several events of transport, most likely from a basement source area. The angular limestone clasts were interpreted to stem from footwall uplift associated with Early Triassic rifting representing short transport (Oftedal et al., 2005).

The 750 meters thick Wordie Creek Formation was deposited within the Induan (Oftedal et al., 2005), which is just 2.2 Myr (million years) long, witnessing of very high sedimentation rates. It coincided with Late Paleozoic and Early Mesozoic tectonic activity in the North Atlantic Barents Sea, which have been reported by several authors (e.g. Seidler, 2000; Wignall and Twitchett, 2002; Müller et al., 2005), and likely caused the footwall uplift mentioned previously.
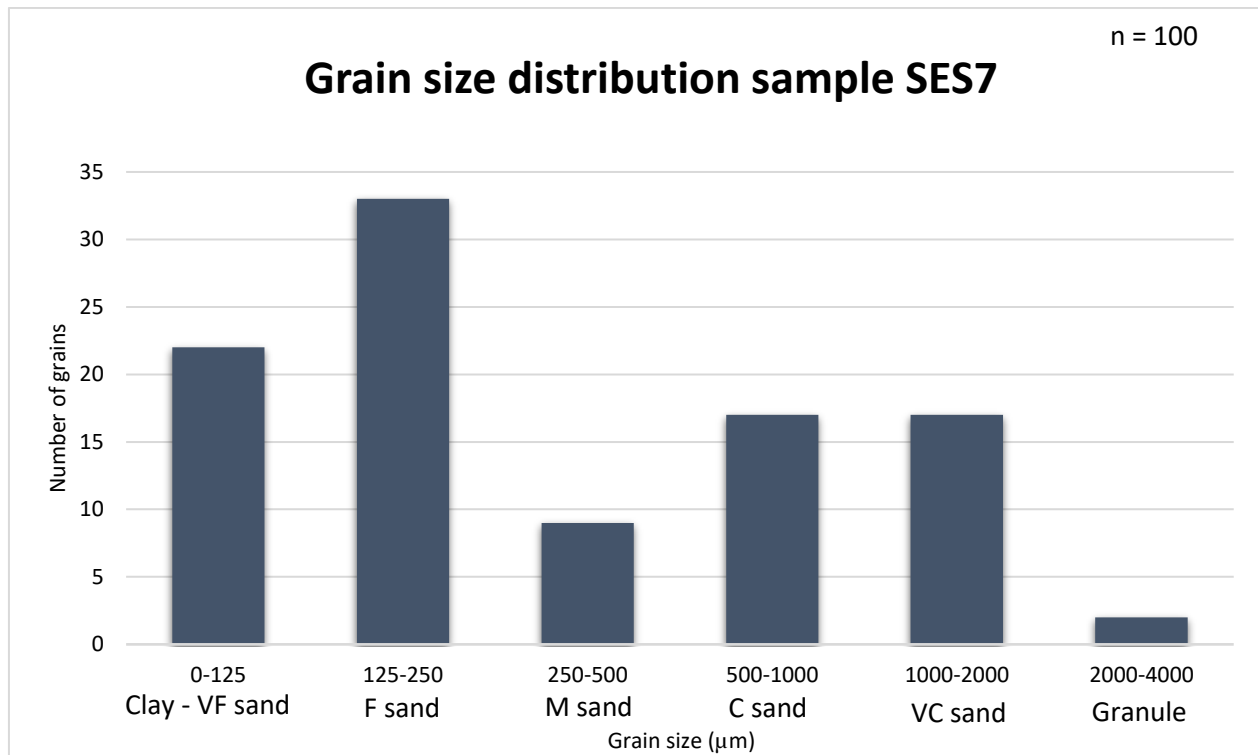
Figure 6.8: Results of the grain size point counting of sample SES7. The column chart displays a clear bimodal sediment distribution with peaks at fine sand as well as coarse sand and granule. Thin section photos of the sample are shown in Fig. 5.8.

Furthermore, the mineralogical maturity of the sandstones in the Vardebukta Formation could falsely be attributed to long sediment transport. However, as the petrographic investigations have shown, this is not in correspondence with the degree of textural immaturity observed in most of the samples. This implies that the main source area must be relatively close. Therefore, this study envisages a similar case as in Oftedal et al. (2005) for the Vardebukta Formation. The generally moderately sorted subangular to poorly rounded grains with low to medium sphericity, which dominate the samples, are inferred to originate from tectonic uplift and subsequent erosion. A similar scenario was proposed in Mørk (2015) where continental blocks between Svalbard and Greenland were mentioned as a potential source for the Sassendalen Group (Fig. 2.5). Contrarily, the coarse sand to granule-sized grains that are well rounded with high sphericity must have been transported further, and are possibly derived from a basement source area. Another explanation for the well-rounded grains is that they have been transported far in an earlier cycle. These grains are only found in one of the studied thin sections (Sample SES7; Fig.

5.8) implying that their sediment source may be more prominent further landwards in the sedimentary system.

Recent work by Heggem (2017) suggested the Sørkapp-Hornsund High (Fig. 6.5), which was acting as a subaerially exposed basement high until mid-Induan (e.g. Nakrem and Mørk, 1991), as a potential local source area for the Vardebukta Formation. This is due to the rather unique detrital U-Pb zircon signature of the Vardebukta Formation compared to the overlying Tvillingodden and Bravaisberget Formations (cf. Pózer Bue and Andresen, 2014; Heggem, 2017), which are all interpreted to stem from northeastern Greenland/Arctic Canada (e.g. Mørk et al., 1982). If this is the case, then the grains speculated of originating from tectonic uplift as mentioned earlier in this subchapter, may also to some extent be derived from the Sørkapp-Hornsund High (Fig. 6.5). However, as Heggem (2017) rightfully pointed out, in order to test this hypothesis samples from the basement high as well as the unconformably overlying basal dimictic conglomerates (Worsley and Mørk, 1978; Vigran et al., 2014) should be analyzed for detrital zircon ages, and further compared to the findings of Pózer Bue and Andresen (2014) from the Vardebukta Formation at Festningen. Additionally, petrographic investigations should be carried out and compared to the present study.

As mentioned previously, the Vardebukta Formation, as well as the entire Lower Triassic on Svalbard are believed to be sourced from the west (Mørk et al., 1982; Mørk, 1999; Riis et al., 2008; Lundschien et al., 2014; Pózer Bue and Andresen, 2014). The deposition was contemporaneous with the thick clastic Wordie Creek Formation investigated by Oftedal et al. (2005), which was interpreted to be partially sourced from footwall uplift. A comparable situation is inferred for the Vardebukta Formation, with tectonic activity to the west of the study area creating topography acting as a major denudation area.

In the Induan, rifting was ongoing between Greenland and mid Norway. Consequently, large amounts of sediments were deposited in the ensuing half-grabens as shown by Müller et al. (2005) and Oftedal et al. (2005). Contemporary with the rifting, deltaic systems were prograding into basins in a distal position to the rift (e.g. the Vardebukta Formation). It is likely that this distal sedimentation was also caused by tectonic uplift by the rift, which created increased topography around the rift leading to increased erosion and sediment transport away from the rift. An analog

from Africa shows a sedimentary system receiving abundant sediment from tectonic uplift, as part of the East African Rift system (Fig. 6.9). Although this sedimentary system is not the same as in this study in terms of sedimentology and processes, it is not unimaginable with a similar tectonic scenario influencing or controlling the deposition of the Vardebukta Formation. Such topographic highs associated with rifting as known from the literature (e.g. ten Brink and Stern, 1992; Daradich et al., 2003).
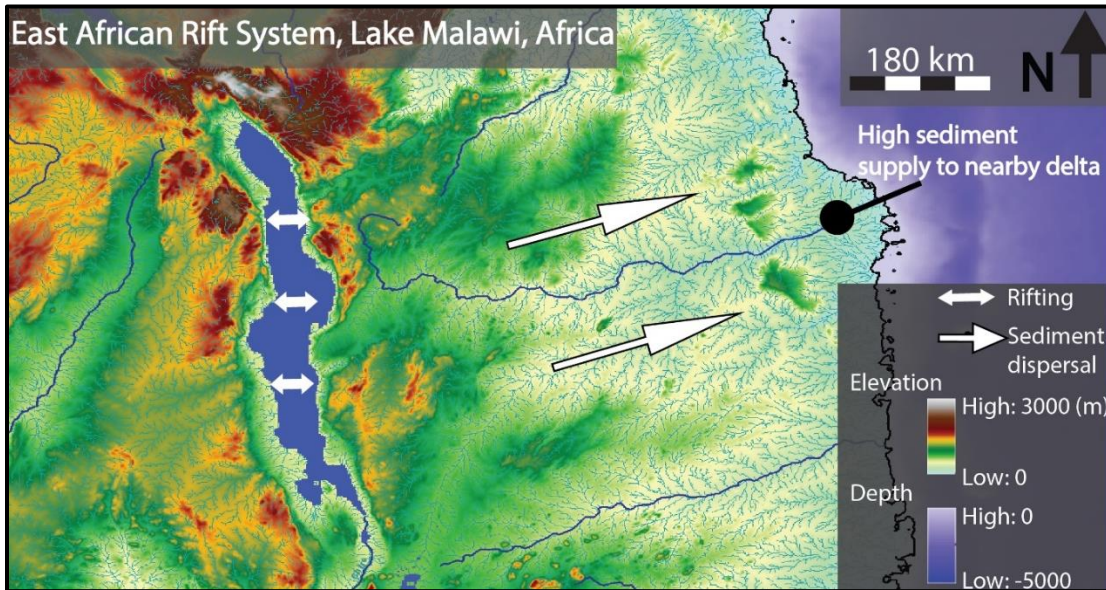
Figure 6.9: Illustration showing the rifting and associated rift shoulder uplift occurring in Africa today. The uplift creates a large denudation area supplying vast amounts of sediments distributed to a nearby delta. A similar tectonic scenario is suggested to have affected the deposition of the Vardebukta Formation. Modified ArcGIS map and the used data is from the ETOPO1 dataset (Amante and Eakins, 2009).

6.4 Reservoir properties and implications for regional reservoir exploration

The Triassic deposits in the Barents Sea are generally associated with rather poor reservoir properties (Fleming et al., 2016). However, the ubiquity of clean, quartz-rich sandstones during the Induan along the cratonward margins in both northern Norway (Mørk, 1999; Fleming et al., 2016) and on Svalbard has important implications for possible reservoir intervals in this area.

The stylolite interfaces seen at several of the sutured contacts coupled with concavo-convex contacts as well as the abundant cementation, effectively remove most of the porosity in the sandstones from the Vardebukta Formation, as evidenced from the two stained thin sections (mentioned in chapter 3, seen in Fig. 5.3 and Fig. 5.4) exhibiting no porosity. This is largely due to the burial history (i.e. temperature and depth) for the sediments along western Spitsbergen,

which have been buried to depths of up to 4-5 kilometers by the fold-thrust belt (Michelsen and Khorasani, 1991). However, a few of the sandstones studied in thin section (e.g. thin section FES3; Fig. 5.3) are well-sorted fine to very fine sublitharenites with a predominance of rounded grains with high to moderate sphericity. Such sandstones could potentially be good reservoirs under different burial conditions.

Deposits of the same age and composition have been documented by Midwinter (2012) from the Early Triassic Bjorne Formation in the Sverdrup Basin (Fig. 6.7). In the study, moderate to very well sorted quartz-rich sandstones were found to exhibit favorable reservoir properties. In some of the samples from the formation, an average porosity of 22% was estimated while all the samples yielded excellent permeabilities in the range of 3-7 darcy (Hu and Dewing, 2010). These sandstones may partially originate from the same source area as the Vardebukta Formation, as contemplated in subchapter 6.2.

Therefore, it is possible that sandstones with desirable reservoir characteristics exist along northeastern Greenland, both on- and offshore, in the most likely continental deposits, which serve as the proximal source for the deposits in the Vardebukta Formation along western Spitsbergen. However, the burial conditions are uncertain for these deposits so further analyses are needed to better understand their properties. The closest available data is from Stoker et al. (2017), which show burial depths of 3-10 kilometers for Triassic strata in the Danmarkshavn Basin (Fig. 6.7) with the shallowest burial occurring closest to the coast.

For the Barents Sea, ramifications of these westerly derived sediments are poorly constrained. Little is known of the strata north of Bjørnøya (Fig. 2.1), as wells are yet to be drilled in this area (NPD, 2017, http://gis.npd.no/factmaps/html_21/). It is not inconceivable that Induan reservoir sandstones, potentially deposited from prograding sedimentary systems similar to the Vardebukta Formation on western Spitsbergen as well as from the Sørkapp-Hornsund High (Fig. 6.5), can be found in the Barents Sea, possibly on the Edgeøya Platform or in the Sørkapp Basin (Fig. 2.1). Seismic and thickness maps of the Sassendalen Group from these locations show the development of stratal packages up to 1200 meters thick (Fig. 3 and Fig. 4; Anell et al., 2014). However, the main constituents are most likely the basinal mud dominated Vikinghøgda and Botneheia Formation (Fig. 2.1A).

7 Conclusions

The aim of this thesis was to establish a viable depositional model for the Vardebukta Formation, to investigate its source-to-sink perspectives, to explore reservoir properties of the formation and synchronous deposits in the Arctic, and furthermore to investigate implications for regional reservoir exploration. The depositional model was established by sedimentological analysis of outcrops on Svalbard, while source-to-sink and reservoir aspects were probed by detailed petrographic work. By incorporating available provenance data, the results of this study have culminated in the following conclusions:

- The Vardebukta Formation was deposited in a mixed type delta with tide-influenced channels as well as the development of tidal flats with desiccation cracks in front of a storm and wave-dominated shelf.

- The depositional environment was characterized by extensive biogenic carbonate production as evidenced by the abundant calcite cement and fossils observed in thin section and shell layers observed in outcrop, making most of the calcite cement early diagenetic.

- Later generations of cement are found, although in subordinate amounts, and the extent of these are poorly constrained.

- Most of the sediments in the Vardebukta Formation express a high compositional maturity, but a low textural maturity, indicating that the source area must have been relatively close and consisted of mature sandstones.

- The relative abundance of quartzite grains and the peculiar curved shape of most of the grains imply that prior to erosion and subsequent deposition in the Vardebukta Formation, the grains were deeply buried giving them this characteristic shape.

- The Vardebukta Formation displays evidence of being supplied with sediments from two contrasting source areas as evidenced by the bimodality expressed in one of the thin sections.

- The Vardebukta Formation is interpreted to have been fed with sediments from tectonically uplifted areas associated with contemporaneous rifting between eastern Greenland and mid Norway.

- Compared to the other sedimentary systems present in the Induan Barents Sea, the Vardebukta Formation displays a much higher likeness to the Fennoscandian System than it does the Uralian system.

- The reservoir properties of the Vardebukta Formation along western Spitsbergen are very poor due to abundant calcite and quartz cementation. However, more favorable reservoir properties connected to the Vardebukta Formation may exist on northeastern Greenland/Arctic Canada and in the Sørkapp Basin or on the Edgeøya Platform.

For further research, this study suggests that the following is investigated in more detail:

- Investigation of Induan deposits on northeastern Greenland/Arctic Canada focusing on sedimentology, provenance ages and petrographic characteristics to unravel the source area for the Vardebukta Formation.

- Investigation of detrital zircon ages and mineralogy for all pre-Triassic basement rocks in Greenland/Arctic Canada to better constrain which have been prolific sources for the deposits in the Vardebukta Formation.

- Investigation of Induan deposits on northeastern Greenland/Arctic Canada regarding tectonic activity and decipher if tectonic uplift created topographic highs acting as major denudation areas supplying sediments eastwards.

- Investigation of the Sørkapp-Hornsund High with emphasis on sediment characteristics for the sake of determining its impact as a sediment source for the Vardebukta Formation.

- Combine the findings of this study with detailed sedimentary, petrographic and structural work from the highly tectonized outcrop at Selmaneset at Oscar II Land. Such work will be presented by master students from NTNU in 2018. Together, this will provide a more comprehensive understanding of the Vardebukta Formation and its depositional conditions.

- Investigate if Induan sands from Svalbard reached the Barents Sea through shallow stratigraphic boreholes strategically placed on the Edgeøya Platform and in the Sørkapp Basin.

References

Ainsworth, B. R., Vakarelov, B. K., and Nanson, R. A., 2011, Dynamic spatial and temporal prediction of changes in depositional processes on clastic shorelines: Toward improved subsurface uncertainty reduction and management: AAPG Bulletin, 95, p. 267-297.

Allen, J. R. L., 1982, Sedimentary Structures: Their Character and Physical Basis, Developments in Sedimentology, Elsevier, Amsterdam, 30A, p. 593.

Amante, C., and Eakins, B. W., 2009, ETOPO1 1 Arc-Minute Global Relief Model: Procedures, Data Sources And Analysis, US Department of Commerce, National Oceanic and Atmospheric Administration, National Environmental Satellite, Data, and Information Service, National Geophysical Data Center, Marine Geology and Geophysics Division Colorado, 19 p.

Andersen, T., Kristoffersen, M., and Elburg, M. A., 2016, How far can we trust provenance and crustal evolution information from detrital zircons? A South African case study: Gondwana Research, 34, p. 129-148.

Anell, I., Braathen, A., and Olaussen, S., 2014, The Triassic — Early Jurassic of the northern Barents Shelf: a regional understanding of the Longyearbyen CO_2 reservoir: Norwegian Journal of Geology, 94, p. 83-98.

Anfinson, O. A., Embry, A. F., and Stockli, D. F., 2016, Geochronologic constraints on the Permian–Triassic northern source region of the Sverdrup basin, Canadian Arctic Islands: Tectonophysics, 691, p. 206-219.

Anfinson, O. A., Leier, A. L., Embry, A. F., and Dewing, K., 2012, Detrital zircon geochronology and provenance of the Neoproterozoic to Late Devonian Franklinian basin, Canadian Arctic Islands: Geological Society of America Bulletin, 124, no. 3-4, p. 415-430.

Arnott, R. W., and Southard, J. B., 1990, Exploratory flow-duct experiments on combined-flow bed configurations, and some implications for interpreting storm-event stratification: Journal of Sedimentary Research, 60, no. 2, p. 211-219.

Baas, J. H., Best, J. L., and Peakall, J., 2016, Predicting bedforms and primary current stratification in cohesive mixtures of mud and sand: Journal of the Geological Society, 173, no. 1, p. 12-45.

Bann, K. L., Fielding, C. R., MacEachern, J. A., and Tye, S. C., 2004, Differentiation of estuarine and offshore marine deposits using integrated ichnology and sedimentology: Permian Pebbley Beach Formation, Sydney Basin, Australia, *in* McIlroy, D., ed., The Application of Ichnology to Palaeoenvironmental and Stratigraphic Analysis, Geological Society of London, Special Publications, 228, p. 179-212.

Bergh, S. G., Braathen, A., and Andresen, A., 1997, Interaction of basement-involved and thin-skinned tectonism in the Tertiary fold-thrust belt of central Spitsbergen, Svalbard: AAPG Bulletin, 81, no. 4, p. 637-661.

Bhattacharya, J. P., 2010, Deltas, *in* James, N. P., and Dalrymple, R. W., eds., Facies models 4, The Geological Association of Canada, St John's, p. 233-264.

Bhattacharya, J. P., and MacEachern, J. A., 2009, Hyperpycnal rivers and prodeltaic shelves in the Cretaceous seaway of North America: Journal of Sedimentary Research, 79, no. 4, p. 184-209.

Bjørkum, P. A., and Walderhaug, O., 1990, Geometrical arrangement of calcite cementation within shallow marine sandstones: Earth-Science Reviews, 29, no. 1-4, p. 145-161.

Blomeier, D., 2015a, Historical Geology - Carboniferous, *in* Dallmann, W., ed., Geoscience Atlas of Svalbard, Norwegian Polar Institute, Report Series, 148, p. 106-109.

Blomeier, D., 2015b, Historical Geology - Permian, *in* Dallmann, W., ed., Geoscience Atlas of Svalbard, Norwegian Polar Institute, Report Series, 148, p. 110-113.

Boggs, S. J., 2014, Principles of Sedimentology and Stratigraphy, 5th edn.: Harlow, Pearson Education Limited, 594 p.

Boyd, R., 2010, Transgressive wave-dominated coasts, *in* Dalrymple, R., ed., Facies Models 4, Geological Association of Canada, St John's, p. 265-294.

Boyd, R., Dalrymple, R., and Zaitlin, B. A., 1992, Classification of clastic coastal depositional environments: Sedimentary Geology, 80, p. 139-150.

Boyd, R., Suter, J., and Penland, S., 1989, Sequence stratigraphy of the Mississippi delta: Gulf Coast Association of Geological Societies, Transactions, 39, p. 331-340.

Braathen, A., Bergh, S. G., and Maher, H. D., 1999, Application of a critical wedge taper model to the Tertiary transpressional fold-thrust belt on Spitsbergen, Svalbard: Geological Society of America Bulletin, 111, no. 10, p. 1468-1485.

Cheel, R. J., and Leckie, D. A., 1993, Hummocky cross-stratification: Sedimentology review, 1, p. 103-122.

Cocks, L. R. M., and Torsvik, T. H., 2006, European geography in a global context from the Vendian to the end of the Palaeozoic, *in* Gee, D. G., and Stephenson, R. A., eds., European Lithosphere Dynamics, Geological Society of London, Memoirs, 32, p. 83-95.

Cocks, L. R. M., and Torsvik, T. H., 2007, Siberia, the wandering northern terrane, and its changing geography through the Palaeozoic: Earth-Science Reviews, 82, no. 1, p. 29-74.

Coe, A. L., and Church, K. D., 2003, Sequence Stratigraphy, *in* Coe, A. L., ed., The Sedimentary Record of Sea-Level Change, Cambridge University Press, New York, p. 57-98.

Collinson, J. D., Mountney, N. P., and Thompson, D. B., 2006, Sedimentary Structures, 3rd edn.: Edinburgh, Scotland, Terra Publishing, 292 p.

Dallmann, W., 2015, Historical Geology - Palaeogene, *in* Dallmann, W., ed., Geoscience Atlas of Svalbard, Norwegian Polar Institute, Report Series 148, p. 126-129.

Dallmann, W., Elvevold, S., Majka, J., and Piepjohn, K., 2015, Tectonics and tectonothermal events, *in* Dallmann, W., ed., Geoscience Atlas of Svalbard, Norwegian Polar Institute, Report Series, 148, p. 175-217.

Dallmann, W. K., 1999, Lithostratigraphic Lexicon of Svalbard: Review and Recommendations for Nomenclature Use: Upper Palaeozoic to Quaternary Bedrock, Norwegian Polar Institute, 318 p.

Dalrymple, R. W., 1992, Tidal depositional systems, *in* Walker, R. G., and James, N. P., eds., Facies Models: Response to Sea Level Change, Geological Association of Canada, St John's, Newfoundland, p. 195-218.

Dalrymple, R. W., 2010, Tidal depositional systems, *in* James, N. P., and Dalrymple, R., eds., Facies Models 4, Geological Association of Canada, St John's, p. 201-231.

Daradich, A., Mitrovica, J. X., Pysklywec, R. N., Willett, S. D., and Forte, A. M., 2003, Mantle flow, dynamic topography, and rift-flank uplift of Arabia: Geology, 31, no. 10, p. 901-904.

Davis Jr, R. A., 2012, Tidal signatures and their preservation potential in stratigraphic sequences, *in* Davis Jr, R. A., and Dalrymple, R. W., eds., Principles of tidal sedimentology, Springer, New York, p. 35-55.

Dickinson, W. R., Beard, L. S., Brakenridge, G. R., Erjavec, J. L., Ferguson, R. C., Inman, K. F., Knepp, R. A., Lindberg, F. A., and Ryberg, P. T., 1983, Provenance of North American Phanerozoic sandstones in relation to tectonic setting: Geological Society of America Bulletin, 94, no. 2, p. 222-235.

Dickinson, W. R., and Suczek, C. A., 1979, Plate tectonics and sandstone compositions: AAPG Bulletin, 63, no. 12, p. 2164-2182.

Dimakis, P., Braathen, B. I., Faleide, J. I., Elverhøi, A., and Gudlaugsson, S. T., 1998, Cenozoic erosion and the preglacial uplift of the Svalbard–Barents Sea region: Tectonophysics, 300, no. 1, p. 311-327.

Duke, W. L., Arnott, R., and Cheel, R. J., 1991, Shelf sandstones and hummocky cross-stratification: new insights on a stormy debate: Geology, 19, no. 6, p. 625-628.

Dumas, S., and Arnott, R., 2006, Origin of hummocky and swaley cross-stratification—The controlling influence of unidirectional current strength and aggradation rate: Geology, 34, no. 12, p. 1073-1076.

Dunham, R. J., 1962, Classification of carbonate rocks according to depositional textures, *in* Ham, W. E., ed., Classification of Carbonate Rocks, AAPG, 1, p. 108-121.

Ehrenberg, S. N., Pickard, N. A. H., Henriksen, L. B., Svana, T. A., Gutteridge, P., and Macdonald, D., 2001, A depositional and sequence stratigraphic model for cold-water, spiculitic strata based on the Kapp Starostin Formation (Permian) of Spitsbergen and equivalent deposits from the Barents Sea: AAPG Bulletin, 85, no. 12, p. 2061-2087.

Eide, C. H., Klausen, T. G., Katkov, D., Suslova, A. A., and Helland-Hansen, W., *in press*, Linking an Early Triassic delta to antecedent topography: Source-to-sink study of the southwestern Barents Sea margin: Geological Society of America Bulletin.

Elvevold, S., Dallmann, W., and Blomeier, D., 2007, Geology of Svalbard, Finnsnes, Norwegian Polar Institute, 36 p.

Emery, D., and Myers, K. J., 1996, Sequence Stratigraphy, Oxford, Blackwell, 297 p.

Faleide, J. I., Gudlaugsson, S. T., and Jacquart, G., 1984, Evolution of the western Barents Sea: Marine and Petroleum Geology, 1, no. 2, p. 129-150.

Faleide, J. I., Tsikalas, F., Breivik, A. J., Mjelde, R., Ritzmann, O., Engen, O., Wilson, J., and Eldholm, O., 2008, Structure and evolution of the continental margin off Norway and the Barents Sea: Episodes, 31, no. 1, p. 82-91.

Fleming, E. J., Flowerdew, M. J., Smyth, H. R., Scott, R. A., Morton, A. C., Omma, J. E., Frei, D., and Whitehouse, M. J., 2016, Provenance of Triassic sandstones on the southwest Barents Shelf and the implication for sediment dispersal patterns in northwest Pangaea: Marine and petroleum geology, 78, p. 516-535.

Folk, R. L., 1966, A review of grain-size parameters: Sedimentology, 6, p. 73-93.

Fürsich, F. T., 1982, Rhythmic bedding and shell bed formation in the Upper Jurassic of East Greenland, Cyclic and event stratification, Springer, p. 208-222.

Gabrielsen, R. H., Færseth, R. B., Jensen, L. N., Kalheim, J. E., and Riis, F., 1990, Structural Elements of the Norwegian Continental Shelf. Part 1: The Barents Sea Region: Norwegian Petroleum Directorate Bulletin, 6, p. 33.

Gee, D. G., and Teben'kov, A. M., 2004, Svalbard: a fragment of the Laurentian margin, *in* Gee, D. G., and Pease, V. L., eds., The Neoproterozoic Timanide Orogen of Eastern Baltica, Geological Society of London, Memoirs, 32, p. 191-206.

Glørstad-Clark, E., Faleide, J. I., Lundschien, B. A., and Nystuen, J. P., 2010, Triassic seismic sequence stratigraphy and paleogeography of the western Barents Sea area: Marine and Petroleum Geology, 27, no. 7, p. 1448-1475.

Goldstein, R. H., Anderson, J. E., and Bowman, M. W., 1991, Diagenetic responses to sea-level change: Integration of field, stable isotope, paleosol, paleokarst, fluid inclusion, and cement stratigraphy research to determine history and magnitude of sea-level fluctuation, *in* Franseen, E. K., Watney, W. L., Kendall, C. G. S., and Ross, W., eds., Sedimentary Modeling: Computer simulations and methods for improved parameter definition, Kansas Geological Survey, 233, p. 139-162.

Grant, R. P., 1985, Cathodoluminescence petrography of syntectonic quartz fibres: Journal of Structural Geology, 7, no. 5, p. 541-553.

Grundvåg, S. A., 2015, Historical Geology - Cretaceous *in* Dallmann, W., ed., Geoscience Atlas of Svalbard, Norwegian Polar Institute, Report Series 148, p. 122-125.

Gudlaugsson, S. T., Faleide, J. I., Johansen, S. E., and Breivik, A. J., 1998, Late Palaeozoic structural development of the south-western Barents Sea: Marine and Petroleum Geology, 15, no. 1, p. 73-102.

Hadler-Jacobsen, F., Johannessen, E. P., Ashton, N., Henriksen, S., Johnson, S. D., and Kristensen, J. B., 2005, Submarine fan morphology and lithology distribution: a predictable function of sediment delivery, gross shelf-to-basin relief, slope gradient and basin topography, *in* Doré, A. G., and Vining, B. A., eds., Petroleum Geology: North-West Europe and Global Perspectives — Proceedings of the 6th Petroleum Geology Conference, Geological Society of London, 1, p. 1121-1145.

Hall, A. M., Sarala, P., and Ebert, K., 2015, Late Cenozoic deep weathering patterns on the Fennoscandian shield in northern Finland: a window on ice sheet bed conditions at the onset of Northern Hemisphere glaciation: Geomorphology, 246, p. 472-488.

Hampson, G. J., and Storms, J. E., 2003, Geomorphological and sequence stratigraphic variability in wave-dominated, shoreface-shelf parasequences: Sedimentology, 50, no. 4, p. 667-701.

Harland, W. B., 1997, The Geology of Svalbard, Geological Society of London, 521 p.

Hassan, M. H. A., Johnson, H. D., Allison, P. A., and Abdullah, W. H., 2013, Sedimentology and stratigraphic development of the upper Nyalau Formation (Early Miocene), Sarawak, Malaysia: a mixed wave-and tide-influenced coastal system: Journal of Asian Earth Sciences, 76, p. 301-311.

Heggem, B., 2017, An analysis of facies in the De Geerdalen Formation and provenance across the Middle to Late Triassic boundary on Spitsbergen, Svalbard, [Master thesis]: Norwegian University of Science and Technology, 175 p.

Henriksen, E., Bjørnseth, H. M., Hals, T. K., Heide, T., Kiryukhina, T., Kløvjan, O. S., Larssen, G. B., Ryseth, A. E., Rønning, K., Sollid, K., and Stoupakova, A. V., 2011a, Uplift and erosion of the greater Barents Sea: impact on prospectivity and petroleum systems, *in* Spencer, A. M., Embry, A. F., Gautier, D. L., Stoupakova, A. V., and Sørensen, K., eds., Arctic Petroleum Geology, Geological Society of London, Memoirs, 35, p. 271-281.

Henriksen, E., Ryseth, A. E., Larssen, G. B., Heide, T., Rønning, K., Sollid, K., and Stoupakova, A. V., 2011b, Tectonostratigraphy of the greater Barents Sea: implications for petroleum systems, *in* Spencer, A. M., Embry, A. F., Gautier, D. L., Stoupakova, A. V., and Sørensen, K., eds., Arctic Petroleum Geology, Geological Society of London, Memoirs, 35, p. 163-195.

Howell, J. A., and Flint, S. S., 2003, Siliciclastics case study: the Book Cliffs, *in* Coe, A. L., ed., The Sedimentary Record of Sea-Level Change, Cambridge University Press, New York, p. 135-208.

Hu, K., and Dewing, K., 2010, Geological and Geochemical Data from the Canadian Arctic Islands. Part X: Core petrophysical data from petroleum exploration boreholes, Geological Survey of Canada, Open File 6669, CD-ROM.

Jopling, A. V., 1963, Hydraulic studies on the origin of bedding: Sedimentology, 2, no. 2, p. 115-121.

Kirkland, C. L., Pease, V., Whitehouse, M. J., and Ineson, J. R., 2009, Provenance record from Mesoproterozoic-Cambrian sediments of Peary Land, North Greenland: implications for the ice-covered Greenland Shield and Laurentian palaeogeography: Precambrian Research, 170, no. 1, p. 43-60.

Klausen, T. G., Ryseth, A. E., Helland-Hansen, W., Gawthorpe, R., and Laursen, I., 2015, Regional development and sequence stratigraphy of the Middle to Late Triassic Snadd formation, Norwegian Barents Sea: Marine and Petroleum Geology, 62, p. 102-122.

Klausen, T. G., Torland, J. A., Eide, C. H., Alaei, B., Olaussen, S., and Chiarella, D., *in press*, Clinoform development and topset evolution in a mud-rich delta–the Middle Triassic Kobbe Formation, Norwegian Barents Sea: Sedimentology.

Knaust, D., 2017, Atlas of Trace Fossils in Well Core: Appearance, Taxonomy and Interpretation, Springer, 209 p.

Komar, P. D., and Miller, M. C., 1975, The initiation of oscillatory ripple marks and the development of plane-bed at high shear stresses under waves: Journal of Sedimentary Research, 45, no. 3, p. 697-703.

Kraft, J. C., Biggs, R. B., and Halsey, S. D., 1973, Morphology and vertical sedimentary sequence models in Holocene transgressive barrier systems, *in* Coates, D. R., ed., Coastal Geomorphology, State University of New York, Binghampton, p. 321-354.

Krajewski, K. P., 2008, The Botneheia Formation (Middle Triassic) in Edgeøya and Barentsøya, Svalbard: lithostratigraphy, facies, phosphogenesis, paleoenvironment: Polish Polar Research, 29, p. 319-364.

Longiaru, S., 1987, Visual comparators for estimating the degree of sorting from plane and thin sections: Journal of Sedimentary Petrology, 57, p. 791-794.

Lord, G. S., Mørk, A., and Høy, T., 2017, Sequence patterns in the Triassic Succession of Svalbard and the northern Barents Sea, *in* Lord, G. S., ed., Sequence stratigraphy and facies development of the Triassic succession of Svalbard and the northern Barents Sea, Norwegian University of Science and Technology, Trondheim, Doctoral thesis, p. 199-237.

Lundberg, M., 2015, Petrology and Provenance of the Upper Cretaceous Strata in Central Utah, [Master thesis]: University of Bergen, 185 p.

Lundschien, B. A., Høy, T., and Mørk, A., 2014, Triassic hydrocarbon potential in the northern Barents Sea; integrating Svalbard and stratigraphic core data: Norwegian Petroleum Directorate Bulletin, 11, p. 3-20.

Maceachern, J. A., Pemberton, S. G., Bann, K. L., and Gingras, M. K., 2005, Departures from the archetypal ichnofacies: Effective recognition of physico-chemical stresses in the rock record, *in* MacEachern, J. A., Bann, K. L., Gingras, M. K., and Pemberton, S. G., eds., Applied Ichnology, Tulsa, Oklahoma, SEPM Short Course Notes, 52, p. 65-93.

McBride, E. F., 1989, Quartz cement in sandstones: a review: Earth-Science Reviews, 26, no. 1-3, p. 69-112.

Michelsen, J. K., and Khorasani, G. K., 1991, A regional study on coals from Svalbard: organic facies, maturity and thermal history: Bulletin de la Société Géologique de France, 162, no. 2, p. 385-397.

Midwinter, D. W., 2012, The Lower Triassic Bjorne Formation: From deposition to diagenesis in the eastern Sverdrup Basin, Ellesmere Island, Nunavut, Canada, [Bachelor thesis]: Dalhousie University, 78 p.

Miller, E. L., Toro, J., Gehrels, G., Amato, J. M., Prokopiev, A., Tuchkova, M. I., Akinin, V. V., Dumitru, T. A., Moore, T. E., and Cecile, M. P., 2006, New insights into Arctic paleogeography and tectonics from U-Pb detrital zircon geochronology: Tectonics, 25, no. 3, p. 1-19.

Mulder, T., Syvitski, J. P., Migeon, S., Faugères, J.-C., and Savoye, B., 2003, Marine hyperpycnal flows: initiation, behavior and related deposits. A review: Marine and Petroleum Geology, 20, no. 6, p. 861-882.

Mulrooney, M. J., Leutscher, J., and Braathen, A., 2017, A 3D structural analysis of the Goliat field, Barents Sea, Norway: Marine and Petroleum Geology, 86, p. 192-212.

Müller, R., Nystuen, J. P., Eide, F., and Lie, H., 2005, Late Permian to Triassic basin infill history and palaeogeography of the Mid-Norwegian shelf—East Greenland region, *in* Wandås, B. T. G., Nystuen, J. P., Eide, E., and Lie, H., eds., Onshore-Offshore Relationships on the North Atlantic Margin, Elsevier, Amsterdam, 12, p. 165-189.

Mørk, A., 2015, Historical Geology - Triassic, *in* Dallmann, W., ed., Geoscience Atlas of Svalbard, Norwegian Polar Institute, Report Series, 148, p. 114-117.

Mørk, A., and Elvebakk, G., 1999, Lithological description of subcropping Lower and Middle Triasic rocks from the Svalis Dome, Barents Sea: Polar Research, 18, no. 1, p. 83-104.

Mørk, A., Elvebakk, G., Forsberg, A. W., Vigran, J. O., and Weitschat, W., 1999, The type section of the Vikinghogda Formation: a new Lower Triassic unit in central and eastern Svalbard: Polar Research, 18, no. 1, p. 51-82.

Mørk, A., Embry, A. F., and Weitschat, W., 1989, Triassic transgressive-regressive cycles in the Sverdrup Basin, Svalbard and the Barents Shelf, Correlation in hydrocarbon exploration, Springer, p. 113-130.

Mørk, A., Knarud, R., and Worsley, D., 1982, Depositional and diagenetic environments of the Triassic and Lower Jurassic succession of Svalbard, *in* Embry, A. F., and Balkwill, H. R., eds., Arctic Geology and Geophysics: Proceedings of the 3rd International Symposium on Arctic Geology, Canadian Society of Petroleum Geologists, Memoir, 8, p. 371-398.

Mørk, A., and Worsley, D., 2006, The Festningen section: Norsk Geologisk Forening (NGF) Abstracts and Proceedings, 3, p. 31-35.

Mørk, M. B. E., 1999, Compositional variations and provenance of Triassic sandstones from the Barents Shelf: Journal of Sedimentary Research, 69, no. 3, p. 690-710.

Nakrem, H. A., and Mørk, A., 1991, New Early Triassic Bryozoa (Trepostomata) from Spitsbergen, with some remarks on the stratigraphy of the investigated horizons: Geological Magazine, 128, no. 2, p. 129-140.

Nemec, W., 1995, The dynamics of deltaic suspension plumes, *in* Oti, M. N., and Postma, G., eds., Geology of deltas, A. A. Balkema, Rotterdam, p. 31-93.

Norina, D. A., Stupakova, A. V., and Kiryukhina, T. A., 2014, Depositional Environments and the Hydrocarbon Generative Potential of Triassic Rocks of the Barents Sea basin: Moscow University Geology Bulletin, 69, no. 1, p. 1-10.

Oftedal, B. T., Andresen, A., and Müller, R., 2005, Early Triassic syn-rift sedimentation at Hold with Hope, Northeast Greenland, *in* Wandås, B. T. G., Nystuen, J. P., Eide, E., and Gradstein, F., eds., Onshore-Offshore Relationships on the North Atlantic Margin, Elsevier, Amsterdam, 12, p. 191-206.

Olaussen, S., Dalland, A., Gloppen, T., and Johannessen, E., 1984, Depositional environment and diagenesis of Jurassic reservoir sandstones in the eastern part of Troms I area, Petroleum Geology of the North European Margin, Springer, p. 61-79.

Patchett, P. J., Embry, A. F., Ross, G. M., Beauchamp, B., Harrison, J. C., Mayr, U., Isachsen, C. E., Rosenberg, E. J., and Spence, G. O., 2004, Sedimentary Cover of the Canadian Shield through Mesozoic Time Reflected by Nd Isotopic and Geochemical Results for the Sverdrup Basin, Arctic Canada: The Journal of Geology, 112, no. 1, p. 39-57.

Pemberton, S. G., MacEachern, J. A., Dashtgard, S. E., Bann, K. L., Gingras, M. K., and Zonneweld, J. P., 2012, Shorefaces, *in* Knaust, D., and Bromley, R. G., eds., Trace Fossils as Indicators of Sedimentary Environments, Elsevier, Amsterdam, Developments in Sedimentology, 64, p. 563-604.

Pettijohn, F., Potter, P. E., and Siever, R., 1987, Diagenesis, Sand and Sandstone, Springer, p. 425-474.

Pickering, K., Stow, D., Watson, M., and Hiscott, R., 1986, Deep-water facies, processes and models: a review and classification scheme for modern and ancient sediments: Earth-Science Reviews, 23, no. 2, p. 75-174.

Plink-Björklund, P., 2012, Effects of tides on deltaic deposition: Causes and responses: Sedimentary Geology, 279, p. 107-133.

Powers, M. C., 1953, A new roundness scale for sedimentary particles: Journal of Sedimentary Petrology, 23, no. 2, p. 117-119.

Pózer Bue, E., and Andresen, A., 2014, Constraining depositional models in the Barents Sea region using detrital zircon U–Pb data from Mesozoic sediments in Svalbard, *in* Scott, R. A., Smyth, H. R., and Morton, A. C., eds., Sediment Provenance Studies in Hydrocarbon Exploration and Production, Geological Society of London, Special Publications, 386, p. 261-279.

Puchkov, V. N., 2009, The evolution of the Uralian orogen, *in* Murphy, J. B., Keppie, J. D., and Hynes, A. J., eds., Ancient Orogens and Modern Analogues, Geological Society of London, Special Publications, 327, p. 161-195.

Reineck, H. E., 1963, Sedimentgefüge im Bereich der südlichen Nordsee: Abhandlungen der Senckenbergischen Naturforschenden Gesellschaft., 505, p. 1-138.

Reineck, H. E., and Singh, I. B., 1980, Depositional Sedimentary Environments, with Reference to Terrigenous Clastics, Depositional Sedimentary Environments, Springer-Verlag, p. 549.

Richter, D. K., Götte, T., Götze, J., and Neuser, R. D., 2003, Progress in application of cathodoluminescence (CL) in sedimentary petrology: Mineralogy and Petrology, 79, p. 127-166.

Riis, F., 1996, Quantification of Cenozoic vertical movements of Scandinavia by correlation of morphological surfaces with offshore data: Global and Planetary Change, 12, no. 1, p. 331-357.

Riis, F., and Fjeldskaar, W., 1992, On the magnitude of the Late Tertiary and Quaternary erosion and its significance for the uplift of Scandinavia and the Barents Sea: Structural and tectonic modelling and its application to petroleum geology, 1, p. 163-185.

Riis, F., Lundschien, B. A., Høy, T., Mørk, A., and Mørk, M. B. E., 2008, Evolution of the Triassic shelf in the northern Barents Sea region: Polar Research, 27, no. 3, p. 318-338.

Rossi, V. M., Perillo, M. M., Steel, R. J., and Olariu, C., *in press*, Quantifying mixed-process variability in shallow-marine depositional systems: What are sedimentary structures really telling us?: Journal of Sedimentary Research, 87, p. 1060-1074.

Røhr, T. S., and Andersen, T., 2009, Detrital zircons from the high Arctic; evidence of extensive recycling of sediment from Devonian through Mesozoic times, *in* Røhr, T. S., ed., Sedimentary Provenance analysis of Lower Cretaceous Sedimentary Successions in The Arctic; Constraints From Detrital Zircon Data, University of Oslo, Doctoral thesis.

Røhr, T. S., Andersen, T., and Dypvik, H., 2008, Provenance of Lower Cretaceous sediments in the Wandel Sea Basin, North Greenland: Journal of the Geological Society, 165, no. 3, p. 755-767.

Saigal, G. C., and Bjørlykke, K., 1987, Carbonate cements in clastic reservoir rocks from offshore Norway—relationships between isotopic composition, textural development and burial depth, *in* Marshall, J. D., ed., Diagenesis of Sedimentary Sequences, Geological Society of London, Special Publications, 36, p. 313-324.

Seidler, L., 2000, Incised submarine canyons governing new evidence of Early Triassic rifting in East Greenland: Palaeogeography, Palaeoclimatology, Palaeoecology, 161, no. 1, p. 267-293.

Senger, K., Roy, S., Braathen, A., Buckley, S. J., Bælum, K., Gernigon, L., Mjelde, R., Noormets, R., Ogata, K., and Olaussen, S., 2013, Geometries of doleritic intrusions in central Spitsbergen, Svalbard: an integrated study of an onshore-offshore magmatic province with implications for CO_2 sequestration: Norwegian Journal of Geology, 93, p. 143-166.

Senger, K., Tveranger, J., Ogata, K., Braathen, A., and Planke, S., 2014, Late Mesozoic magmatism in Svalbard: A review: Earth-Science Reviews, 139, p. 123-144.

Smelror, M., Petrov, O. V., Larssen, G. B., and Werner, S. C., 2009, Geological History of the Barents Sea, Trondheim, Geological Survey of Norway, 135 p.

Solomon, M., 1963, Counting and sampling errors in modal analysis by point counter: Journal of Petrology, 4, no. 3, p. 367-382.

Steel, R. J., and Worsley, D., 1984, Svalbard's post-Caledonian strata—an atlas of sedimentational patterns and palaeogeographic evolution, Petroleum geology of the North European margin, Springer, p. 109-135.

Stemmerik, L., Elvebakk, G., and Worsley, D., 1999, Upper Palaeozoic carbonate reservoirs on the Norwegian arctic shelf; delineation of reservoir models with application to the Loppa High: Petroleum Geoscience, 5, no. 2, p. 173-187.

Stoker, M. S., Stewart, M. A., Shannon, P. M., Bjerager, M., Nielsen, T., Blischke, A., Hjelstuen, B. O., Gaina, C., McDermott, K., and Ólavsdóttir, J., 2017, An overview of the Upper Palaeozoic–Mesozoic stratigraphy of the NE Atlantic region, *in* Péron-Pinvidic, G., Hopper, J. R., Funck, T., Stoker, M. S., Gaina, C., Doornenbal, J. C., and Árting, U. E., eds., The NE Atlantic Region: A Reappraisal of Crustal Structure, Tectonostratigraphy and Magmatic Evolution, Geological Society of London, Special Publications, 447, p. 11-68.

Storvoll, V., and Bjørlykke, K., 2004, Sonic velocity and grain contact properties in reservoir sandstones: Petroleum Geoscience, 10, p. 215-226.

Taylor, A. M., and Goldring, R., 1993, Description and analysis of bioturbation and ichnofabric: Journal of the Geological Society, 150, no. 1, p. 141-148.

Taylor, J. M., 1950, Pore-space reduction in sandstones: AAPG Bulletin, 34, no. 4, p. 701-716.

ten Brink, U., and Stern, T., 1992, Rift Flank Uplifts and Hinterland Basins: Comparison of the Transantarctic Mountains With the Great Escarpment of Southern Africa: Journal of Geophysical Research: Solid Earth, 97, p. 569-585.

Vigran, J. O., Mangerud, G., Mørk, A., Bugge, T., and Weitschat, W., 1998, Biostratigraphy and sequence stratigraphy of the Lower and Middle Triassic deposits from the Svalis Dome, central Barents Sea, Norway: Palynology, 22, no. 1, p. 89-141.

Vigran, J. O., Mangerud, G., Mørk, A., Worsley, D., and Hochuli, P. A., 2014, Palynology and geology of the Triassic succession of Svalbard and the Barents Sea, Geological Survey of Norway Special Publication, 14, p. 270.

Walderhaug, O., 1990, A fluid inclusion study of quartz-cemented sandstones from offshore mid-Norway--possible evidence for continued quartz cementation during oil emplacement: Journal of Sedimentary Research, 60, no. 2, p. 203-210.

Walker, R. G., 1984, Shelf and shallow marine sands, *in* Walker, R. G., ed., Facies Models, 2nd edn.: Geological Association of Canada, Geoscience Canada Reprint Series, 1, p. 141-170.

Wentworth, C. K., 1922, A Scale of Grade and Class Terms for Clastic Sediments: The Journal of Geology, 30, no. 5, p. 377-392.

Wignall, P. B., Bond, D. P., Sun, Y., Grasby, S. E., Beauchamp, B., Joachimski, M. M., and Blomeier, D. P., 2016, Ultra-shallow-marine anoxia in an Early Triassic shallow-marine clastic ramp (Spitsbergen) and the suppression of benthic radiation: Geological Magazine, 153, no. 2, p. 316-331.

Wignall, P. B., Morante, R., and Newton, R., 1998, The Permo-Triassic transition in Spitsbergen: δ 13 C org chemostratigraphy, Fe and S geochemistry, facies, fauna and trace fossils: Geological Magazine, 135, no. 1, p. 47-62.

Wignall, P. B., and Twitchett, R. J., 2002, Permian–Triassic sedimentology of Jameson Land, East Greenland: incised submarine channels in an anoxic basin: Journal of the Geological Society, 159, no. 6, p. 691-703.

Worsley, D., 2008, The post-Caledonian development of Svalbard and the western Barents Sea: Polar Research, 27, no. 3, p. 298-317.

Worsley, D., Johansen, R., and Kristensen, S., 1988, The Mesozoic and Cenozoic succession of Tromsøflaket: A lithostratigraphic scheme for the Mesozoic and Cenozoic succession offshore mid- and northern Norway: Norwegian Petroleum Directorate Bulletin, no. 4, p. 42-65.

Worsley, D., and Mørk, A., 1978, The Triassic stratigraphy of southern Spitsbergen: Norsk Polarinstitutt Årbok 1977, p. 43-60.

Online Resources

Naturhistorisk Museum., 2013, Barents Sea Chart:

http://www.nhm2.uio.no/norges/litho/Barents_Chart.html (accessed 03.09.2017)

Norwegian Petroleum Directorate (NPD)., 2017, Factpages:

http://gis.npd.no/factmaps/html_21/ (accessed 02.11.2017)

Appendix A:

Sedimentary logs from outcrop

LEGEND

☐ Sandstone

☐ Mudstone

☐ Limestone

☒ No data

☰ Planar parallel stratification

≈ Crude laminations

𝄇𝄇𝄇 Tangential cross-stratification

/// Angular cross-stratification

≈ Flaser bedding

∼ Wavy bedded sandstone

∼ Wavy bedded mudstone

∼ Lenticular bedding

≈ 3D current ripple cross-lamination

╱ Low-angle cross-stratification

〜〜〜 Erosion surface/ incutting surface

Unidirectional current orientation
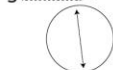
Oscillatory current orientation

Facies associations (FA):
A: Tidally influenced channel
B: Tidal sandflat
C: Supratidal deposits
D: Delta front deposits
E: Offshore transition zone
F: Prodelta deposits

⌒ Wave ripples

── Plane parallel laminations

Ω Soft-sediment deformation

⬚✕ ➤ Shell fragments, shell hash

⋀ Indistinct ripples

/// Current ripples

〜 Mud drapes

◗ ◖ Organic fragments

⊕ Fe Iron concretion

⊥ Very cemented

◗ ◗ Clasts of sandstone

● ◗ ● Mud clasts, rounded rip-up clasts

⌄⌄ Desiccation cracks

⊕ Undifferentiated concretions

( ) Planolites

⌣ Bivalves

U Arenicolites

= Undifferentiated, horizontal burrows

V Undifferentiated, vertical burrows

⫽ Cylindrichnus

(≋) Teichichnus

♀ Rosselia

( ) Palaeophycus

◎ Ammonite

98

Log A Festningen

Coordinates for start of log location:

78° 5'43.01"N

13°51'7.48"E

Rose diagram for unidirectional paleocurrent measurements

n = 10
Mean direction 50.8°

Rose diagram for oscillatory paleocurrent measurements

n=1
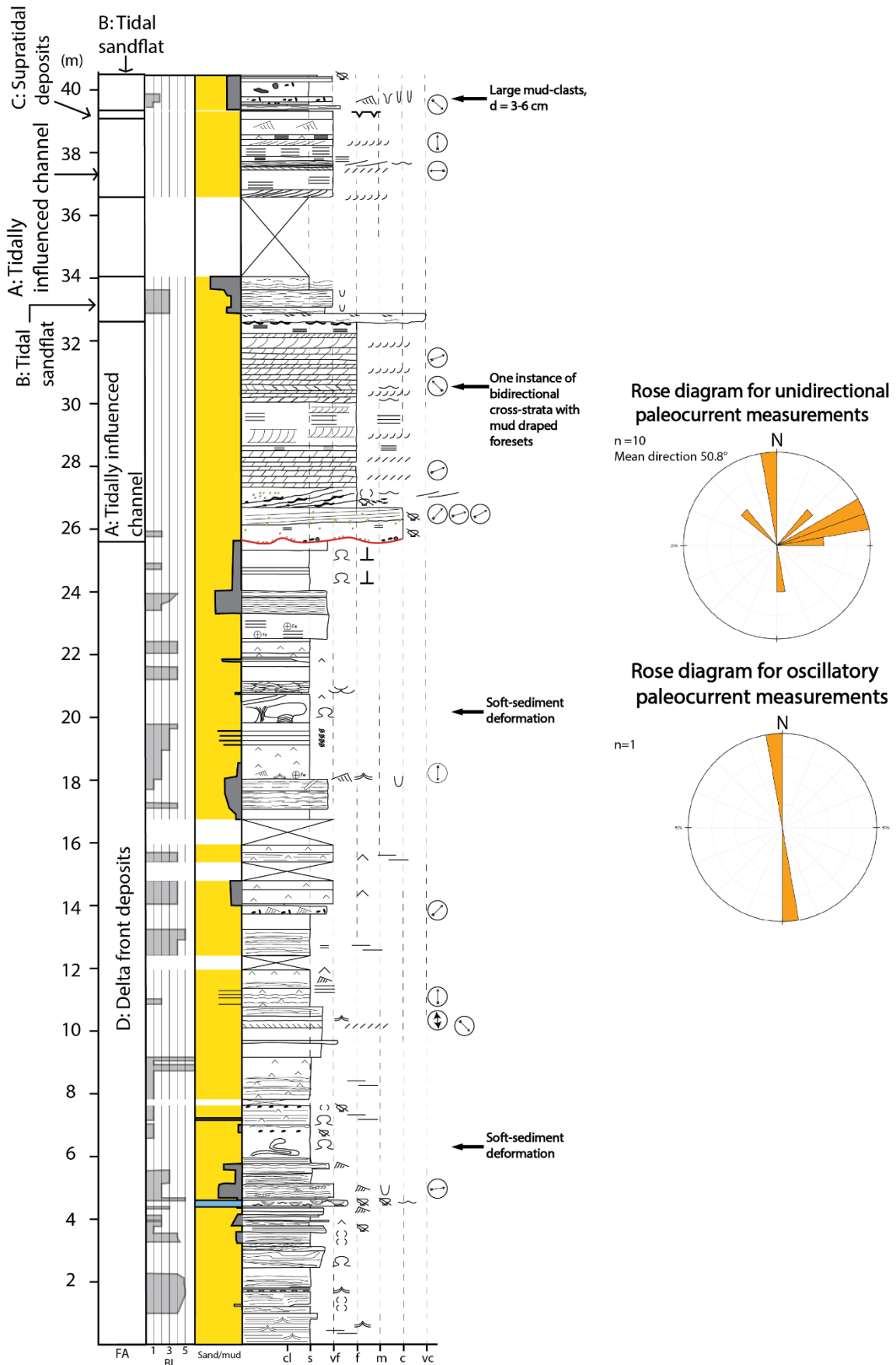
Log B Festningen

Coordinates for start of log location:

78° 5'39.39"N

13°50'35.93"E

Log C Festningen

Coordinates for start of log location:

78° 5'44.28"N

13°51'35.98"E

E: Offshore transition zone

D: Delta front deposits

(m)

7

6

5

4

3

2

1

FA   1 3 5   Sand/mud   cl   s   vf   f   m   c   vc
        Bl
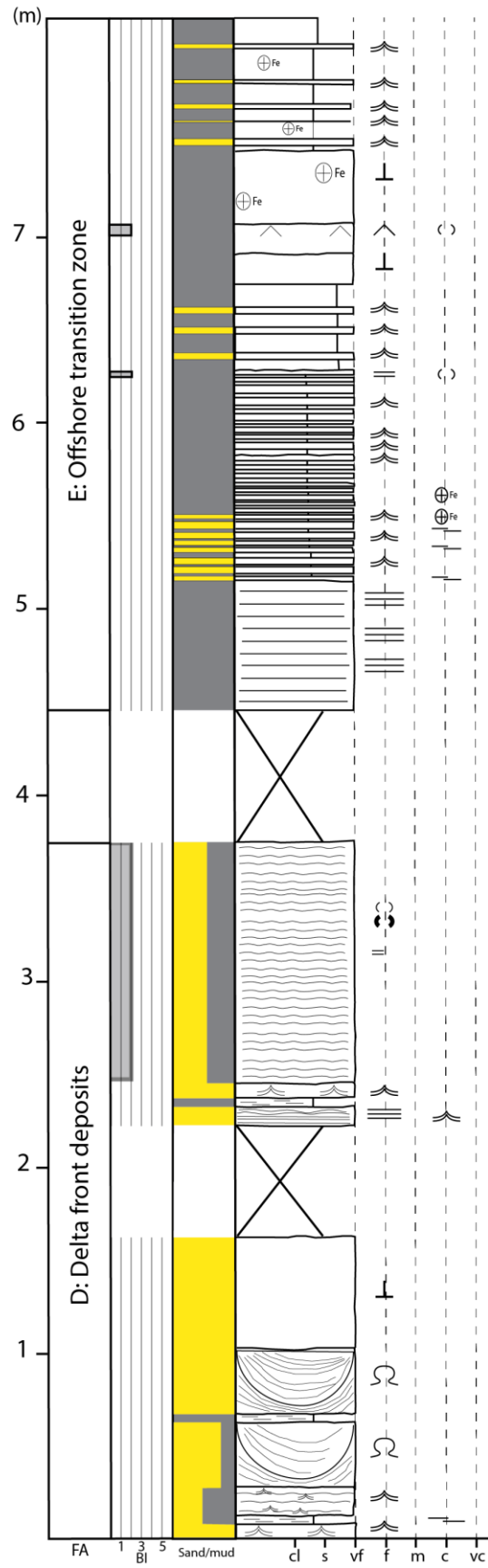
Log D Studentdalen

Coordinates for start of log location:

78°29'3.19"N

15°50'55.67"E
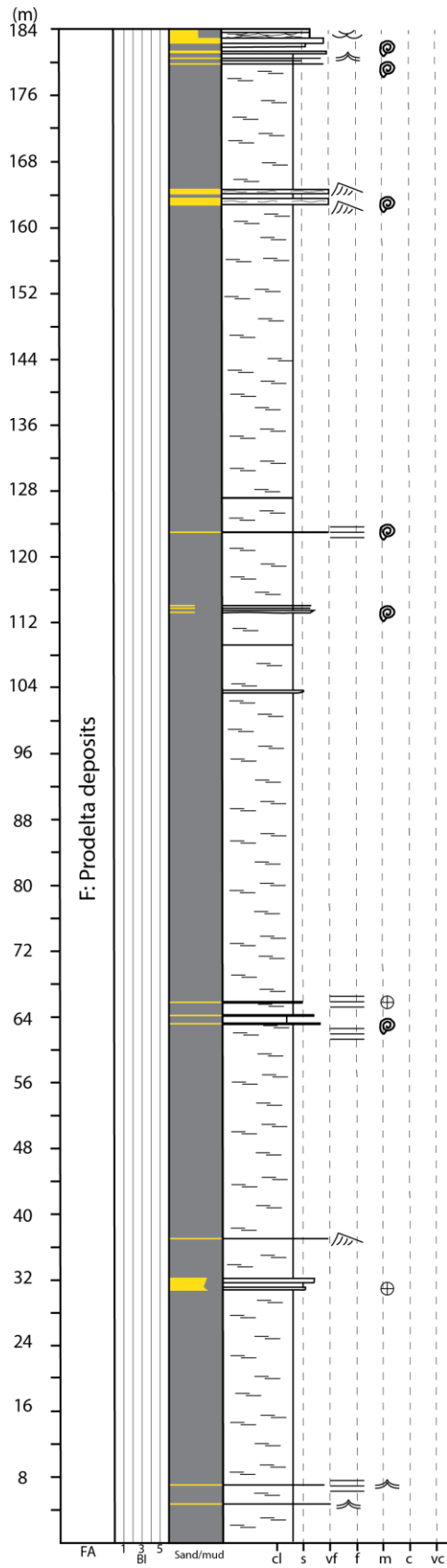
Log E Studentdalen

Coordinates for start of log location:

78°29'47.44"N

15°49'18.46"E
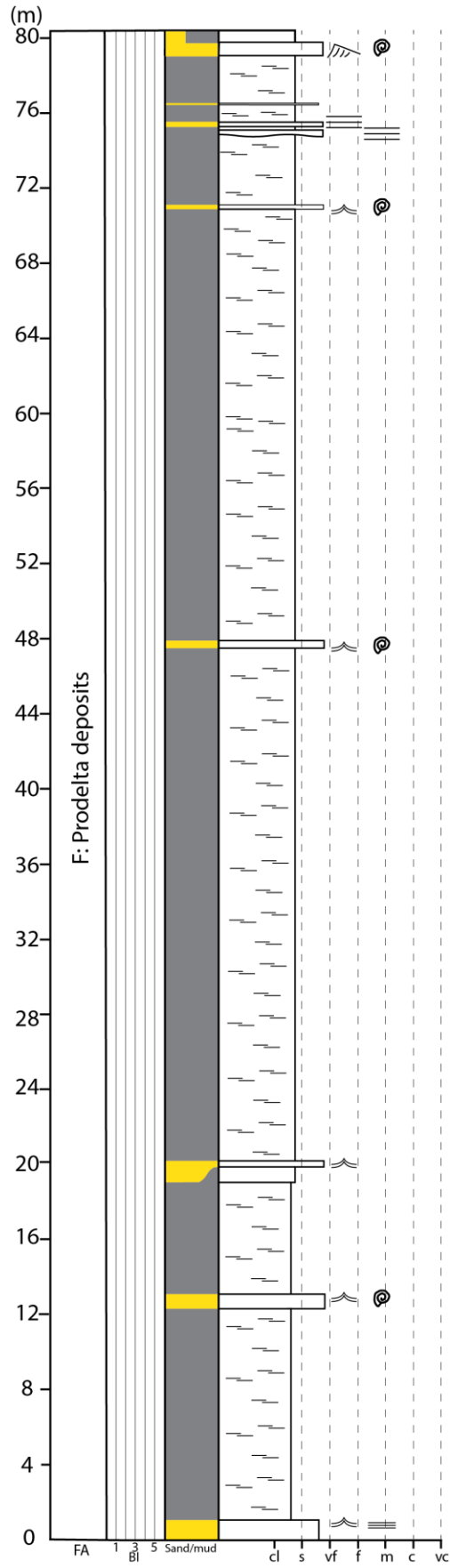
Log F Studentdalen:

Coordinates for start of log location:

78°29'27.37"N

15°50'4.73"E
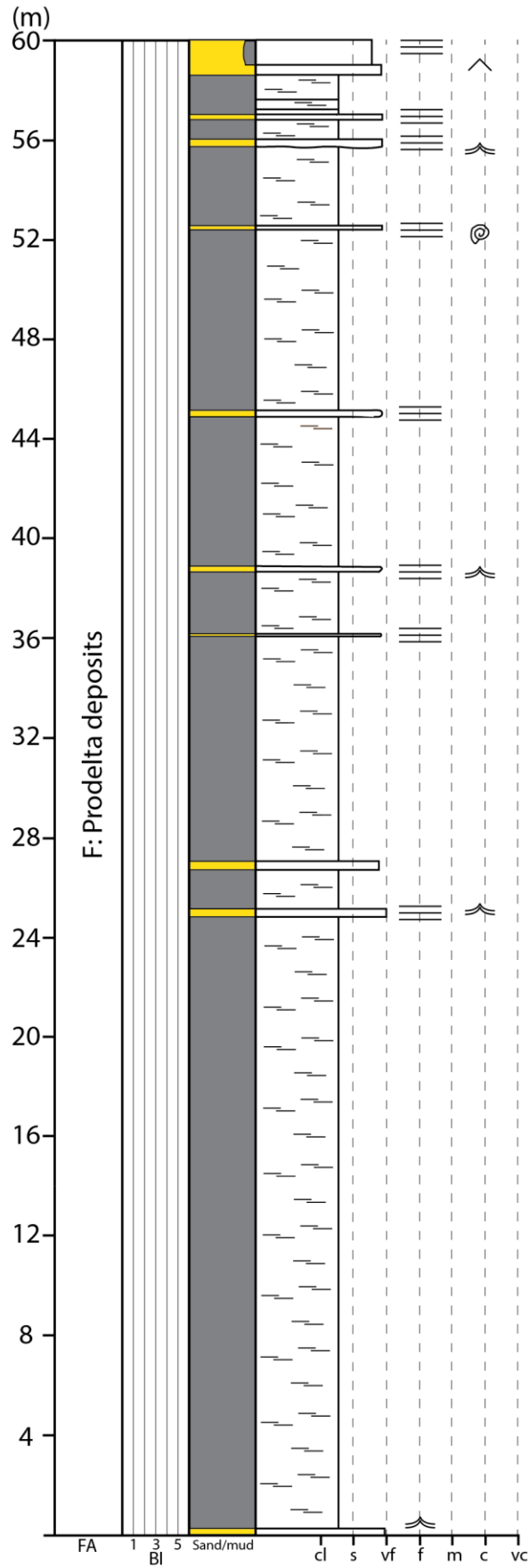
Appendix B:

Table showing in which facies samples were collected

Location	Sample	Facies	Facies association
Festningen	FES1	M	C
	FES2	J	B
	FES3	A	A
	FES6	K	A
	FES9	C	A
	FES19	K	A
	FES20	K	A
Selmaneset	SES2	B	-
	SES3	K	-
	SES5	A	-
	SES7	O	A